Thermal Effects and Temperature Profiles in Capillary Electrophoresis

by

Christopher John Evenhuis

A thesis submitted in fulfillment of the requirements for the degree of Doctor of Philosophy

January 2007

Declaration

To the best of my knowledge, this thesis contains no copy or paraphrase of material previously written or published, except where due reference is made.

This thesis may be made available for loan, and limited copying in accordance with the *Copyright Act 1968.*

Christopher John Evenhuis

10 January 2007

Acknowledgements

I would like to thank the following people for their help and encouragement over the last three years.

My primary supervisor Dr Miroslav Macka for his guidance, enthusiasm and generosity with his time and resources to support my project.

My research supervisor Dr Rosanne M Guijt for her help, encouragement and invaluable proofreading of numerous drafts of manuscripts.

My associate supervisors Prof. Paul R. Haddad and Prof Philip J. Marriot for their wisdom and guidance and polishing of manuscripts.

Dr Cameron Johns for getting me started in capillary electrophoresis.

Dr Michael C. Breadmore for many helpful suggestions and instructing me on how to maintain and repair my capillary electrophoresis instrument.

Dr Emily F. Hilder for her assistance and encouragement.

All members of the Australian Centre for Research on Separation Science

John Davis and Paul Waller for electronic technical assistance.

Dr I. Koev for the gift of PMMA capillary.

Xiangchun Xuan and Donqing Li for supply of original data files for **Figures 1- 7** to **1- 9**.

Vlastmil Hruška for assistance in performing ionic strength corrections to electrophoretic mobilities and for useful collaboration in Prague.

Mrs. Violet Giblin for her continued interest and enthusiasm.

My parents Dr A. J. Evenhuis and Dr E.K. Evenhuis for their encouragement.

My friend and prayer partner Omar Venegas for his encouragement and prayer support throughout the course of my research.

My daughters Ruth and Elyse for their continued interest and encouragement.

My wife Rosanne for her help in supporting our family during the course of my research and for her constant friendship and encouragement.

Finally I thank God for leading me back in to academia and for supplying all my needs. This work is dedicated to Him.

Trust in the LORD with all your heart, and lean not on your own understanding; in all your ways acknowledge Him, and He shall direct your paths. Proverbs 3:5-6 (NKJ)

Glossary of Terms

Abbreviation	Quantity	Unit
α	Thermal diffusivity	m^2s^{-1}
β	Reciprocal of film temperature	K^{-1}
γ	Temperature coefficient of electrical conductivity	$^oC^{-1}$
γ^*	Temperature-dependence of the diffusion coefficient	Dimensionless
δ_t	thickness of the thermal boundary layer	m
$\left(\frac{\partial p}{\partial L}\right)_i$	Pressure gradient in section *i* of the capillary.	$kgm^{-2}s^{-2}$
ΔT_{Air}	Temperature difference across air layer surrounding capillary (see **Figure 1- 4**)	^{o}C
$\Delta T_{Across\ Wall}$	Temperature difference across the capillary wall (sum of ΔT_{FS} and ΔT_{PI} (see **Figure 1- 4**)	^{o}C
$\Delta T_{At\ Axis}$	Change of electrolyte temperature at capillary axis as a result of Joule heating	^{o}C
$\Delta T_{Coolant}$	Temperature difference across coolant layer surrounding capillary	^{o}C
ΔT_{FS}	Temperature difference across fused-silica wall (see **Figure 1- 4**)	^{o}C
ΔT_{Mean}	Change in mean temperature of the electrolyte as a result of Joule heating (see **Figure 1- 4**)	^{o}C
ΔT_{PI}	Temperature difference across poly(imide) coating (see **Figure 1- 4**)	^{o}C
$\Delta T(r)$	Temperature difference between electrolyte and the inner wall of the capillary at a distance r from the axis.	^{o}C
ΔT_{Radial}	Radial temperature difference across electrolyte (see **Figure 1- 4**)	^{o}C
$\Delta T_{Rad\,i}$	Radial temperature difference across electrolyte in section i of the capillary (see **Figure 1- 11**)	^{o}C
ΔT_{ref}	Characteristic temperature rise	^{o}C
ΔT_{Wall}	Change of electrolyte temperature near capillary wall as a result of Joule heating	^{o}C
ε	Electrical permittivity of electrolyte	Fm^{-1}
ε_0	Electrical permittivity of a vacuum	8.8542×10^{-12} Fm^{-1}
ε_{Wall}	Electrical permittivity of electrolyte neat the inner wall of section i of the capillary (see **Figure 1- 11**)	Fm^{-1}
ε_r	Dielectric constant of water	Dimensionless

ζ	Zeta potential	V
η	Dynamic viscosity of electrolyte	$kgm^{-1}s^{-1}$
η_{iwall}	Viscosity of electrolyte at the wall in section i of the capillary (see **Figure 1- 11**)	$kgm^{-1}s^{-1}$
κ	Electrical conductivity of electrolyte	Sm^{-1}
$\overline{\kappa}$	Average electrical conductivity of electrolyte	Sm^{-1}
κ_0	Electrical conductivity of electrolyte at set temperature	Sm^{-1}
λ	Thermal conductivity of electrolyte	$Wm^{-1}K^{-1}$
λ_{Air}	Thermal conductivity of air	$Wm^{-1}K^{-1}$
λ_{FS}	Thermal conductivity of fused-silica	$Wm^{-1}K^{-1}$
λ_{PI}	Thermal conductivity of poly(imide)	$Wm^{-1}K^{-1}$
λ_{Wall}	Thermal conductivity of wall	$Wm^{-1}K^{-1}$
μ_{EOF}	Electroosmotic mobility	$m^2s^{-1}V^{-1}$
μ_{EOF}^0	Electroosmotic mobility free from Joule heating	$m^2s^{-1}V^{-1}$
$\mu_{EOF}^0(25\ ^oC)$	Electroosmotic mobility free from Joule heating at 25 ºC	$m^2s^{-1}V^{-1}$
μ_{ep}	Electrophoretic mobility	$m^2s^{-1}V^{-1}$
μ_{ep}^0	Electrophoretic mobility at zero ionic strength (equivalent to limiting ionic mobility)	$m^2s^{-1}V^{-1}$
$\mu_{ep}(0\ Wm^{-1})$	Effective electrophoretic mobility free from Joule heating effects	$m^2s^{-1}V^{-1}$
μ_{epA}	Electrophoretic mobility of analyte ion	$m^2s^{-1}V^{-1}$
μ_{epB}	Electrophoretic mobility of co-ion in electrolyte	$m^2s^{-1}V^{-1}$
$\mu_{epi\ Wall}$	Electrophoretic mobility of ion at the inner wall of section i of the capillary (see **Figure 1- 11**)	$m^2s^{-1}V^{-1}$
μ_{epR}	Electrophoretic mobility of counter-ion in electrolyte	$m^2s^{-1}V^{-1}$
μ_{osm}	Electroosmotic mobility	$m^2s^{-1}V^{-1}$
ν	Kinematic viscosity	m^2s^{-1}
ρ	Density	kgm^{-3}
σ	Standard deviation of Gaussian peak	s
σ_w	Charge density	Cm^{-2}
$\overline{\sigma}_w$	Mean charge density	Cm^{-2}
ψ	Electrical potential	V
ω_i	Radial viscosity distribution in section *i* of the capillary (see **Figure 1- 11**)	Dimensionless
a	Gradient of graph of power versus increase of electrolyte temperature	WK^{-1}
*a**	Reciprocal of *a*	KW^{-1}
A	Area	m^2

Bi_{OA}	Overall Biot number	Dimensionless
Bi'_{OA}	Average of experimentally-determined Biot numbers calculated at 25 kV and 30 kV	Dimensionless
c	Molar concentration	$molL^{-1}$
c_A	Molar concentration of analyte ion	$molL^{-1}$
C	Constant used for calculation of the Nusselts number	Dimensionless
C_A	Charge transported of analyte per unit volume	CL^{-1}
CEC	Capillary electrochromatography	Analytical technique
CGC	Capillary gas chromatography	Analytical technique
d_{FS}	External diameter of fused-silica	m
d_i	Internal diameter of capillary	m
d_o	External diameter of capillary	m
D	Diffusion coefficient	m^2s^{-1}
D_{Eff}	Effective dispersion coefficient	m^2s^{-1}
D_{Taylor}	Taylor-Aris dispersion coefficient	m^2s^{-1}
D_{Wall}	Diffusion coefficient at the wall,	m^2s^{-1}
E	Electrical field strength	Vm^{-1}
E_i	Electrical field strength in section i of the capillary (see **Figure 1- 11**)	Vm^{-1}
EDL	Electrical double layer	(Concept)
EOF	Electroosmotic flow	(Concept)
F	Faraday's constant	96487 $Cmol^{-1}$
FEP	Fluorinated ethylene-propylene copolymer	Capillary Material
FS	Fused-silica	Capillary Material
G	Conductance	S
G_r	Grashof number	Dimensionless
h	Heat transfer coefficient	$Wm^{-2}K^{-1}$
h_{Active}	h for the actively cooled section of the capillary	$Wm^{-2}K^{-1}$
$h_{Passive}$	h for the passively cooled capillary sections	$Wm^{-2}K^{-1}$
H	Height of theoretical peak	m
H_{axT}	Contribution to theoretical plate height due to effects of axial temperature differences	m
H_{Joule}	Contribution of Joule heating to the theoretical plate height	m
H_{Taylor}	Contribution to the theoretical plate height stemming from Taylor dispersion	m
I	Electric current	A
I_s	Ionic strength	$molL^{-1}$
k	Boltzmann constant	1.3807×10^{-23} JK^{-1}
k_1	Defined constant $k_1 = G_0/2\pi L h_{OA} r_i$.	Dimensionless

k^*	Autothermal parameter	Dimensionless
$k^{*\prime}$	Critical value of autothermal parameter	Dimensionless
k_{Taylor}	Constant which depends on the geometry of the lumen	1/48 ≈ 0.0208 for circular capillary
K	Capacity factor	Dimensionless
K_D	Advective dispersion coefficient	m^2s^{-1}
K_{diss}	Dissociation constant	Not applicable
K_E	Electromigrational dispersion coefficient	m^2s^{-1}
K^*	Overall dispersion coefficient	m^2s^{-1}
L_{det}	Length of the capillary to the detector	m
L_{tot}	Total length of the capillary	m
M	Hydrodynamic conductivity	m^3skg^{-1}
M_i	Hydrodynamic conductivity in section i of the capillary (see **Figure 1- 11**)	m^3skg^{-1}
^{n}	Constant used for calculation of the Nusselts number	Dimensionless
n	Refractive index	Dimensionless
N	Number of theoretical plates	Dimensionless
N_u	Nusselts number	Dimensionless
p	Pressure	Pa
P	Power	W
P/L	Power per unit length	Wm^{-1}
PDMS	Poly(dimethylsiloxane)	Material for chips
Pe	Peclet number	Dimensionless
PEEK	Poly(etherether ketone)	Capillary Material
PI	Poly(imide)	Capillary Material
PMMA	Poly(methyl methacrylate)	Capillary Material
P_r.	Prandtl number	Dimensionless
q	Charge	C
q^*	Parameter in Debye-Hückel-Onsager equation	0.586
Q	Rate of heat production per unit volume	Wm^{-3}
r	Distance from the axis of the capillary	m
r_h	Hydrodynamic radius of solvated ion	
r_i	Internal radius of capillary	m
r_{Mean}	Distance from axis to the location where $T = T_{Mean}$	m
R	Ideal gas constant	$8.3144\ Jmol^{-1}K^{-1}$
R_a	Rayleigh number	Dimensionless
R_e	Reynolds number	Dimensionless
t_A	Time for analyte to migrate to detector	s

t_{EOF}	Time for EOF marker to migrate to the detector	s
T	Temperature or absolute temperature	ºC or K
T_{Axis}	Temperature of the electrolyte at axis of capillary (see **Figure 1- 4**)	ºC
T_{Cavity}	Temperature measured in instrument cavity	ºC
$T_{Effective}$	Effective temperature of the electrolyte without Joule heating	ºC
T_{Film}	Film temperature (average of temperature of the external wall of the capillary and of the ambient temperature of the coolant)	K
T_{Mean}	Mean temperature of the electrolyte in the capillary (see **Figure 1- 4**)	ºC
T_{Set}	Set temperature of air used for active-cooling of cassette (see **Figure 1- 4**)	ºC
T_{Wall}	Temperature of the electrolyte near the inner wall of capillary (see **Figure 1- 4**)	ºC
$T_{Wall\ (EOF)}$	Temperature of the electrolyte near the inner wall of capillary determined using electroosmotic mobility	ºC
$T_{Wall\ (G)}$	Temperature of the electrolyte near the inner wall of capillary determined using conductance	ºC
$T_{Wall\ i}$	Temperature of the electrolyte near the inner wall of section i of capillary (see **Figure 1- 11**)	ºC
$\bar{v}_A$	Mean velocity of analyte over cross section	ms^{-1}
$v_{Coolant}$	Speed of coolant flow	ms^{-1}
v_{ep}	Electrophoretic velocity	ms^{-1}
v_{EOF}	Velocity of the electroosmotic flow	ms^{-1}
$v_{EOF\ i}(y)$	Electroosmotic velocity profile using a dimensionless radial coordinate	ms^{-1}
v_{obs}	Observed velocity of analyte	ms^{-1}
v_{parab}	Average velocity of the parabolic flow	ms^{-1}
$v_{pd\ i}$	Hydrodynamic velocity in section i of the capillary (see **Figure 1- 11**)	ms^{-1}
V	Applied voltage	V
Vol	Volume of electrolyte in capillary	m^3
$w_{1/2}$	width of peak at half height	s
x	Thickness of stationary air layer surrounding capillary	m
x_S	Thickness of Stern layer (see **Figure 1- 2**)	m
y	Dimensionless radial coordinate	Dimensionless
z	Valency of ion	Dimensionless
z_A	Valency of analyte ion	Dimensionless

List of Publications

Type of Publication	Number	Reference
Papers in refereed journals	6	[1-6]
Book chapter	1	[7]
Refereed posters at international meetings	6	[8-13]
Contributions to talks at international meetings	2	[14, 15]

[1] Evenhuis, C. J., Guijt, R. M., Macka, M., Haddad, P. R., Determination of inorganic ions using microfluidic devices, *Electrophoresis* 2004, *25*, 3602-3624.

[2] Guijt, R. M., Evenhuis, C. J., Macka, M., Haddad, P. R., Conductivity detection for conventional and miniaturised capillary electrophoresis systems, *Electrophoresis* 2004, *25*, 4032-4057.

[3] Evenhuis, C. J., Guijt, R. M., Macka, M., Marriott, P. J., Haddad, P. R., Internal Electrolyte Temperatures in Polymer and Fused-silica Capillaries during Capillary Electrophoresis, *Electrophoresis* 2005, *26*, 4333-4344.

[4] Evenhuis, C. J., Guijt, R. M., Macka, M., Marriott, P. J., Haddad, P. R., Variation of Zeta-Potential with Temperature in Fused-silica Capillaries Used for Capillary Electrophoresis, *Electrophoresis* 2006, *27*, 672-676.

[5] Evenhuis, C. J., Guijt, R. M., Macka, M., Marriott, P. J., Haddad, P. R., Temperature Profiles and heat Dissipation in Capillary Electrophoresis, *Anal. Chem.* 2006, *78*, 2684-2693.

[6] Kuban, P., Evenhuis, C. J., Macka, M., Haddad, P. R., Hauser*, P. C., Comparison of different contactless conductivity detectors for the determination of small inorganic ions by capillary electrophoresis, *Electroanalysis* 2006, *18*, 1289-1296.

[7] Evenhuis, C. J., Guijt, R. M., Macka, M., Marriott, P. J., Haddad, P. R., in: Landers, J. P. (Ed.), *Handbook of Capillary Electrophoresis*, CRC Press, Boca Raton 2006, p. Submitted.

[8] Evenhuis, C. J., Guijt, R. M., Macka, M., Marriott, P. J., Haddad, P. R., Measuring Temperatures In Capillaries Used For CE, 28th International Symposium on Capillary Chromatography & Electrophoresis, May 22-25, 2005, Las Vegas, poster no.59

[9] Evenhuis, C. J., Guijt, R. M., Macka, M., Marriott, P. J., Haddad, P. R., How Cool Is My CE?- Measuring the heat transfer coefficient in CE, International Symposium on Chromatography, Copenhagen, August 21-25, 2006 poster no. Pe01.

[10] Evenhuis, C. J., Guijt, R. M., Macka, M., Marriott, P. J., Haddad, P. R., Get it right! Measuring electrophoretic mobilities free of Joule Heating, International Symposium on Chromatography, Copenhagen, August 21-25, 2006 poster no. Pe 03.

[11] Evenhuis, C. J., Guijt, R. M., Macka, M., Marriott, P. J., Haddad, P. R., Post-Blast Identification of Improvised Explosive Devices, International Symposium on Chromatography, Copenhagen, August 21-25, 2006 poster no. Pe 04.

[12] Evenhuis, C. J., Guijt, R. M., Macka, M., Marriott, P. J., Haddad, P. R., A New Approach to Measuring the Variation of Zeta-Potential with Temperature Studied in Fused-silica Capillaries in Capillary Electrophoresis, International Symposium on Chromatography, Copenhagen, August 21-25, 2006 poster no. Pe 05

[13] Evenhuis, C. J., Guijt, R. M., Macka, M., Marriott, P. J., Haddad, P. R., Quantifying temperature increases due to Joule heating in electrodriven separations, International Symposium on High Performance Liquid Phase Separations & Related Techniques - HPLC-2005, Stockholm, June 26-30, 2005 poster no.7:25

[14] Evenhuis, C. J., Johns, C.,Yang, W.-C., Schuman, P., Guijt, R. M., Haddad, P. R., Marriott, P. J., Macka, M., New Approaches to Simultaneous Separations of Inorganic Anions and Cations by Capillary Electrophoresis: Use of High-Magnitude EOF Capillaries and UV-transparent Fluoropolymer Capillary, 25th International Symposium on Capillary Chromatography (ISCC), Riva del Garda, 31 May - 4 June 2004, oral keynote presentation No. KNL.10.

[15] Evenhuis, C. J., Guijt, R. M., Haddad, P. R., Marriott, P. J., Macka, M., At what effective temperatures do we actually run electro-driven separations? International Symposium on Separation Science, Parubice, 12-15 September 2005, oral presentation No. L33, p. 43.

Table of Contents

Thermal Effects and Temperature Profiles in Capillary Electrophoresis i

Declaration ii

Acknowledgements iii

Glossary of Terms v

List of Publications x

Abstract 1

1. Introduction and Literature Review: 3

1.1. Basic Theory of Electrophoresis 3

1.2. Electroosmotic Flow 4

1.2.1 Origin of Electroosmotic flow 5

1.3. Heating Effects in Electrophoresis 7

1.3.1 Quantifying Temperature Differences 8

1.3.2 The heat transfer coefficient (h) 13

1.3.3 Investigations of Joule heating and cooling efficiency 17

1.4. Joule Heating and Separation Efficiency 21

1.4.1 The Effect of Electrolyte Temperature on Separation Efficiency 22

1.4.2 The Effect of Radial Temperature Differences on Separation Efficiency. 24

1.4.3 The Effect of Axial Temperature Differences on Separation Efficiency ... 34

1.5. Temperature Measurement in CE 40

1.6. Project Aims 48

2 Experimental 50

2.1 Instrumentation 50

2.2 Reagents 51

2.3 Conductance Measurements 51

2.4 Electroosmotic Mobility Measurements 51

2.5 Temperature Measurements 52

3 The Radial Temperature Profile of the Electrolyte During CE 54
3.1 Modeling the Radial Temperature Profile 54
3.2 Conclusions 57

4. Using Conductance and Electroosmotic Mobility as Temperature Probes for the Mean Electrolyte Temperature 58
4.1 Introduction 58
4.2 Calibrating Conductance as a Temperature Probe 58
4.2.1 Experimental 58
4.2.2 Results and Discussion 60
4.2.3 Conclusions 67
4.3 Calibrating Electroosmotic Mobility as a Temperature Probe 67
4.3.1 Experimental 67
4.3.2 Results and Discussion 68
4.3.3 Conclusions 71
4.4 Comparison of μ_{EOF} and G as temperature probes 71
4.4.1 Introduction 71
4.4.2 Results and Discussion 71
4.4.3 Conclusions 74
4.5 Using G to find T_{Wall} 74
4.5.1 Introduction 74
4.5.2 Results and Discussion 75
4.5.3 Conclusions 75
4.6 Calculation of a complete temperature profile for a fused-silica capillary 75
4.6.1 Introduction 75
4.6.2 Theory 78
4.6.3 Experimental 79
4.6.4 Results and Discussion 80
4.6.5 Conclusions 83
4.7 Investigation of an alternative method for determining h. 85
4.7.1 Introduction 85
4.7.2 Theory 85
4.7.3 Experimental 86
4.7.4 Results and Discussion 87

4.7.5 Conclusions 91

5 The Variation of Zeta-Potential with Temperature 92

5.1 Introduction 92

5.2 Experimental 94

5.3 Results and Discussion 94

5.4 Conclusions 96

6 Temperature Increases in Polymer Capillaries 99

6.1 Introduction 99

6.2 Theory 101

6.3 Experimental 102

6.4 Results and Discussion 103

6.5 Conclusions 111

7 Measurement of Electrophoretic Mobilities Free from the Effects of Joule Heating 112

7.1 Introduction 112

7.2 Experimental 116

7.2.1 Chemicals 116

7.2.2 Procedures 117

7.3 Results and Discussion 117

7.4 Conclusions 122

8 General Conclusions 123

9 References: 126

10 Appendices 136

Appendix 1 - Derivation of Modified Debye-Hückel-Onsager Equation 136

Appendix 2 – Calculation of *h* for Passively-cooled Capillaries 139

Appendix 3 – Derivations of Eqns 4- 27 and 4- 28 141

Abstract

Whilst temperature control is usually employed in capillary electrophoresis (CE) to aid heat dissipation and provide acceptable precision, internal electrolyte temperatures are almost never measured. In principle this limits the accuracy, repeatability and method robustness. This work presents a fundamental study that combines the development of new equations characterising temperature profiles in CE with a new method of temperature determination. New equations were derived from first principles relating the mean, axial and inner wall electrolyte temperatures (T_{Mean}, T_{Axis} and T_{Wall}). T_{Mean} was shown to occur at a distance $1/\sqrt{2}$ times the internal radius of the capillary from the centre of the capillary and to be the average of T_{Axis} and T_{Wall}. Conductance (G) and electroosmotic mobility (μ_{EOF}) were used to determine T_{Mean} and T_{Wall}, respectively. Extrapolation of curves of μ_{EOF} *versus* power per unit length (P/L) at different temperatures was used to calibrate the variation of μ_{EOF} with temperature (T), free from Joule heating effects. μ_{EOF} increased at 2.22 % per ºC. The experimentally-determined temperatures using μ_{EOF} agreed to within 0.2 ^{o}C with those determined using G. The accuracy of G measurements was confirmed independently by measuring the electrical conductivity (κ) of the bulk electrolyte over a range of temperatures and by calculating the variation of G with T from the Debye-Hückel-Onsager equation. T_{Mean} was found to be up to 20 ^{o}C higher than the external temperature under typical conditions using active air-cooling and a 74.0 µm internal diameter (d_i) fused-silica capillary. A combination of experimentally-determined and calculated temperatures enabled a complete temperature profile for a fused-silica capillary to be drawn, the thickness of the stationary air layer to be determined and the heat transfer coefficient (h) for the capillary to be determined.

Similar techniques based on the variation of G with P/L were used to explore temperature profiles in polymer capillaries used for CE. For each type of capillary material, it was found that the average increase in the mean temperature of the electrolyte (ΔT_{Mean}) was directly proportional to P/L and inversely proportional to the thermal conductivity (λ) of the capillary material. At 7.5 Wm^{-1}, values for ΔT_{Mean} for fluorinated ethylene-propylene copolymer (FEP), poly(methyl methacrylate) (PMMA) and poly(etherether ketone) (PEEK) were determined to be 36.6 °C, 33.8 °C and 30.7 °C, respectively. Under identical conditions, ΔT_{Mean} for FS capillaries was 20.4 °C.

The temperature variation of electroosmotic mobility corrected for the effects of Joule heating (μ_{EOF}^{0}) was employed to investigate the variation of the zeta-potential (ζ) with temperature in fused-silica capillaries. Experimentally-determined values for ζ increased at 0.39 % per ºC, a rate that is about 4 to 5 times smaller than reported previously. Experimentally-determined values of ζ were directly proportional to the absolute temperature although values were also influenced slightly by changes to the dielectric constant. It was found that the effective charge density at the inner surface of the capillary was independent of temperature.

Invariably, electrophoretic mobilities (μ_{ep}) determined from capillary electrophoresis (CE) experiments are different to accepted values based on limiting ionic conductance. While the effect of ionic strength on μ_{ep} has been long understood, the increase in μ_{ep} that results from Joule heating has been largely overlooked. A simple method for obtaining reliable and reproducible values of μ_{ep} is introduced. μ_{ep} is measured over a range of power values and extrapolation to zero power dissipation is employed to eliminate the effect of Joule heating. Agreement between experimentally-determined mobilities and literature values may be improved by an order of magnitude.

1. Introduction and Literature Review:

1.1. Basic Theory of Electrophoresis

Electrophoresis is an analytical technique used to separate charged species by means of an intense electrical field. Separation is based on differences in velocity (*v*) of charged species when the electrical field (*E*) is applied. It may be shown that the velocity of a solvated ion in free solution with a charge, *q* in an electrical field, *E* is given by Eqn 1- 1.

$$v_{ep} = \frac{Eq}{6\pi r_h \eta} \qquad 1\text{- }1$$

where v_{ep} is the electrophoretic velocity, q is the charge on the ion, r_h is the hydrodynamic radius of the solvated ion and η is the dynamic viscosity of the electrolyte.

The electrophoretic mobility (μ_{ep}) is defined in Eqn 1- 2; it conveniently compares the electromigrational velocities of analytes independent from variations to the electrical field strength [16].

$$\mu_{ep} = \frac{v_{ep}}{E} = \frac{q}{6\pi r_h \eta} \qquad 1\text{- }2$$

The time for a separation depends on the velocities of the analytes. Clearly the stronger the electrical field strength used, the greater are the electrophoretic velocities and the shorter is the time required for separation to occur.

For a detailed description on modes of capillary electrophoresis (CE), electrolytes, sample injection methods, detection methods, stacking, peak shape and resolution, the reader is referred to excellent works by Andrews [17], Baker [18], Bartle [19], Camilleri [20], Deyl and Svec [21], El Rassi [22], Foret [23], Frazier, Ames and Nursten [24] Grossman and Colburn [25], Heiger [26], Jandik and Bonn [16], Kuhn and Hoffstetter-Kuhn [27], Krull et al. [28], Landers [29, 30], Li [31], Lunn[32], Lunte and Radzik [33], Rathore and Guttman [34], Righetti [35], Shaw [36], Shintani and Polonský [37], Thibault and Honda [38],and Weinberger [39].

1.2. Electroosmotic Flow

In capillaries, the movement of analytes is not just the result of the force acting on ions in an applied electrical field; in fact neutral species are also moved by a flow of the bulk electrolyte called the electroosmotic flow (EOF). This is similar to logs being carried by a current of water. **Figure 1- 1** illustrates the movement of ions and of a neutral molecule carried by the EOF. The difference in speeds of the ions comes from their different charge to radius ratios (see Eqn 1- 1) and the speed of the neutral molecule is a result of the EOF only.

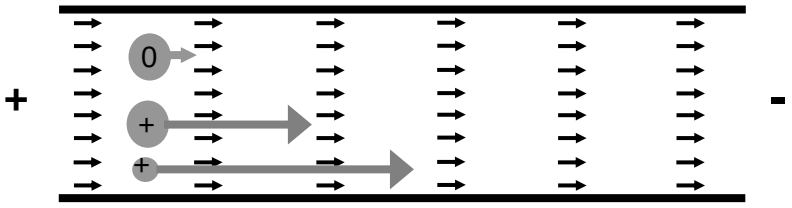

Figure 1- 1: Movement of charged and neutral species in a capillary during CE. Length of vector is a measure of relative speed.

Eqn 1- 3 shows that the observed velocity (v_{obs}) of an ion is the vector sum of its electrophoretic velocity and the electroosmotic velocity (v_{EOF}).

$$v_{obs} = v_{ep} + v_{EOF} \qquad 1\text{- }3$$

v_{EOF} can be simply measured by adding a neutral marker to the mixture of analytes and recording the time at which it is detected (t_{EOF}). As the marker travels more slowly than the ions, it is usually observed well after the ions as a symmetrical peak.

$$v_{EOF} = \frac{L_{\text{det}}}{t_{EOF}} \qquad 1\text{- }4$$

It follows that the electrophoretic velocity of an ion cannot be found directly by timing when it reaches the detector; instead the velocity of the electroosmotic flow must be subtracted from the observed velocity. Eqn 1- 5 shows that the electroosmotic mobility (μ_{EOF}) is defined similarly to μ_{ep}.

$$\mu_{EOF} = \frac{v_{EOF}}{E} \qquad 1\text{- }5$$

Rearranging Eqns 1- 2 and 1- 3, it is possible to derive Eqn 1- 6, an expression that enables practical measurement of electrophoretic mobilities to be made.

$$\mu_{ep_A} = \mu_{obs\,A} - \mu_{EOF} = \frac{v_{obs\,A} - v_{EOF}}{E} = \frac{L_{\det} L_{tot}}{V}\left(\frac{t_{EOF} - t_A}{t_{EOF} t_A}\right) \qquad 1\text{- }6$$

where the subscript A refers to the analyte of interest and t_A is its migration time.

The velocity of the electroosmotic flow (v_{EOF}) is given by Smoluchovski's equation (Eqn 1- 7**)**

$$v_{EOF} = -\frac{\varepsilon\zeta}{\eta} \bullet E \qquad 1\text{- }7$$

where ε is the electrical permittivity of the electrolyte and ζ is the zeta-potential (discussed in detail in Section 1.2.1 and Chapter 5.1). Substituting Eqn 1- 7 into Eqn 1- 5 results in Eqn 1- 8.

$$\mu_{EOF} = -\frac{\varepsilon\zeta}{\eta} \qquad 1\text{- }8$$

1.2.1 Origin of Electroosmotic flow

EOF arises as a result of a charged double-layer on the inner wall of the capillary which develops when an ionic solution is in contact with a charged surface. In the case of fused-silica capillaries, the ionised silanol groups on the wall have a negative charge. The charge on the capillary wall has an associated electrical field, which draws oppositely charged ions (counterions) towards it and drives similarly charged ions (co-ions) away (see **Figure 1- 2**). Hydronium ions, polar water molecules and counterions from the electrolyte are preferentially attracted and adsorbed onto the surface to form what is called the inner Helmholtz layer or Stern layer. This layer is relatively stable and organised.

The second layer, known as the outer Helmholtz layer, or diffuse layer, contains solvated cations and less organised dipolar water molecules. These two layers make up an electrical double-layer (EDL) usually with a thickness of a few angstroms to tens of nanometres [40, 41].

Electroneutrality does not exist within the EDL so that a potential gradient arises perpendicular to the surface [42]. When an electrical field is applied tangential to the capillary wall, the cations in the outer Helmholtz layer are attracted to the cathode.

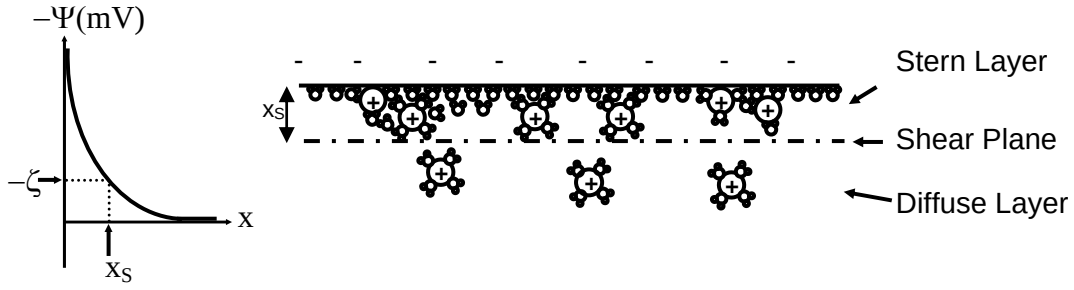

Figure 1- 2: The origins of electroosmotic flow -interactions of the wall charges with ions and molecules in the liquid phase.
Diagram adapted from Jandik and Bonn [43].

These cations in the EDL are interlocked within the water structure and drag the bulk electrolyte with them by means of viscous forces to generate an electroosmotic flow. Since the driving force for the EOF exists only within the thin EDL, the EOF has an almost flat profile in which most parts of the fluid travel at the same speed (see **Figure 1- 3**) [41]. This contributes to the excellent resolving power of capillary electrophoresis. In contrast, pressure-driven flows exhibit parabolic profiles in which fluid at the centre of the capillary travels considerably more quickly than at the sides.

Figure 1- 3: Flow profiles for pressure-driven and electrically driven flows.
Pressure-driven flow has a parabolic profile due to viscous forces between the walls and the liquid. EOF has an almost flat profile. Diagram adapted from Li [44].

The boundary between the inner Helmholtz layer and the outer Helmholtz layer in which counterions just begin to move is called the shear plane (see **Figure 1- 2**). The electrical potential at this plane is known as the zeta-potential, (ζ) [40, 45]. It is the zeta-potential of the surface in question that controls v_{EOF}. The size of ζ depends on the charge of the capillary wall and varies inversely with the concentration of counterions

and their valency. It is also strongly pH-dependent. In their comprehensive review of zeta-potentials in polymers and fused-silica, Kirby and Hasselbrink [40, 46] discussed the factors affecting ζ and noted the scarcity of experimental data on its variation with temperature.

1.3. Heating Effects in Electrophoresis

Resistive heating, known as Joule heating, is inevitable when a current passes through an electrolyte. The power (*P*) produced during electrophoresis is given by Eqn 1- 9.

$$P = GV^2 = \frac{\kappa A V^2}{L} \qquad 1\text{- }9$$

where *G* is the conductance of the electrolyte, V is the separation voltage, κ is the conductivity, *A* is the cross-sectional area and *L* is the length of the medium.

Joule heating produces adverse effects during CE including peak broadening [29, 47-55], changes to migration times [53, 56], instability of the baseline when using indirect detection [57], volume expansion and loss of sample due to initial self-heating [58, 59], boiling or superheating of the sample zone and/or electrolyte [29, 55, 60, 61] and decomposition of thermally labile compounds [62-64].

Even though Joule heating is always problematic, in some cases resolution can be improved at higher temperatures [29]. However, in practice it would be better to elevate the temperature set by thermostat and limit the Joule heating by using efficient cooling or a lower separation voltage. These measures are in the interests of method repeatability and ruggedness. Recently Giordano et al. [65] exploited Joule heating in the sample zone in the presence of a fluorescent dynamic labelling reagent to achieve an order-of-magnitude increase in the fluorescence detection sensitivity of their proteins. Even more recently, in a somewhat different experimental set-up employing isoelectric focussing, Kates and Ren [66] used Joule heating in divergent microchannels to establish a pH gradient in chips.

As an analytical technique, electrophoresis started in free solution as opposed to gels or capillaries. Temperature differences in the liquid led to the problem of band broadening due to convection [67]. A partial solution to the problem was the use of slab gels [68] or paper impregnated with the electrolyte solution [69-71] but properties of

these media and safety considerations restricted the size of the electrical field that could be used and led to long separation times.

In 1967, Hjerten recognised that thermal effects due to currents could be reduced by carrying out electrophoresis in narrow diameter tubes (capillaries) [68]. It was also found that the favourable physical properties of materials from which the capillaries were made allowed very high voltages to be used, enabling faster electrophoretic separations to be performed [72].

Eqn 1- 9 can be modified to produce Eqn 1- 10, which shows the power generated during CE in capillaries with an internal diameter (d_i).

$$P = \frac{\pi \kappa d_i^2 V^2}{4 L_{tot}} \qquad 1\text{- }10$$

Clearly, the rate of heat generation can be minimised by lowering the conductivity of the electrolyte and the voltage used, by decreasing the internal diameter of the capillary and increasing the length of the capillary. Unfortunately, these measures may not be in the interests of separation efficiency (lowering V) or detection sensitivity (decreasing d_i) or separation times (increasing L_{tot}). Symmetrical peak shapes occur when the mobility of analytes match the mobility of the co-ion in the electrolyte, so a low conductivity electrolyte may not be appropriate [73, 74]. Reducing the internal diameter of the capillary obviously decreases the detection pathlength, which for most detection methods is associated with an increase in detection limits.

Mori et al. [75] found that the use of zwitterionic surfactants was effective for lowering the conductivity of high ionic strength electrolytes, enabling bromide and nitrate to be determined in untreated seawater. It was thought that the reduction in conductivity was largely the result of increased viscosity and changes to the permittivity of the electrolyte or the partition of the salt into the neutral micelles in the electrolyte.

1.3.1 Quantifying Temperature Differences

In order to be able to predict the effects of Joule heating quantitatively, a detailed knowledge of the electrolyte temperature profile and the way that heat is dissipated through the capillary walls is needed.

The description of temperature profiles in electrokinetic separations started in isotachophoresis with Konstantinov and Oshurkova [76] and was quickly taken up in

capillary electrophoresis. As early as 1967, Hjerten [48] recognised that a parabolic radial temperature profile existed between the centre of the capillary and its inner wall.

Knox [52] came to the same conclusion and modelled the dissipation of heat from capillaries and predicted the temperature profiles that exist during a CE separation. He derived equations for the temperature difference across the electrolyte (ΔT_{Radial}, Eqn 1- 11) and for the temperature difference across the capillary wall (ΔT_{Wall}, Eqn 1- 12) based on the power generated per unit volume (Q)

$$\Delta T_{Radial} = \frac{Q d_i^{\,2}}{16\lambda} = \frac{E^2 \kappa d_i^{\,2}}{16\lambda} \qquad 1\text{- }11$$

$$\Delta T_{Across\ Walll} = \frac{Q d_i^{\,2}}{8\lambda_{Wall}} \ln\left(\frac{d_o}{d_i}\right) \qquad 1\text{- }12$$

where λ_{Wall} is the average thermal conductivity of wall material, d_o is the external diameter of the capillary and the other symbols have their usual meaning.

Figure 1- 4 shows how ΔT_{Radial} and $\Delta T_{Across\ Wall}$ are defined. In the case of a fused-silica capillary, Eqn 1- 12 needs to be applied twice (once for the fused-silica wall ΔT_{FS} and once for the poly(imide) coating ΔT_{PI}). Grushka, McCormick, and Kirkland [54] did precisely this and extended the equations of Knox to take into account the contribution of the static layer of coolant surrounding the capillary.

Eqn 1- 13 gives an expression for the temperature just inside the capillary wall T_{Wall} at the edge of the migrating electrolyte (see **Figure 1- 4**).

$$T_{Wall} = T_{Set} + \frac{Q d_i^{\,2}}{8}\left[\frac{1}{\lambda_{FS}} \ln\left(\frac{d_{FS}}{d_i}\right) + \frac{1}{\lambda_{PI}} \ln\left(\frac{d_o}{d_{FS}}\right) + \frac{2}{d_o h}\right] \qquad 1\text{- }13$$

where T_{Set} is the ambient temperature of the coolant (usually air or a liquid) surrounding the capillary, λ_{FS} is the thermal conductivity of fused-silica, λ_{PI} is the thermal conductivity of the poly(imide), d_{FS} is the diameter of the fused-silica and h is the heat transfer coefficient for the capillary surface in the particular instrumental set-up.

Knox [52] pointed out for air-cooled capillaries that the temperature gradient is greatest in the thin layer of air surrounding the capillary (see **Figure 1- 5**) so that the last term in Eqn 1- 13 is the most significant. This is due to the relative values of the thermal conductivities of air and the capillary materials (see **Table 1- 1**).

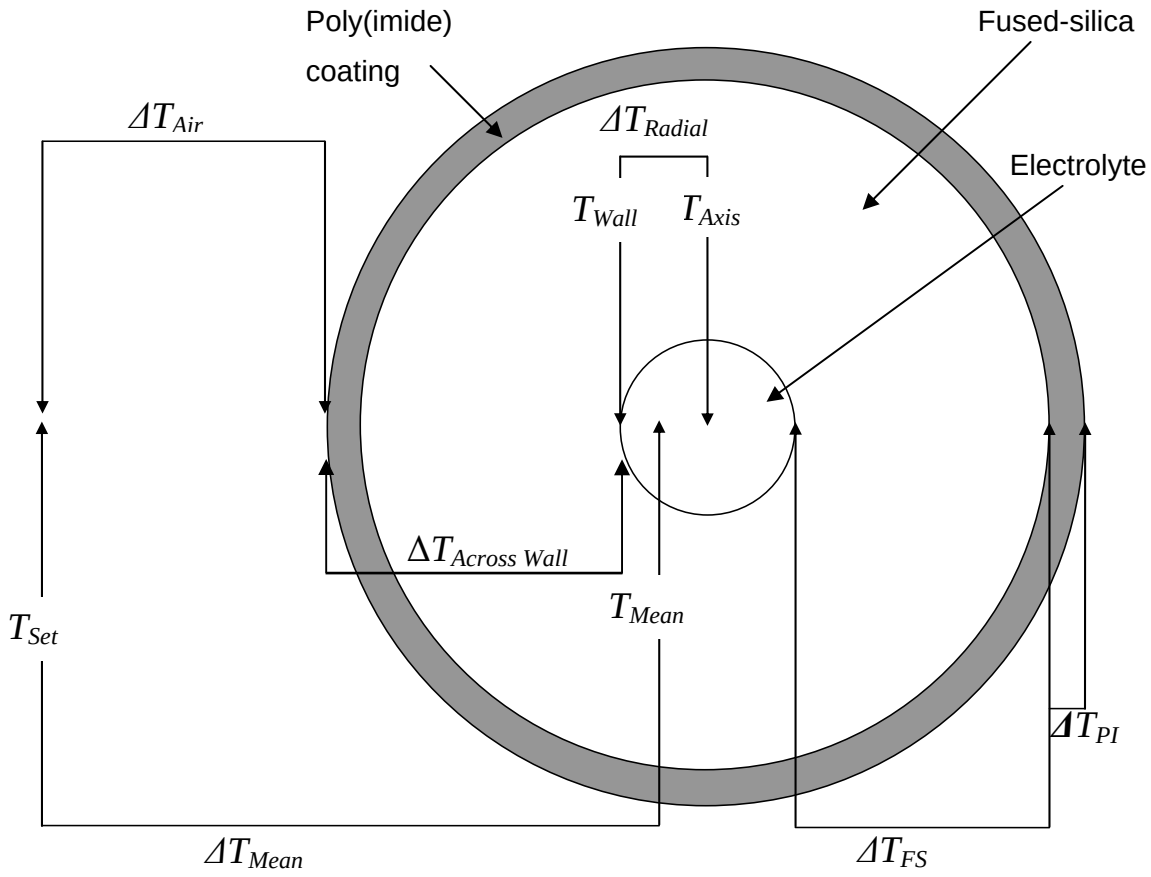

Figure 1- 4: Schematic diagram of a radial cross section of an air cooled poly(imide) coated fused-silica capillary showing the locations at which the temperature determinations are made.

Table 1- 1: Thermal conductivity of materials at 25 ºC

Material	λ ($Wm^{-1}K^{-1}$)	Reference
Water	0.605	[77]
Fused-silica	1.40	[16]
Poly(imide)	0.155	[78]
Air	0.0266	[79]

Later, Grushka et al. [54] used a parabolic temperature profile in their study of Joule heating effects on efficiency and derived Eqn 1- 14 to describe the variation of temperature with distance from the central axis of the capillary.

$$T(r) = T_{Wall} + \frac{Q r_i^2}{4\lambda}\left(1 - \frac{r^2}{r_i^2}\right) \qquad 1\text{- }14$$

where *T(r)* is the temperature of the electrolyte at a distance *r* from the central axis, T_{Wall} is the temperature at the inner wall, *Q* is the heat generated per unit volume, r_i is the internal radius of the capillary and λ is the thermal conductivity of the electrolyte. In the same year Jones and Grushka [80] derived an expression for the radial temperature profile of the electrolyte that took into account radial differences in electrical conductivity. They concluded that Eqn 1- 14 was valid for radial temperature differences of up to 1.5 ºC but that for higher power levels, it tended to slightly underestimate the axial temperature. The parabolic nature of the electrolyte's radial temperature profile was confirmed experimentally by Liu, Davis and Morris [81] using Raman microthermometry.

Early in 2004, Tang et al. [82] published their study on the effects of Joule heating on electroosmotic flow and mass transport during CE. Unlike previous studies, which yielded averaged data for temperature, this study used finite volume-based computation fluid dynamics techniques to provide radial, axial and temporal temperature information. The model predicted a parabolic radial temperature profile along almost the whole length of the capillary but showed that the maximum axial temperature is typically reached after a distance of about 10 capillary radii. These findings were largely independent of the cooling efficiency [82].

Figure 1- 5 was calculated using Knox's equations for heat dissipation and assumed that the stagnant air layer surrounding the capillary acted in a similar way to the poly(imide) coating in that the temperature decreased in a logarithmic fashion until the coolant temperature reached the ambient temperature. The temperature at the central axis of the capillary (T_{Axis} see **Figure 1- 4**) is the sum of the temperature changes across the electrolyte (ΔT_{Radial}), the fused-silica (ΔT_{FS}), the poly(imide) layer (ΔT_{PI}) and the air layer surrounding the capillary (ΔT_{Air}). Using the conditions from **Figure 1- 5** and the data from **Table 1- 1**, yields the following results.

$$\Delta T_{Radial} = \frac{Qd_i^{\,2}}{16\lambda} = \frac{2.325x10^{8} W m^{-3} x 74.0x10^{-6} m)^2}{16x0.605 W m^{-1} K^{-1}} = 0.132 K$$

$$\Delta T_{FS} = \frac{Qd_i^{\,2}}{8\lambda_{FS}} \ln\left(\frac{d_{FS}}{d_i}\right) = \frac{2.325x10^{8} W m^{-3} x 74.0x10^{-6} m)^2}{8x1.40 W m^{-1} K^{-1}} x \ln\left(\frac{321.0x10^{-6} m}{74.0x10^{-6} m}\right) = 0.166 K$$

$$\Delta T_{PI} = \frac{Qd_i^{\,2}}{8\lambda_{PI}} \ln\left(\frac{d_{PI}}{d_{FS}}\right) = \frac{2.325x10^{8} W m^{-3} x 74.0x10^{-6} m)^2}{8x0.155 W m^{-1} K^{-1}} x \ln\left(\frac{362.8x10^{-6} m}{321.0x10^{-6} m}\right) = 0.125 K$$

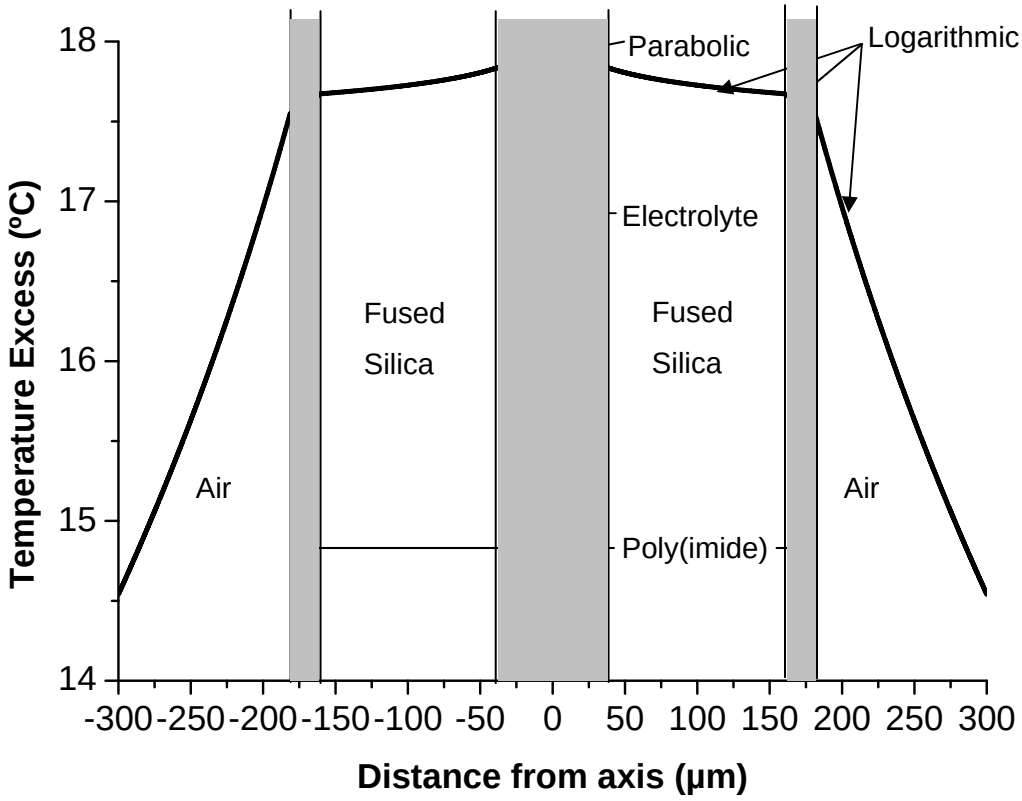

Figure 1- 5: Calculated temperature profile for a passively-cooled poly(imide) coated fused-silica capillary.
Conditions: d_i = 74.0 µm, d_{FS} = 321.0 µm, d_{PI} = 362.8 µm, P/L = 1.00 Wm^{-1} equivalent to Q = 2.325 x 10^8 Wm^{-3}, h = 50.0 $Wm^{-2}K^{-1}$.
Diagram adapted from Knox [52]

$$\Delta T_{Air} = \frac{Q d_i^{\,2}}{4 d_{PI} h} = \frac{2.325\,x\,10^{8}\,W m^{-3} x\,(74.0\,x\,10^{-6} m)^2}{4\,x\,362.8\,x\,10^{-6} m\,x\,50 W m^{-2} K^{-1}} = 17.5 K$$

$$T_{Axis} = T_{Set} + \Delta T_{Radial} + \Delta T_{FS} + \Delta T_{PI} + \Delta T_{Air} \qquad 1\text{- }15$$

$$\therefore T_{Axis} = 25.0\,^{o}C + 0.132\,^{o}C + 0.166\,^{o}C + 0.125\,^{o}C + 17.5\,^{o}C = 43.0\,^{o}C$$

It follows that the maximum rise in temperature of the electrolyte was 43.0 ºC – 25.0 ºC = 18.0ºC

As stated above and shown in **Figure 1- 5,** a parabolic temperature profile exists within the electrolyte. A complete expression for the temperature of the electrolyte at a distance *r* from the central axis of the capillary (*T(r)*) can be derived by combining Eqns 1- 11, 1- 12 and 1- 14. Eqn 1- 16 shows that *T(r)* depends only on the physical

parameters of the capillary, the cooling system, the conductivity of the electrolyte and the voltage used.

$$T(r) = T_{Set} + \frac{Qd_i^{\,2}}{8}\left(\frac{1}{\lambda_{FS}}\ln\left(\frac{d_{FS}}{d_i}\right) + \frac{1}{\lambda_{PI}}\ln\left(\frac{d_{PI}}{d_{FS}}\right) + \frac{2}{d_{PI}h} + \frac{1}{2\lambda}\left(1 - \frac{r^2}{r_i^{\,2}}\right)\right)$$

$$= T_{Set} + \frac{\kappa V^2 d_i^{\,2}}{8L^2}\left(\frac{1}{\lambda_{FS}}\ln\left(\frac{d_{FS}}{d_i}\right) + \frac{1}{\lambda_{PI}}\ln\left(\frac{d_{PI}}{d_{FS}}\right) + \frac{2}{d_{PI}h} + \frac{1}{2\lambda}\left(1 - \frac{r^2}{r_i^{\,2}}\right)\right) \qquad 1\text{- }16$$

If as Knox concluded and has been demonstrated above, the temperature change across the coolant is much larger than within the capillary, an accurate knowledge of ΔT_{Air} or $\Delta T_{Coolant}$ (the temperature difference between the outside of the capillary and the ambient temperature of the coolant) is critical for determining the temperature of the electrolyte itself.

Eqn 1- 16 illustrates the influence of *h* on the overall rise in temperature of the electrolyte. The smaller the value of *h*, the greater will be the value of *T(r)*. The following sections illustrate how *h* can be determined from experimental results or from empirical equations for passively-cooled and actively-cooled capillaries.

1.3.2 The heat transfer coefficient (h)

For fused-silica capillaries the heat transfer coefficient (*h*) indicates the effectiveness of the heat removal from the air film on the capillary poly(imide) coating to the surroundings. Newton's Law of Cooling (Eqn 1- 17) shows the relationship between the rate at which heat is removed and the temperature difference across the air film [61, 83].

$$P = \frac{\lambda_{Air} A \Delta T_{Air}}{x} = hA\Delta T_{Air} \qquad 1\text{- }17$$

where *P* is the rate at which heat is generated in the electrolyte and conducted through the outer wall, λ_{Air} is the thermal conductivity of air, *A* is the outside curved surface area of the capillary and *x* is the thickness of the static air layer.

1.3.2.1 Calculating h from experimental results

Eqn 1- 17 can be rearranged to give Eqn 1- 18, which is an expression for *h* that depends on the power per unit length (*P*/*L*) or the power per unit volume (*Q*).

$$h = \frac{P}{A\Delta T_{Air}} = \frac{P}{\pi d_o L \Delta T_{Air}} = \frac{1}{\pi d_o \Delta T_{Air}} \bullet \frac{P}{L} = \frac{Q d_i^{\,2}}{4 d_o \Delta T_{Air}} \qquad 1\text{- }18$$

h can be calculated from experimental data using Eqn 1- 18 or Eqn 1- 19 if ΔT_{Air} or $\Delta T_{Coolant}$ (the temperature difference between the outside of the capillary and the ambient temperature of the coolant) is known [54, 55].

$$h = \frac{Q d_i^{\,2}}{4 d_o \Delta T_{Coolant}} \qquad 1\text{- }19$$

For passive cooling in air, a value of h can be calculated using the experimental data of Knox and McCormack [53]. In an experiment using a fused-silica capillary with d_i = 5.00 x 10^{-5} m, d_{FS} = 3.35x10^{-4} m, d_{PI} = 3.75x10^{-4} m, and Q = 1.54 x 10^{9} Wm^{-3}, ΔT_{Mean} was estimated to be 29.6 ºC. Subtracting ΔT_{FS}, ΔT_{PI} and $^1/_2\Delta T_{Radial}$ (discussed in Chapter 3.1) yields $\Delta T_{Air} \approx$28.3 ºC

Substituting into Eqn 1- 19 gives:

$$h = \frac{Q d_i^{\,2}}{4 d_o \Delta T_{Coolant}} = \frac{1.54 x 10^{9} W m^{-3} x (5.00 x 10^{-5} m)^2}{4 \; x \; 3.75 x 10^{-4} m \; x \; 28.3 K} = 90.6 \, W m^{-2} K^{-1}$$

Comparison with reported values from other researchers (see **Table 1- 2**) shows that this value is among the largest of the reported values. Knox and McCormack [53] suggested that their apparatus may have been subjected to small air currents.

Table 1- 2: Heat transfer coefficients for passively-cooled capillaries reported in the literature – Porras et al.[1] [49], Knox and McCormack[2] [53], Petersen et al.[3] [55] and Nishikawa and Kambara[4] [84]

Cooling Method	Length of Capillary (cm)	Internal Diameter (µm)	External Diameter (µm)	h (Wm^{-2}K^{-1})
Passive[1]	34	50	375	130*
Passive[2]	100	50	375	90.6
Passive[3]	30	50	375	7*
Passive[4]	50	100	200	84
Passive[4]	50	100	375	56

*The extreme values come from reference books rather than from experimental results.

1.3.2.2 *Calculating h for passively-cooled capillaries using empirical equations*

h may also be calculated using empirical equations such as Eqn 1- 20, developed by mechanical engineers for the cooling of pipes [85]. Passive cooling refers to cooling that occurs when the capillary is surrounded by still air.

$$h = \frac{N_u \lambda_{Coolant}}{d_o} \qquad 1\text{- }20$$

where N_u is called the Nusselts number, $\lambda_{Coolant}$ is the thermal conductivity of the coolant and d_o is the outer diameter of the capillary.

By equating Eqn 1- 19 and Eqn 1- 20, an expression for the Nusselts number can be obtained, which shows that it is inversely proportional to the change in temperature of the coolant. Eqn 1- 21 shows that the larger the value of N_u, the greater will be the cooling efficiency.

$$\frac{Q}{4d_o \Delta T_{Coolant}} = \frac{Pd_i^{\,2}}{4\pi r_i^{\,2} L d_o \Delta T_{Coolant}} = \frac{P}{\pi L d_o \Delta T_{Coolant}} = \frac{EI}{\pi d_o \Delta T_{Coolant}} = \frac{N_u \lambda_{Coolant}}{d_o}$$

$$\therefore N_u = \frac{EI}{\pi d_o \Delta T_{Coolant}} \bullet \frac{d_o}{\lambda_{Coolant}} = \frac{EI}{\pi \lambda_{Coolant} \Delta T_{Coolant}} \qquad 1\text{- }21$$

For passive cooling, calculation of the Nusselts number is somewhat complicated and requires a knowledge of the temperature of the external wall of the capillary. The calculations have been well described by Knox and McCormack [53] and are shown in detail in **Appendix 2**. A typical value for the Nusselts number for passive cooling in air is N_u = 0.753. Substitution into Eqn 1- 9 and using the thermal conductivity of air at the film temperature (a temperature halfway between the ambient temperature and the external wall temperature) yields h_s = 53.9 $Wm^{-2}K^{-1}$.

$$h_s = \frac{N_u \lambda_{Coolant}}{d_o} = \frac{0.753\, x\, 0.02684\, Wm^{-1}K^{-1}}{3.75x10^{-4}\, m} = 53.9\ Wm^{-2}K^{-1}$$

This value agrees very well with the value of Nishikawa and Kambara [84] who used miniature thermocouples to measure the external temperature of capillaries but is about 61 % of the value for h_s previously calculated for Knox and McCormack's experimental

data [53]. The discrepancy corroborates their hypothesis that tiny air currents were present.

To summarise for passively-cooled capillaries, the heat transfer coefficient is typically between 50 and 100 $Wm^{-2}K^{-1}$. Capillaries with smaller outer diameters tend to have higher values of h, however it should be made clear that when comparing the temperature increases for capillaries with different external diameters, that the product hd_o determines the overall temperature rise. Due to their larger surface areas, capillaries with larger external diameters tend to transfer heat more efficiently resulting in smaller rises in temperature. Prediction of h for passively-cooled capillaries from first principles is not possible as it relies on knowing $\Delta T_{Coolant}$ (the difference between the ambient temperature and the temperature of the external wall of the capillary).

1.3.2.3 *Calculating h for actively-cooled capillaries using empirical equations*

For active-cooling, the size of the heat transfer coefficient and the Nusselts number depend on the speed of the coolant flow ($v_{Coolant}$) and the kinematic viscosity of the coolant (ν) [86, 87]. When a stream of coolant is directed at a cylinder, the way in which the boundary layer develops determines the heat transfer characteristics. The Reynolds number (R_e) gives a measure of whether the flow is laminar or turbulent. The higher the value of R_e, the greater is the turbulence that exists at the trailing edge of the cylinder and the more efficient is the cooling.

$$R_e = \frac{v_{Coolant} d_o}{\nu} \qquad \text{1- 22}$$

In commercial CE instruments with Peltier fan-forced cooling systems, typical air speeds are about 10 ms^{-1}, so for air with ambient temperature 25.0 ºC and film temperature 25.8 ºC, the Reynolds number based on an outer capillary diameter of 375 µm is:

$$R_e = \frac{v_{Coolant} d_o}{\nu} = \frac{10 ms^{-1} x\, 3.75x10^{-4} m}{1.56x10^{-5} m^2 s^{-1}} \approx 240$$

The Nusselts number is calculated from the Reynolds number using Eqn 1- 23,

$$N_u = C(R_e)^n \qquad \text{1- 23}$$

where C and n are constants whose values depend on the size of the Reynolds number and the Prandtl number in the case of liquid coolants [85].

Table 1- 3: Constants for use with Eqn 1- 23 [85]

R_e	*C* for gases	*C* for liquids	*n*
0.4-4	0.891	$0.989Pr^{1/3}$	0.330
4-40	0.821	$0.911Pr^{1/3}$	0.385
40-4 $x10^3$	0.615	$0.683Pr^{1/3}$	0.466
4 $x10^3$-4 $x10^4$	0.174	$0.193Pr^{1/3}$	0.618
4 $x10^4$-4 $x10^5$	0.0239	$0.0266Pr^{1/3}$	0.805

It follows that for the air cooled capillary with $R_e \approx 239$ described above,

$$N_u = C(R_e)^n = 0.615\,x\,239^{0.466} = 7.91$$

$$h = \frac{N_u \lambda_{Coolant}}{d_o} = \frac{7.91x\,0.02616\,Wm^{-1}K^{-1}}{3.75x10^{-4}m} = 552\,Wm^{-2}K^{-1}$$

Table 1- 4 illustrates the significant variations in values of *h* reported in the literature; it would appear that a variety of methods has been used to calculate *h*. A straightforward approach to determining *h,* which does not require knowledge of the coolant velocity, is demonstrated in Section 4.6.2 using Eqn 4- 13 (previously 1- 18) and Eqn 4- 14.

1.3.3 Investigations of Joule heating and cooling efficiency

A number of research groups have investigated Joule heating and cooling efficiency in CE since the pioneering work of Knox and McCormack in 1988 [86]. The following section describes the contributions of each group.

In 1989, Nelson et al. [62] investigated solid-state cooling using a Peltier cooled alumina block containing grooves for the capillary. They found that cooling was improved by using ethylene glycol to make thermal contact between the capillary wall and the alumina.

Table 1- 4: Heat transfer coefficients for actively-cooled capillaries reported in the literature: Nishikawa and Kambara[1] [84], Petersen et al.[2] [55], Xuan and Li[3] [88] Bello and Righetti[4] [89], Vinther and Soeberg[5] [61] and Nelson et al.[6] [62]

Cooling Method	Length of Capillary (cm)	Internal Diameter (μm)	External Diameter (μm)	Velocity of Cooling fluid (ms^{-1})	h ($Wm^{-2}K^{-1}$)
Active Air[1]	50	100	375	0.1	81
Active Air[1]	50	100	375	2.6	285
Active Air[3]	30	50	360	?	4 000*
Active Air[4]	?	75	375	?	240
Active Air[5]	100	50	192	?	369
Active Liquid[2]	30	50	375	?	760
Active Liquid[2]	100	50	375	?	940
Active Liquid[4]	?	75	375	?	1 176
Active Liquid[5]	100	75	375	?	501
Solid State[6]	?	100	357	Not applicable	2 600

*Palonen [87] suggested that unexpectedly large values of h have appeared in the literature when authors have consulted engineering references and not considered whether the values are appropriate for the experimental conditions. Working backwards using Eqns 1- 20, 1- 22 and 1- 23 reveals for h = 4000 $Wm^{-2}K^{-1}$, $v_{Air} \approx 496$ ms^{-1}! (This is about $1^1/_2$ times the speed of sound.)

Gobie and Ivory [60] explained the autothermal effect in 1990. This is the positive feedback that occurs between conductivity and temperature at a constant operating voltage. When the voltage is first applied, Joule heating produces an increase in temperature which in turn increases the electrical conductivity so that the temperature rises further until a steady state is achieved in which the rate at which heat is generated is exactly balanced by the rate at which heat is conducted to the surroundings. The time taken for the steady state to be achieved (referred to as the transient time) decreases with increasing cooling efficiency. If the cooling efficiency is inadequate, the steady state can occur at a temperature that exceeds the boiling point of the electrolyte. This can lead to superheating or boiling of the electrolyte.

Gobie and Ivory [60] derived Eqn 1- 24, an expression for the autothermal parameter (k^*) a dimensionless constant which is the fractional increase in electrical conductivity associated with a characteristic temperature rise (ΔT_{ref}).

$$k^* = \sqrt{\gamma \Delta T_{ref}} \qquad 1\text{- }24$$

ΔT_{ref} is an increase in temperature equivalent to $4\Delta T_{Radial}$ (see Eqn 1- 11) assuming that the conductivity of the electrolyte is constant.

$$\Delta T_{ref} = \frac{\kappa_0 E^2 r_i^{\,2}}{\lambda} = \frac{Q d_i^{\,2}}{4\lambda} = 4\Delta T_{Radial} \qquad 1\text{- }25$$

Eqn 1- 26 defines γ as the fractional increase in electrical conductivity per unit temperature (equivalent to the fractional increase in electrical conductance with temperature) which has a value of about 0.02 K^{-1} for most electrolytes [90].

$$\gamma = \frac{\kappa - \kappa_0}{\kappa_0 \Delta T} = \frac{G - G_0}{G_0 \Delta T} \qquad 1\text{- }26$$

where κ and G are the conductivity and conductance at an elevated temperature (T) and κ_0 and G_0 are the conductivity and conductance at a reference temperature (T_0) and $\Delta T = T - T_0$.

Gobie and Ivory [60] found that at a critical value of the autothermal parameter k^*', autothermal runaway would occur. Under such conditions, thermal equilibrium is never reached but the electrolyte temperature increases until vapour bubbles form and the current is cut off. The onset of autothermal runaway is controlled by the overall Biot number Bi_{OA} which compares the rate of heat conduction through the wall with the rate at which heat is removed by the coolant.

$$Bi_{OA} = \frac{h_{OA} r_i}{\lambda} \qquad 1\text{- }27$$

where h_{OA} is the overall heat transfer coefficient defined in Eqn 1- 28, r_i is the internal radius of the capillary and λ is the thermal conductivity of the electrolyte. The overall heat transfer coefficient is a composite value that takes into account conduction of heat energy through each of the layers.

$$h_{OA} = \frac{1}{r_i}\left(\frac{1}{\frac{\ln\left(\frac{d_{FS}}{d_i}\right)}{\lambda_{FS}} + \frac{\ln\left(\frac{d_o}{d_{FS}}\right)}{\lambda_{PI}} + \frac{2}{d_o h}} \right) \qquad 1\text{- }28$$

For example, for a passively-cooled fused-silica capillary with d_i = 75 µm, d_{FS} = 335 µm and d_o = 375 µm and a heat transfer coefficient of 50 $Wm^{-2}K^{-1}$, h_{OA} = 246 $Wm^{-2}K^{-1}$. Not surprisingly, the overall heat transfer coefficient increases with the efficiency of the cooling system. For the same capillary with effective active-cooling h = 500 $Wm^{-2}K^{-1}$, the corresponding value of h_{OA} is 2140 $Wm^{-2}K^{-1}$. The corresponding Biot numbers for the passive and active-cooling are 0.152 and 1.33, respectively.

Gobie and Ivory expressed the predicted temperature rise in a rather complicated equation involving Bessel functions which took into account the radial temperature gradient in the electrolyte. In 1992, Bello and Righetti [89] simplified the model and derived an equation for the temperature rise that involved the reference temperature, the Biot number and the autothermal parameter

$$T_{Mean} = T_{Set} + \frac{\Delta T_{ref}}{2Bi'_{OA} - (k^*)^2} \qquad 1\text{- }29$$

where T_{Mean} is the mean temperature of the electrolyte when a steady state is achieved and $Bi'_{OA}$is the average of the Biot numbers at 25 kV and at 30 kV. Eqn 1- 29 shows that the higher the Biot number, the lower will be the final temperature of the electrolyte. As k^{*2} approaches $2Bi'_{OA}$ the electrolyte is more likely to boil or superheat, which may not necessarily involve autothermal runaway. Autothermal runaway occurs when the denominator equals 0. It follows that Eqn 1- 30 can be used to predict the critical value of the autothermal parameter (k*')

$$k^{*'} = \sqrt{2Bi'_{OA}} \qquad 1\text{- }30$$

Gobie and Ivory had previously found that for passive cooling $k^{*'}$ was approximately equal to the square root of the Biot number [60]. This apparent discrepancy appears to have been due to their use of a rather large value for the temperature coefficient of electrical conductivity (γ = 0.045 $^oC^{-1}$) that was slightly more than double the accepted value.

Bello and Righetti [89] also modelled unsteady heat transfer in CE. They found that the transient time (the time taken for the temperature to stabilise) varied according to whether the instrument was current-stabilised resulting in the shortest transient time, power-stabilised or voltage-stabilised yielding the longest transient time. They did not

calculate values of *h* from their own experimental work but used information supplied by Beckman Instruments.

Nishikawa and Kambara [84] used thermocouples to measure the external temperatures of capillaries with the same internal diameter but different external diameters. They also investigated the effect of changing the air velocity for actively-cooled capillaries. Values of *h* were calculated from their temperature measurements and were corroborated using empirical equations developed by Fujii et al. [91] for passive cooling and by Hilpert for active-cooling [85]. There was excellent agreement between their measurements and predictions, except at high electrical field strengths where autothermal runaway was observed. As expected from an examination of Eqn 1- 20, their experimentally-determined values of *h* were inversely proportional to the external diameter of the capillary and increased with the velocity of the air flow used for active-cooling.

Petersen et al. [55] investigated the effect of Joule heating on efficiency and performance for microchip-based and capillary based electrophoretic separation systems and found that the cooling efficiency in glass chips that employed passive cooling was comparable to that of liquid cooled fused-silica capillaries. Their values of *h* were calculated from their experimental data in which temperature measurement was based on variations in conductivity.

1.4. Joule Heating and Separation Efficiency

Giddings [92] introduced the concept of the height of a theoretical plate (*H*) into CE. The width of a Gaussian peak can be characterised by its standard deviation (σ), the width at the baseline is approximately 4σ [93]. The peak variance (σ^2) depends on the diffusion coefficient (*D*) and the time (*t*) for which the analyte has migrated. The relationship (Eqn 1- 31) is known as the Einstein Equation [94].

$$\sigma^2 = 2Dt \qquad 1\text{- }31$$

The height of a theoretical plate is equal to the rate of change of variance with length along the capillary and can be found by differentiating Eqn 1- 31 [94]

$$H = \frac{d\sigma^2}{dL} = 2D\frac{dt}{dL} = 2D \div \frac{dL}{dt} = \frac{2D}{v_{obs}} \qquad 1\text{- }32$$

Jorgenson and Lukacs [72] showed that when sample dispersion is only the result of longitudinal diffusion, then the higher the voltage, the greater would be the separation efficiency. The maximum possible number of theoretical plates (*N*) that can be achieved in CE is given by Eqn 1- 33.

$$N = \frac{L_{\text{det}}}{H} = \frac{L_{\text{det}} v_{obs}}{2D} = \frac{L_{\text{det}} \mu_{obs} E}{2D} = \frac{L_{\text{det}} \mu_{obs} V}{2D L_{tot}} \approx \frac{\mu_{obs} V}{2D} \qquad 1\text{- }33$$

In practice, *N* is calculated using Eqn 1- 34 by measuring the migration time for an analyte (t_A) and the width of its peak at half height, $w_{1/2}$ [94].

$$N = \frac{5.55 t_{(A)}^{\,2}}{w_{1/2}} \qquad 1\text{- }34$$

1.4.1 The Effect of Electrolyte Temperature on Separation Efficiency

Knox and McCormack [53] modelled the temperature-dependence of *D* and viscosity in their prediction of the number of theoretical plates and deduced that temperature increases as a result of Joule heating would have a serious detrimental effect on *N*. They calculated that a 35 ºC increase in the temperature of the electrolyte would result in a 50 % decrease in *N*.

$$N = \frac{\mu_{obs} V 6\pi\eta r_h L_{\text{det}}}{2kTL_{tot}} = \frac{\mu_{obs} V 6\pi r_h L_{\text{det}} \left(2.761 x 10^{-3} e^{\left(\frac{1713}{T}\right)} \right)}{2kTL_{tot}} \qquad 1\text{- }35$$

where μ_{obs} is the observed electrophoretic mobility, η is the viscosity, L_{det} is the length to the detector, *T* is the absolute temperature, *k* is Boltzmann's constant and L_{tot} is the total length of the capillary. Petersen et al. [55] refined Eqn 1- 35 by taking into account the temperature-dependence of the observed electrophoretic mobility (μ_{obs}). Eqn 1- 36 combines Eqns 1- 2, 1- 6 and 1- 8 to give an expression for μ_{obs}.

$$\mu_{obs} = \mu_{ep} + \mu_{EOF} = \frac{q}{6\pi\eta r_h} + \frac{\varepsilon\zeta}{\eta} = \frac{1}{\eta}\left(\frac{q}{6\pi r_h} + \varepsilon\zeta \right) \qquad 1\text{- }36$$

Substituting Eqn 1- 36 into Eqn 1- 35 gives Eqn 1- 37, an expression for the number of theoretical plates that takes into account the dependence of μ_{obs} on viscosity [55].

$$N = \frac{1}{\eta}\left(\frac{q}{6\pi r_h} + \varepsilon\zeta \right) \frac{V 6\pi\eta r_h L_{\text{det}}}{2kTL_{tot}} = \frac{3\pi V r_h L_{\text{det}}}{kTL_{tot}} \left(\frac{q}{6\pi r_h} + \varepsilon\zeta \right) \qquad 1\text{- }37$$

Petersen et al. [55] deduced that *N* would be independent of viscosity. They asserted that in accordance with previous literature reports, the product $\varepsilon\zeta$ is independent of temperature [48, 53, 55, 95, 96] and they deduced that *N* was inversely proportional to the absolute temperature. They concluded that the influence of longitudinal diffusion from the increase in temperature of the electrolyte would be much less significant than suggested previously by Knox and McCormack [53]. **Figure 1- 6** compares the variation in the relative number of theoretical plates using the equation of Knox and McCormack [53] (which overlooked the influence of η on μ_{obs}) with that of Petersen et al. [55] Eqn (1- 37).

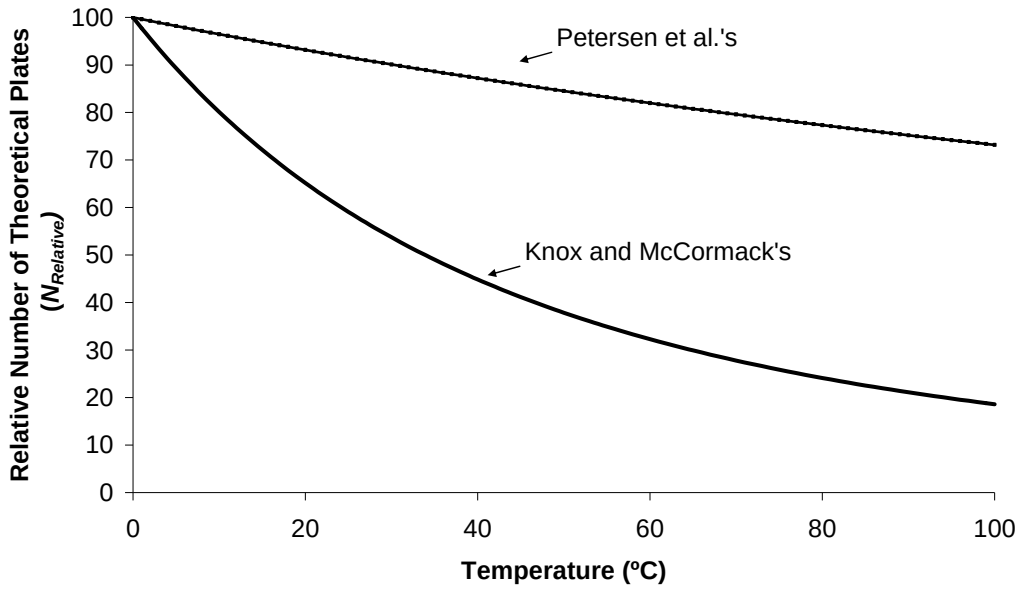

Figure 1- 6: Variation in the relative number of theoretical plates with temperature based on Eqn 1- 35 (lower curve) and Eqn 1- 37 (upper curve).
Diagram adapted from Petersen et al. [55].

For example, if the temperature of the electrolyte uniformly increases from 25 ºC to 35 ºC, *N* would decrease by about 17 % if μ_{obs} were constant but by less than 3.3 % if its dependence on η is taken into account. Ignoring changes to the product $\varepsilon\zeta$ with temperature, Eqn 1- 37 predicts that the number of theoretical plates decreases by about 0.3 % for each degree rise in electrolyte temperature over the temperature range 0 ºC to 100 ºC. If, as illustrated in Chapter 5, $\varepsilon\zeta$ decreases by 0.07 % per ºC, *N* would still be expected to decrease by less than 0.4 % per ºC.

It would appear that problems of peak broadening cannot be attributed to a rise in temperature of the electrolyte alone and that the effects of radial temperature differences and of axial temperature differences are also important.

1.4.2 The Effect of Radial Temperature Differences on Separation Efficiency

The heat generated in the electrolyte can only be dissipated through the walls so it is not surprising that the temperature at the axis is larger than at the inner wall of the capillary. It follows that the viscosity of the electrolyte at the wall will be greater than at the axis so that the electrophoretic mobility of analytes at the axis will be greater than that of analytes near the wall (see Eqn 1- 36). These variations in velocity associated with temperature are a significant source of band broadening. Hjerten [47] calculated that a radial temperature difference of just 2 ºC would result in almost a 6 % difference in velocities of analytes at the wall and at the central axis. He also showed that the percentage band broadening as a result of Joule heating increased with the square of the field strength.

Petersen et al. reasoned that Taylor-Aris dispersion (that is the radial diffusion of "fast" species from the axis towards the wall and of "slow" species from the wall towards the axis) tends to decrease the effects of radial temperature differences. They derived an expression for the contribution of Joule heating to the theoretical plate height (H_{Joule}) that took into account radial differences in viscosity; this derivation has been adapted below. The purpose of this next section is to model the contribution of Joule heating to the overall theoretical plate height.

For a parabolic flow profile, the effective dispersion coefficient (D_{Eff}) is given by the sum of the axial diffusion coefficient (D) and the Taylor-Aris dispersion coefficient (D_{Taylor}) [55].

$$D_{Eff} = D + D_{Taylor} = D(1 + k_{Taylor} Pe^2) \qquad 1\text{- }38$$

where k_{Taylor} is a constant which depends on the geometry of the lumen = 1/48 for circular capillaries and Pe is the Peclet number a number which describes the ratio of bulk or convective heat transfer with conductive heat transfer [97]. Eqn 1- 39 gives an expression to calculate Pe.

$$Pe = \frac{v_{parab} r_i}{D} \qquad 1\text{- }39$$

where v_{parab} is the average velocity of the parabolic flow.

The contribution to the overall plate height stemming from Taylor dispersion is given by Eqn 1- 40.

$$H_{Taylor} = \frac{2D_{Taylor}}{v_{parab}} = \frac{2Dk_{Taylor}Pe^2}{v_{parab}} = \frac{2k_{Taylor}v_{parab}r_i^2}{D} = \frac{v_{parab}r_i^2}{24D} \qquad 1\text{- }40$$

The electrophoretic flow is a combination of a temperature-induced parabolic flow profile and a plug-shaped profile. Eqn 1- 41 gives the time taken (t_A) for an analyte band (A) to reach the detector, as the distance travelled to the detector divided by the observed velocity.

$$t_A = \frac{L_{\text{det}}}{v_{obs}} \qquad 1\text{- }41$$

During this time, the middle of the analyte band travels a distance L_{app} defined in Eqn 1- 42.

$$L_{app} = \frac{v_{parab}}{v_{obs}} L_{\text{det}} \qquad 1\text{- }42$$

The quotient H_{Joule}/H_{Taylor} is equivalent to the quotient v_{parab} / v_{obs} enabling Eqn 1- 43 to be derived for the contribution of the parabolic temperature profile to the plate height.

$$H_{Joule} = \frac{L_{\text{det}}}{L_{app}} H_{Taylor} = \frac{v_{parab}r_i^2}{24D} \bullet \frac{v_{parab}}{v_{obs}} = \frac{v_{obs}r_i^2}{24D}\left(\frac{v_{parab}}{v_{obs}}\right)^2 \qquad 1\text{- }43$$

The value of v_{parab} / v_{obs} is critical to calculating H_{Joule}. Petersen et al. [55] asserted that the average parabolic flow velocity is half sum of the velocity at the wall and at the axis. (This appears to be based on the assumption that the average temperature can be calculated in a similar way [49, 55]).

As μ_{obs} is inversely proportional to the viscosity (see Eqn 1- 36), Petersen et al. [55] deduced that Eqn 1- 44 would apply for calculating the quotient v_{parab} / v_{obs}.

$$\frac{v_{parab}}{v_{obs}} = \frac{1}{2}\frac{\Delta\eta}{\eta} \qquad 1\text{- }44$$

Knox and McCormack [53] had previously fitted an equation for the variation of the viscosity of water with temperature.

$$\eta = 2.761x10^{-3}e^{\left(\frac{1713K}{T}\right)} \qquad 1\text{- }45$$

where η is measured in cP (centipoise = 10^{-3} $kgm^{-1}s^{-1}$).
Differentiation of this equation leads to Eqn 1- 46.

$$\frac{\Delta\eta}{\eta} = \frac{1713\Delta T_{Radial}}{T^2} \qquad 1\text{- }46$$

Substitution of Eqns 1- 44 and 1- 46 into Eqn 1- 43 gives Eqn 1- 47.

$$H_{Joule} = \frac{v_{obs}r_i^2}{24D}\left(\frac{1713\Delta T_{Radial}}{2T^2}\right)^2 = \frac{1713^2 v_{obs}r_i^2\Delta T_{Radial}^2}{96DT^4} \qquad 1\text{- }47$$

Substituting Eqn 1- 11 for ΔT_{Radial} in Eqn 1- 47 leads to Eqn 1- 48.

$$H_{Joule} = \frac{1713^2\mu_{obs}Er_i^2}{96DT^4}\left(\frac{E^2\kappa d_i^2}{16\lambda}\right)^2 = \frac{1713^2\mu_{obs}\kappa^2E^5r_i^6}{1536\lambda^2DT^4}$$
$$\approx \frac{1910\mu_{obs}\kappa^2E^5r_i^6}{\lambda^2DT^4} \qquad 1\text{- }48$$

Eqn 1- 48 demonstrates that in order to minimise the contribution of Joule heating to the theoretical plate height, the radius of the capillary and the conductivity of the electrolyte should be minimised, but as mentioned earlier this can lead to reduced sensitivity and inferior peak shapes due to electromigrational dispersion. It might also appear expedient to run the separation at a higher temperature as H_{Joule} is inversely proportional to T^4 however, it is the ratio $\mu_{obs}\kappa^2/\lambda^2DT^4$ that needs to be examined. At 25 ºC, μ_{obs}, κ and D all increases at a rate of approximately 2 % per ºC and λ increases at about

0.3 % per ºC. It follows that the numerator $\mu_{obs}\kappa^2$ increases at about 6.1 % per ºC, however the denominator $\lambda^2 D T^4$ only increases at about 3.9 % per ºC[77], so H_{Joule} increases at a rate of about 2.1 % per ºC. Therefore in terms of axial diffusion and the effects of radial temperature differences, the temperature at which the separation is carried out should be minimised.

Grushka et al. [54] calculated that *H* should not increase substantially with *E* until ΔT_{Radial} reaches 1.5 ºC. This was corroborated by Petersen et al. [55] who calculated the variation of *N* with *E* for rhodamine-110 in capillaries and on a glass microfluidic device. In the 50 µm id capillary, values of *N* reached a maximum at $E \approx 50\ 000\ Vm^{-1}$ for which ΔT_{Radial} was about 1.1 ºC. In the 5.3 µm deep glass chip there appeared to be a linear increase in *N* with *E* until the maximum value of 70 000 Vm^{-1} was reached due to more efficient heat transfer and the smaller radial temperature increase.

Gobie and Ivory [60] found that when Joule heating limited performance, *N* could be improved substantially by applying a small counter pressure to counteract the radial velocity profile. They found the method to be particularly effective in wider bore capillaries for which Taylor–Aris dispersion was inefficient at achieving radial diffusive averaging.

Tallarek et al. [98] used pulsed magnetic field gradient NMR to investigate flow profiles and dispersion during CE and capillary electrochromatography (CEC). Their results suggested that provided that $P/L < 2.5\ Wm^{-1}$ ($\Delta T_{Radial} < 0.33$ ºC), increased dispersion could be accounted for entirely by increased axial dispersion and that there was no need to consider Taylor-Aris dispersion.

Porras et al. [49] investigated the effect of solvent composition on peak broadening. They found that plate heights in organic solvents tended to be significantly larger than in aqueous solutions. As the thermal conductivity of organic solvents is typically three times lower than that of water, the radial temperature gradient for a particular value of *P/L* will be three times greater. Despite the larger radial temperature gradients and lower separation efficiency for organic solvents, Porras et al. [49] found that axial diffusion was still the major contributor to *H*.

In 2004, Xuan and Li [50] published what appears to be the most comprehensive theoretical study on the effects of Joule heating on peak broadening. Their model took into account the variation of molecular diffusion, electroosmotic flow, electrophoretic velocity based on their temperature-dependence of the diffusion constant, the dynamic

viscosity and electrical conductivity. Eqn 1- 49 gives their expression for the plate height in CE in the presence of Joule heating.

$$H = \frac{2D_{Wall}}{\bar{v}_{(A)}} + \frac{2K_E}{\bar{v}_{(A)}} + \gamma\left[\frac{2D_{Wall}}{\bar{v}_{(A)}} - \frac{2K_D}{\bar{v}_{(A)}(1+\gamma^*)}\right] \qquad 1\text{- }49$$

In Eqn 1- 49, D_{Wall} is the diffusion coefficient at the wall, $\bar{v}_{(A)}$ is the mean velocity of the analyte over the cross section, K_E is the electromigrational dispersion coefficient, K_D is the advective dispersion coefficient and γ^* is the temperature-dependence of the diffusion coefficient. The first term of Eqn 1- 49 indicates the contribution from enhanced diffusive dispersion, the second term gives the contribution from the non-plug like electroosmotic flow and electrophoretic flow and the final term is attributed to the radial variation of the diffusion coefficient across the capillary. Expressions for K_E and K_D were derived from first principles and were found to depend on the temperature at the inner wall of the capillary.

Plots of calculated theoretical plate heights (H) versus the internal radius (r_i) for three different electrical field strengths are shown in **Figure 1- 7**. Not surprisingly Xuan and Li's [50] model confirmed that plate heights and wall temperatures increase with internal diameter for passively-cooled capillaries. Key data from their calculations are shown in **Table 1- 5**. Values of the heat produced per unit volume (Q), the power per unit length (P/L) and the radial temperature difference ΔT_{Radial} were calculated using Eqns 1- 10 and 1- 11. Xuan and Li [50] concluded that the elevation of the electrolyte temperature was the main factor that limits the performance of CE. This was not surprising given that the maximum radial temperature difference was less than 0.1 ºC but the electrolyte temperature was predicted to increase by almost 65 ºC.

Table 1- 5: Theoretical plate heights for r_i = 60.0 µm using data supplied for **Figure 1- 7** [50]

E (kVm^{-1})	Q (Wm^{-3})	P/L (Wm^{-1})	ΔT_{Radial}	H_0 (µm)	H-H_0 (µm)	ΔT_{Wall} (ºC)
20	0.60 x 10^8	0.170	0.022	0.4972	0.0127	7.28
30	1.35 x 10^8	0.382	0.050	0.3315	0.0249	21.3
40	2.40 x 10^8	0.679	0.089	0.2487	0.0578	64.8

NB In this case ΔT_{Wall} refers to the increase in temperature of the electrolyte at the wall rather than the temperature difference across the wall ($\Delta T_{Across\ Wall}$).

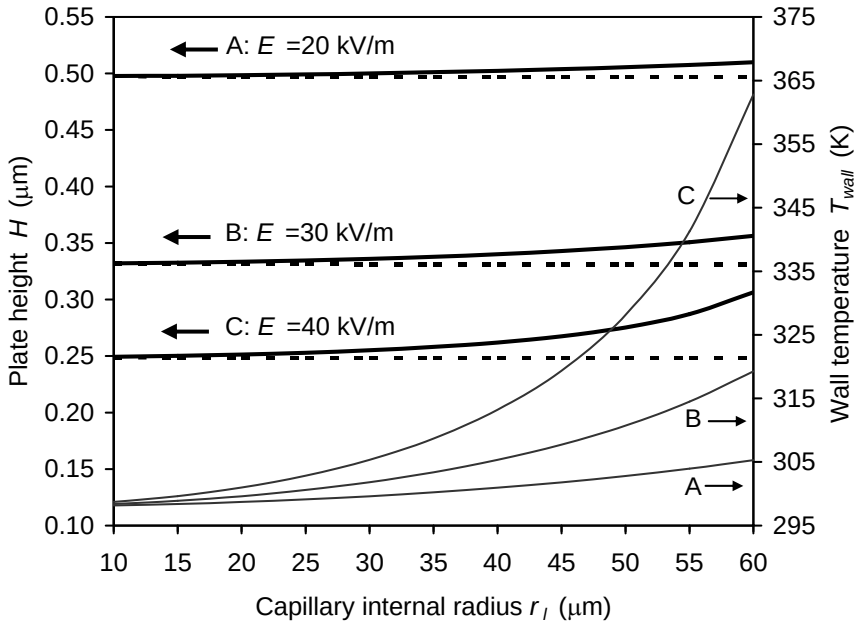

Figure 1- 7: Calculated variation of theoretical plate height *H* of cations with internal radius (r_i)

H at different electric fields strengths (thick solid lines as labelled in the figure). The horizontal dashed dot-lines show calculated plate heights in the absence of Joule heating. Thin dark grey solid lines show the temperatures measured at the inner wall. Horizontal arrows link curves to the appropriate scales.
Simulation conditions electrical conductivity (κ =0.150 Sm^{-1}), heat transfer coefficient for passive air cooling (h = 100 $Wm^{-2}K^{-1}$), valence of cations (z = 1), electrophoretic mobility of cation at ambient temperature of 25 ºC (μ_{ep} = 9.8 x 10^{-9} $m^2s^{-1}V^{-1}$). Diagram adapted from Xuan and Li [50] with minor modifications, used with permission.

It is possible to compare the relative sizes of the contributions of the elevated electrolyte temperature and the radial temperature difference by calculating the relative decrease in the number of theoretical plates in the presence of Joule heating. As *N* is inversely proportional to *H,* the fractional decrease in *N* can be calculated using Eqn 1- 50.

$$\frac{N}{N_0} = \frac{H_0}{H} \qquad \text{1- 50}$$

Table 1- 6: Comparison of predicted fractional decrease in number of theoretical plates for a passively-cooled capillary.
N/N_0 (Petersen et al. [57]) (see Eqn 1- 37) and N/N_0 (Xuan and Li [52]) (see Eqn 1- 49)
Conditions: As in **Table 1- 5**

E (kVm^{-1})	P/L (Wm^{-1})	ΔT_{Radial} (ºC)	ΔT_{Wall} (ºC)	N/N_0 (Petersen et al.)	N/N_0 (Xuan and Li)
20	0.170	0.022	7.28	0.976	0.975
30	0.382	0.050	21.3	0.933	0.930
40	0.679	0.089	64.8	0.821	0.811

Petersen et al.'s [57] model is based on an inverse relationship between N and T, whereas Xuan and Li's [52] model also takes into account the radial temperature difference within the electrolyte. **Table 1- 6** shows that the effect of radial temperature differences are relatively small in passively-cooled capillaries as the rise in temperature of the electrolyte may be three orders of magnitude greater than the radial temperature difference.

Xuan and Li [52] also predicted that the minimum plate height would vary with the valency of the analyte (see **Figure 1- 8**). Once again they compared plate heights with and without the effects of Joule heating. The size of H increased in the order: cations < neutral species < anions for normal EOF. The differences can be understood in terms of the longer migration times for anions. The fractional decrease in N as a result of Joule heating for a particular field strength, was virtually identical for each of the species considered.

Finally Xuan and Li's [50] modeling revealed that no matter how efficiently the capillary was cooled (values of h ranged from 100 to 10 000 Wm^{-2}K^{-1}), Joule heating produced minima in curves of plate height versus concentration (see **Figure 1- 9**).
In the absence of Joule heating, H decreases with increasing concentration due to a reduction in electrokinetic dispersion producing sharper peaks. However in the presence of Joule heating, Xuan and Li explained that the value of H reflects a compromise between the overall dispersion coefficient K^* and the mean velocity of the analyte $\bar{v}_{(A)}$ (see Eqn 1- 51).

$$H = \frac{K^*}{\bar{v}_{(A)}} \qquad 1\text{- }51$$

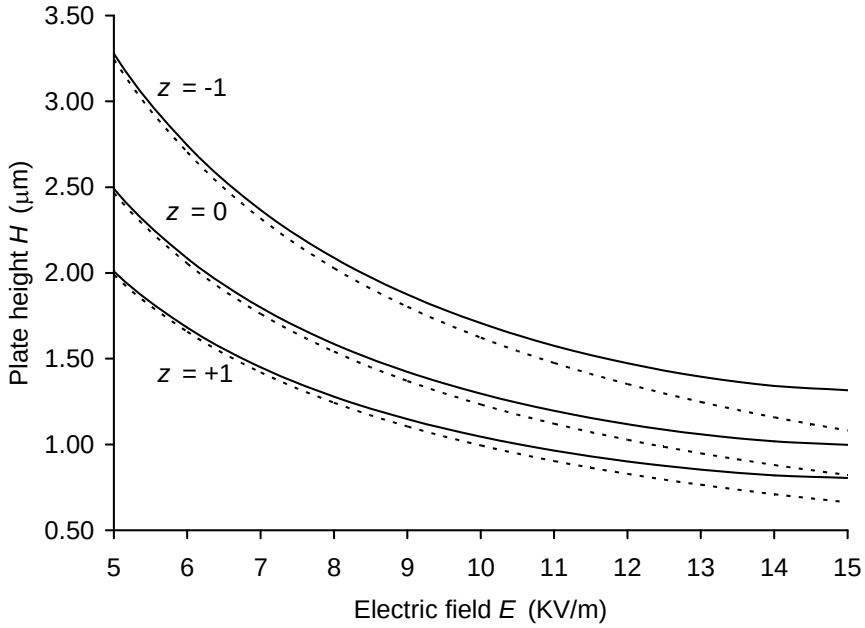

Figure 1- 8: Calculated plate height H against electrical field strength E for differently charged ions

Broken lines represent cases in the absence of Joule heating effects.

Simulation conditions: Internal radius (r_i = 60 μm), electrical conductivity (κ =0.750 Sm^{-1}), heat transfer coefficient for passive air cooling (h = 100 $Wm^{-2}K^{-1}$), electrophoretic mobility of cation at ambient temperature of 25 ºC (μ_{ep} = 9.8 x 10^{-9} $m^2s^{-1}V^{-1}$).

Diagram from Xuan and Li [50] used with permission.)

Joule heating increases the mean velocity of analytes $\overline{v}_{(A)}$ and the dispersion coefficients K_E and K_D. For passively-cooled capillaries the minimum value of H comes at a low concentration of the electrolyte as Joule heating produces a significant increase in the electrolyte temperature. As expected, efficient cooling of the capillary allows higher concentrations of the electrolyte to occur [50]. It is reassuring to note that increasing h from 1000 $Wm^{-2}K^{-1}$ to 10 000 $Wm^{-2}K^{-1}$ only makes a minor difference to H and to ΔT_{Radial}. (Even to achieve h = 4 000 $Wm^{-2}K^{-1}$ using air cooling would require supersonic air speeds.)

It is interesting to compare the effects of increasing electrolyte temperature and increasing radial temperature difference on theoretical plate heights with passive and active-cooling.

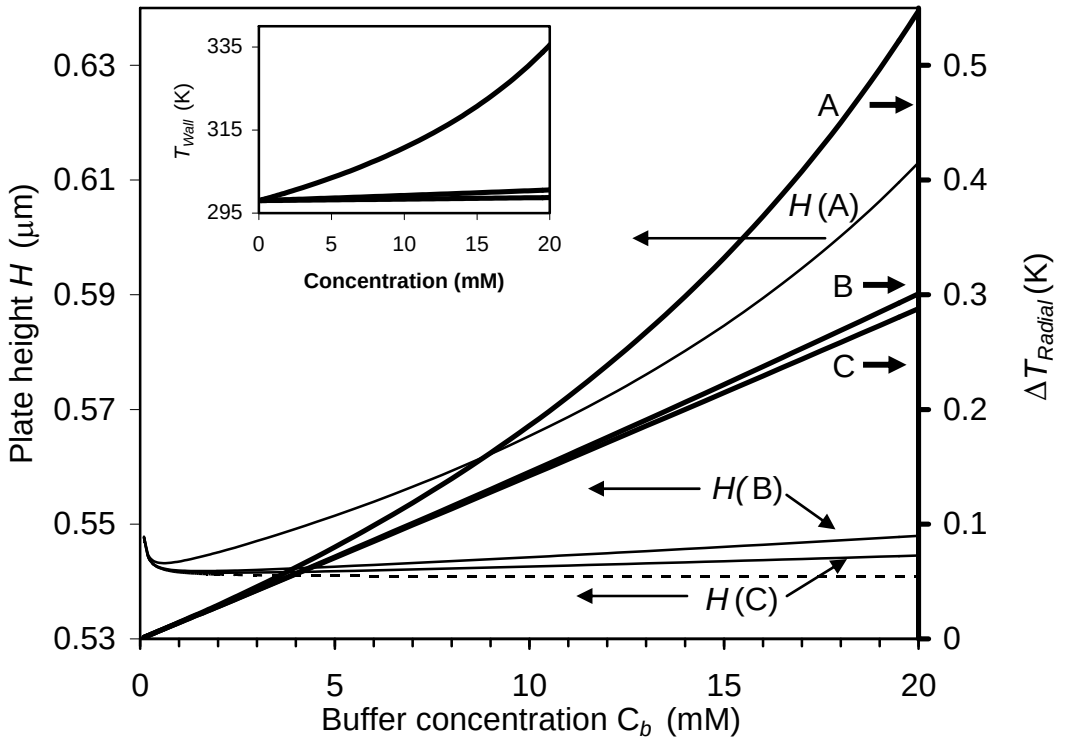

Figure 1- 9: Variation of theoretical plate height (*H*) of anions with concentration of the electrolyte solution (*c*) for different cooling efficiencies.
The broken line gives the case where Joule heating is absent. Thin solid lines show the variation in *H* with *c* in the presence of Joule heating. Thick solid lines in the main graph show the variation of ΔT_{Radial} with *c*. Horizontal arrows link curves to the appropriate scales. The inset shows the variation of the temperature at the inner wall (T_{Wall}) with *c*.
Simulation conditions: Electrical field strength (E = 50 kVm^{-1}) internal radius (r_i = 25 μm), valence of anions (z = -1), Case A, h = 100 $Wm^{-2}K^{-1}$ (passive cooling), Case B, h = 1000 $Wm^{-2}K^{-1}$ (efficient cooling), Case C, h = 10 000 $Wm^{-2}K^{-1}$ (super-efficient cooling).
Diagram adapted from Xuan and Li [50] used with permission.)

Table 1- 7 illustrates the importance of active-cooling in limiting the autothermal effect. In every case, the use of a more efficient cooling system led to smaller theoretical plate heights. This trend becomes more significant as the concentration of the electrolyte increases. Obviously for capillaries of greater internal diameter, the increase in electrolyte temperature wil be greater for the same electrical field strength, leading to greater values of *H* and reduced values of *N*. For passive cooling (h = 100 $Wm^{-2}K^{-1}$, the effect of increasing electrolyte temperature with concentration to produce increased axial diffusion dominates the effects of the radial temperature difference. For highly efficient

active-cooling (h = 1000 $wm^{-2}K^{-1}$), the contribution to decreasing N from the radial temperature difference was about 50 % of that from increased electrolyte temperature. For super efficient cooling (h = 10 000 $Wm^{-2}K^{-1}$), the effect of the radial temperature difference became twice as important as the increase in electrolyte temperature. However in practice, such a high heat transfer coefficient is not achieved in capillaries [87].

Table 1- 7: The effect of concentration on peak broadening
r_i = 25.0 µm using data supplied for **Figure 1- 9** [50]
N/N_0 (Petersen et al. [55] (see Eqn 1- 37) and N/N_0 (Xuan and Li [52]) (see Eqn 1- 49) Conditions: As in **Figure 1- 9**

c (mM)	P/L (Wm^{-1})	h ($Wm^{-2}K^{-1}$)	ΔT_{Radial}(ºC)	ΔT_{Wall} (ºC)	N/N_0 (Petersen et al.)	N/N_0 (Xuan and Li)
10	1.413	100	0.186	12.7	0.959	0.957
10	1.105	1 000	0.145	1.24	0.996	0.994
10	1.080	10 000	0.142	0.361	0.999	0.997
15	2.526	100	0.332	22.7	0.929	0.925
15	1.687	1 000	0.222	1.89	0.994	0.991
15	1.632	10 000	0.215	0.544	0.998	0.992
20	4.164	100	0.548	37.5	0.888	0.882
20	2.288	1 000	0.301	2.56(5)	0.991	0.987
20	2.189	10 000	0.288	0.730	0.998	0.993
25	6.814	100	0.896	61.3	0.829	0.821
25	2.911	1 000	0.383	3.26	0.989	0.983
25	2.753	10 000	0.362	0.917	0.997	0.991

In summary, for passive cooling the effects of the increased electrolyte temperature to enhance molecular diffusion are far more important than effects of radial temperature differences. During active-cooling, radial temperature differences are typically <1 ºC except under extreme conditions when P/L exceeds 8 Wm^{-1}, so that the thermal plate height is usually small compared to that caused by molecular diffusion.

1.4.3 The Effect of Axial Temperature Differences on Separation Efficiency

In CE, axial temperature differences occur as a result of fluid dynamics [82], instrumental design [99] and differences in conductivity between sample zones and the bulk electrolyte [73, 100].

Tang et al. [82] demonstrated that the thermal entrance of the electroosmotic flow (the distance from the start of the capillary to where the full EOF is developed) is significant when Joule heating occurs but is insignificant in its absence. This relates to the fact that μ_{EOF} is temperature-dependent and that there is a significant axial temperature gradient at the wall near the entrance and exit of the capillary as discussed in Section 1.3.1.

Instrumental design is a major source of axial temperature differences because parts of the capillary are often outside the cooling system and are surrounded by stagnant air or electrolyte in the vials (see **Figure 1- 10**) [5, 49]. Rathore [99] pointed out that as much as 50 % of the length of the capillary may be outside the zone of active-cooling.

Superimposed on these instrumentally-induced changes in axial temperature are differences that occur as a result of differences in conductivity between sample zones and the bulk electrolyte [73]. This is particularly the case when transient isotachophoretic stacking or field-amplified stacking is employed. As the conductivity of the sample is generally much less than that of the bulk electrolyte, the resistance of the zone and hence the electrical field strength across it will be much greater than in the bulk electrolyte. Temperatures in sample zones may be significantly different to those in the bulk electrolyte even after stacking has been completed. Analytes with greater mobilities than the co-ions in the electrolyte will tend to be at a lower temperature and produce fronting peaks, analytes with lower mobilities will tend to be at a higher temperature and produce tailing peaks [73].

Hjerten [47] demonstrated that the difference in conductivity ($\Delta\kappa$) between a sample zone and the electrolyte is given by Eqn 1- 52.

$$\Delta\kappa = \frac{C_A}{\mu_{epB}}\left(\mu_{epB} - \mu_{epA}\right)\left(\mu_{epR} - \mu_{epA}\right) \qquad \text{1- 52}$$

where C_A is the charge transported of the sample per unit volume measured in coulombs per litre and μ_{ep} refers to the electrophoretic mobility. The subscripts: A, B and R refer to

the analyte, co-ion in the electrolyte and counter-ion in the electrolyte respectively. Eqn 1- 53 may be used to calculate the charge transported per unit volume.

$$C_A = z_A c_A F \qquad 1\text{- }53$$

where z_A is the valency of the analyte ion, c_A is its molar concentration measured in $molL^{-1}$ and F is Faraday's constant = 9.6487 x 10^4 $Cmol^{-1}$. For cations, mobility and concentration are assigned positive values and for anions they are assigned negative values. Hjerten concluded that the difference in conductivity is minimised by having a low concentration of analyte with mobility close to that of the co-ion in the electrolyte and by using a counter-ion with a low mobility.

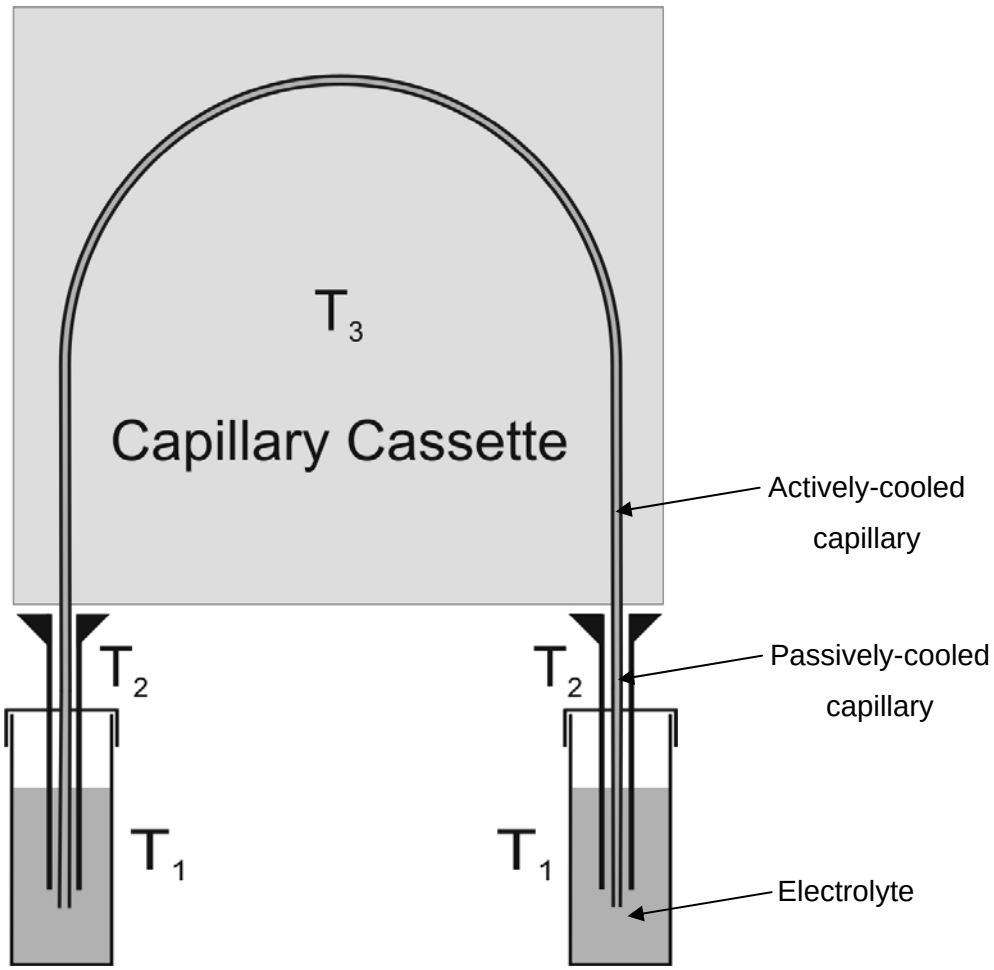

Figure 1- 10: Schematic diagram of an actively-cooled capillary in an Agilent $3D^{CE}$ instrument.

Vinther and Soeberg [61] predicted that the elevation in temperature of the sample would be several times greater than that of the bulk electrolyte, but were unable to confirm this experimentally. Recently, Giordano et al. [65] were able to corroborate these predictions by making continuous temperature measurements at the detection window of the capillary using the temperature-dependence of the fluorescence response of Rhodamine B.

Gas [100] showed both theoretically and experimentally that in the presence of axial temperature variations, the flow of heat energy from the electrolyte does not travel solely through the walls but that an axial flux of heat also occurs. This can lead to oscillation of the concentration profile of the electrolyte appearing at sites where there are sudden changes in the radial heat flux, for example, where the capillary exits the active-cooling zone.

Xuan et al. [51, 88, 101] demonstrated numerically and experimentally that axial temperature gradients produce non-uniform electrical fields and velocity fields along the length of the capillary and that these result in axial pressure variations induced by the temperature-dependent variations of electrical conductivity and viscosity. The following section is adapted from Xuan and Li [88] and demonstrates how differences in axial temperature induce variations in the electric field strength and pressure (p).

Figure 1- 11 shows schematically the variation of T, E and p in different sections of the capillary. The diagram divides the capillary into three parts. The injection end of the capillary to the start of the temperature-controlled section is assigned the subscript 1. The actively-cooled part is assigned 2 and the remainder of the capillary 4

The following section explains how variations in the electrical field strength are induced. By Kirchhoff's current law, the electric current (I) must be the same in each section of the capillary.

$$I_1 = I_2 = I_4 \qquad \text{1- 54}$$

Electric current is the product of conductance and voltage.

$$I = GV = \frac{\kappa A V}{L} = \frac{\pi r_i^{\,2} \kappa V}{L} = \pi r_i^{\,2} \kappa E \qquad \text{1- 55}$$

As the internal radius of the capillary is the same throughout, Eqn 1- 56 applies.

$$\bar{\kappa}_1 E_1 = \bar{\kappa}_2 E_2 = \bar{\kappa}_4 E_4 \qquad \text{1- 56}$$

As electrical conductivity increases with temperature, it follows that the temperature and therefore the conductivity in the passively-cooled sections of the capillary will be greater than in the actively-cooled section. By the same reasoning the electrical field strength, and therfore the rate of migration of ions in these sections, must be less than in the actively-cooled section. Whether or not the temperature in the sample zone is higher or lower than the surrounding electrolyte depends on their relative conductivities. Consider a sample zone with a lower conductivity than the surrounding electrolyte. *E* in the sample zone will be greater so that continuity of current occurs. The rate at which heat is produced depends on E^2 so that the temperature of the sample zone will be greater than its surroundings.

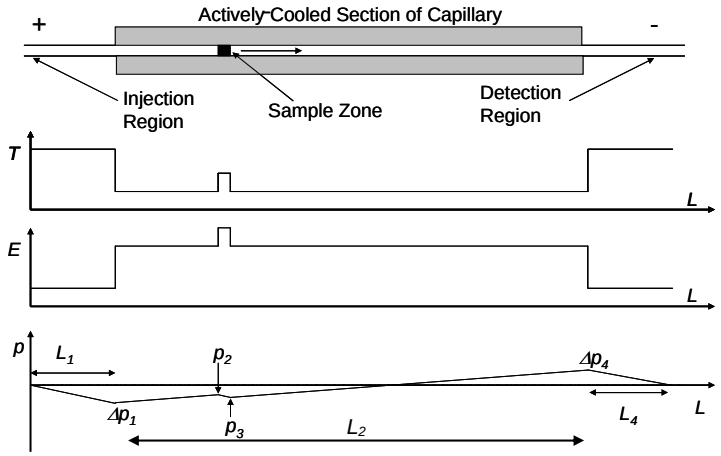

Figure 1- 11: Schematic diagram showing axial variations in temperature *T*, electrical field strength *E* and pressure *p* in a capillary resulting from Joule heating. For simplification the sample contains a single analyte zone with a lower electrical conductivity than the bulk electrolyte.
Diagram adapted from Xuan and Li [88].

Electroosmotic mobility increases with temperature [5, 53, 102] so v_{EOF} varies in different parts of the capillary, however in order to maintain mass continuity, pressure differences are induced to preserve a constant flow rate of the bulk electrolyte There is a slight decrease in pressure at the inlet end and a slight increase in pressure near the outlet. The effect of this pressure gradient is to produce a convex velocity profile near the inlet and outlet and a slightly concave profile in the actively-cooled section of the capillary [88]. Xuan and Li's [88] model suggested that the velocity of analytes in the passively-cooled sections of the capillary were less than in the actively-cooled section

due to the smaller electrical field strength in these passively-cooled zones. Eqn 1- 57 gives their equation for the electroosmotic velocity profile using a dimensionless radial coordinate $y = r / r_i$.

$$v_{EOF\,i}(y) = -\frac{\varepsilon_{iWall}\zeta E_i}{\eta_{iWall}} - \left(\frac{\partial p}{\partial L}\right)_i \frac{{r_i}^2}{4\eta_{iwall}}\left[1 + \tfrac{1}{2}\omega_i - \frac{r^2}{{r_i}^2}\left(1 + \omega_i - \tfrac{1}{2}\omega_i \frac{r^2}{{r_i}^2}\right)\right] \qquad 1\text{- }57$$

The subscript i can take the values 1,2 or 4 corresponding to the sections of the capillary shown in **Figure 1- 11** which are passively-cooled near the inlet (1) and outlet (4) and actively-cooled (2). The subscript *Wall* refers to the inside wall. $\left(\frac{\partial p}{\partial L}\right)_i$ is the pressure gradient in section i of the capillary. ω_i describes the radial distribution of viscosity in section i of the capillary.

$$\omega_i = \frac{1713K\, x\, \Delta T_{(r)_i}}{{T_{Wall\,i}}^2} \qquad 1\text{- }58$$

where $\Delta T_{(r)\,i}$ describes the radial temperature profile of the electrolyte at a distance r from the central axis in section i of the capillary (see Chapter 3.1).

Xuan and Li [88] introduced the term hydrodynamic conductivity (M) as an analogy to thermal conductivity. M relates the hydrodynamic velocity (v_{pd}) to the pressure gradient in a radial temperature field. The size of $v_{pd\,i}$ can be calculated using Eqn 1- 59, a modified form of the Poiseuille equation that takes into account the radial temperature profile.

$$v_{pd\,i} = -M_i \bullet \left(\frac{\partial p}{\partial L}\right)_i = -(1 + \tfrac{1}{3}\omega_i)\frac{{r_i}^2}{8\eta_{iWall}} \bullet \left(\frac{\partial p}{\partial L}\right)_i \qquad 1\text{- }59$$

The size of the pressure gradient depends on the difference in the electroosmotic mobility between adjacent sections of the capillary. The decrease in pressure (from atmospheric pressure) at the junction between the inlet and the cooled zone (Δp_1) is given by Eqn 1- 60.

$$\Delta p_1 = \frac{\mu_{EOF2}E_2 - \mu_{EOF1}E_1}{\left[\frac{M_1}{L_1} + \frac{M_2}{L_2}\left(1 + \frac{L_4}{L_1}\right)\right]} \qquad 1\text{- }60$$

where μ_{EOF1} and μ_{EOF2} are the electroosmotic mobilities in section 1 and 2 of the capillary corresponding to the temperatures of their internal walls.

To maintain mass continuity, it may be shown that the decrease in pressure between the inlet and the active-cooling zone is related to the increase in pressure after the cooling zone by the relative lengths of the passively-cooled zones [88].

$$\Delta p_1 = -\frac{\Delta p_4 L_4}{L_1} \qquad 1\text{- }61$$

For charged analytes, the velocity profile given by Eqn 1- 62, is the sum of a plug like electroosmotic flow, an almost parabolic Poiseuille (hydrodynamic) flow, induced by the pressure gradient and a parabolic electrophoretic profile induced by the radial temperature profile which correspond to the first, second and third parts of Eqn 1- 62.

$$v_i(y) = -\frac{\varepsilon_{iw}\zeta E_i}{\eta_{iWall}} - \left(\frac{\partial p}{\partial L}\right)_i \frac{{r_i}^2}{4\eta_{iWall}}\left[1+\tfrac{1}{2}\omega_i - \frac{r^2}{{r_i}^2}\left(1+\omega_i - \tfrac{1}{2}\omega_i \frac{r^2}{{r_i}^2}\right)\right] + \mu_{epiWall} E_i \left[1+\omega_i\left(1-\frac{r^2}{{r_i}^2}\right)\right] \qquad 1\text{- }62$$

The pressure-driven term causes Taylor–Aris dispersion (see Eqn 1- 39) which contributes to the overall theoretical plate height due to the effects of axial temperature differences (H_{axT}) [88].

$$H_{axT} = \frac{{r_i}^2}{24 L_{\text{det}}} \sum_i \frac{(v_{pd\,i})^2 t_i}{D_i} \qquad 1\text{- }63$$

where $v_{pd\,i}$ is the average pressure-driven velocity of the analyte at the average fluid temperature in section $_i$ of the capillary, D_i is its local diffusion coefficient and t_i is the time spent in that section. It is assumed in Eqn 1- 63, that the time that the analyte spends in each section of the capillary is much greater than the time for radial diffusion to occur $\approx r_i^2/D_i$.

Xuan and Li [88] calculated the total theoretical plate height by summing the contributions from axial diffusion, the axial pressure gradient, the radial temperature profile, injection and detection. They stated that that their model tends to slightly underestimate the overall plate height when compared to experimental measurements using Eqn 1- 34. Possible reasons for this are that: the variation in zeta-potential with temperature has not been taken into account and the value of *h* used for the calculations is unrealistically high [87]. The zeta-potential increases slightly with temperature (see Chapter 5) so that the velocity of the electroosmotic flow and the corresponding pressure gradients will also be slightly underestimated. Conversely, the effect of using a very large value of *h* is to underestimate the temperature of the electrolyte in the actively-

cooled section of the capillary and to exaggerate the axial temperature differences and the corresponding pressure gradients.

1.5. Temperature Measurement in CE

During the past two decades, a considerable amount of research has been conducted toward electrolyte temperature measurements in CE [3, 5, 53, 60, 61, 65, 81, 84, 87, 98, 102-113]. For the reader's convenience **Table 1- 8** summarises the methods that have been used to date for temperature measurement in CE.

In 1975 Ryslavy et al. [106] used an external thermocouple as a means of detecting sample zones during isotachophoresis. They recognized that the differing sample zones varied in their conductivity and electrical field strength and so were at different temperatures. They found that the sharpness of zone boundaries could be improved by applying a counter flow to compensate for the parabolic velocity profile that resulted from Joule heating. This approach was later corroborated by the work of Gobie and Ivory [60].

In 1985, Terabe et al. [107] observed that the capacity factor (*K*) measured at different voltages during CEC changed with the applied voltage. Using thermodynamic data they were able to estimate the electrolyte temperature from the variation of *K*.

$$T = \frac{\Delta H^0}{R \ln K - \Delta S^0} \qquad 1\text{- }64$$

where ΔH^0 is the enthalpy of formation, R is the ideal gas constant and ΔS^0 is the standard entropy of formation. Increases of 40 ºC or more were observed at P/L = 1.89 Wm^{-1} suggesting that only passive cooling was in operation.

Table 1- 8: Temperature measurement in electrokinetic separations

Year	Research Group	Separation Method	Method for Measuring T
1975	Ryslavy, Vacik, and Zuska [106]	ITP	External thermocouple
1985	Terabe, Otsuka and Ando [107]	CEC	Capacity factor
1990	Gobie and Ivory [60]	CE	Conductivity (κ)
1991	Burgi, Salomon and Chien [102]	CE	κ and electroosmotic mobitlity (μ_{EOF})
1991	Vinther and Soeberg [61]	CE	μ_{EOF} and κ
1992	Watzig [114]	CE	Thermochromic solution
1993	Davis, Liu, Lanan, and Morris [105]	CE	Raman thermometry
1994	Knox and McCormack [53]	CE	κ, μ_{EOF}, and electrophoretic mobility (μ_{ep})
1996	Nishikawa and Kambara [84]	CE	External thermocouples
1998	Cross and Cao [108]	CE	μ_{ep}
2000	Tallarek et al. [98]	CE	μ_{EOF}
2000	Lacey, Webb and Sweedler [103]	CE	NMR
2001	Swinney and Bornhop [110]	Chip CE	Refractive index (n)
2001	Ross, Gaitan, and Locascio [113]	Chip CE	Fluorescence of Rhodamine B
2002	Rathore, Reynolds and Colon [112]	CE	κ
2003	Porras et al. [49]	CE	κ
2004	Berezovski and Krylov [104],	CE	Rate constant
2006	Giordano et al. [65]	CE	Fluorescence of Rhodamine B

In 1990, Gobie and Ivory [60] found that there was a linear relationship between conductivity (κ) and temperature T in the range 20 ºC – 100 ºC. However the temperature coefficient of electrical conductivity ($\gamma \approx 0.046$ ºC^{-1}) reported in their study appears to be much greater than values reported elsewhere for which $\gamma \approx 0.02$ ºC^{-1} is more typical [90, 102]. Nevertheless they were able to demonstrate good agreement between their experimentally measured temperatures and the temperatures that they predicted using their "autothermal theory" (see Section 1.3.1 pp.20-23).

In 1991, Burgi et al. [102] used the variation of conductivity and electroosmotic mobility (μ_{EOF}) as probes for the average temperature of the electrolyte. Their techniques were based on the idea that there would be little effect of Joule heating at

5 kV so that the ratio of κ: κ(5 kV) or μ_{EOF} : μ_{EOF}(5kV) could be used to determine the temperature increase. The size of the error introduced by this assumption would increase with the concentration of the electrolyte used. For higher conductivity electrolytes, Joule heating can exert an influence even at 5 kV [3]. Porras et al. [49] used a similar approach but measured the conductivity at 1kV rather than 5kV to reduce this influence, however, Chapter 4.7 of this thesis illustrates that serious errors may be introduced by using this technique. Burgi et al. [102] used Eqn 1- 65 to find the increase in the mean electrolyte temperature.

$$\Delta T_{Mean} = \frac{\left(\frac{\kappa}{\kappa(5kV)} - 1\right)}{0.0205\,^{o}C^{-1}} \qquad 1\text{- }65$$

The denominator 0.0205 $^{o}C^{-1}$ is the temperature coefficient for electrical conductivity of the phosphate electrolyte that they used.

Burgi et al.'s [102] second method of determining temperature assumed that the variation of electroosmotic mobility with temperature was due solely to changes in the viscosity of the electrolyte. Eqn 1- 66 takes into account the exponential variation of viscosity that occurs with temperature when the ambient temperature is 25 ^{o}C.

$$T_{Mean} = \frac{1820\,K}{\ln(\mu_{EOF}(5kV) - \ln(\mu_{EOF}) + 6.11} \qquad 1\text{- }66$$

As the same electrolyte was used throughout, they assumed that the product of the dielectric constant (ε) and zeta-potential (ζ) would be constant (see Eqn 1- 8). This assumption is challenged in Chapter 5 of this work.

During the same year, Vinther and Soeberg [61] used electroosmotic mobility as a temperature probe. Unlike Burgi et al. [102] or Knox and McCormack [53], they took into account the temperature-dependence of ε, η, and ζ. For the variation in zeta-potential, Vinther and Soeberg [61] assumed that ζ is directly proportional to the absolute temperature. They also used the variation in electrical conductivity as a temperature probe. Based on the difference of electrical conductivity of the sample zone to the electrolyte, they calculated that the increase in temperature of the sample zone could be several times larger than that of the bulk electrolyte. They predicted that a linear relationship would exist between the temperature increase and the power dissipated due to Joule heating.

$$\Delta T_{Mean} = \frac{P}{a} \qquad 1\text{- }67$$

where a is the gradient of the graph of P versus ΔT_{Mean}. They assumed that a would be the same for the sample and the bulk electrolyte. It follows that the expected increases in temperature for the bulk electrolyte and sample are given by Eqns 1- 68 and 1- 69.

$$\Delta T_{MeanB} = \frac{P_B}{a} \qquad 1\text{- }68$$

$$\Delta T_{MeanS} = \frac{P_S}{a} \qquad 1\text{- }69$$

where the subscripts B and S refer to the bulk electrolyte and the sample respectively. 1- 70 can be derived by rearranging Eqn 1- 9 with the aid of Ohm's Law.

$$P = I^2 R = \frac{I^2 L}{\kappa A} \qquad 1\text{- }70$$

As the electric current (I) and the cross-sectional area (A) are the same throughout the capillary, it follows that the relative increase in temperature of the sample to the bulk electrolyte is given by Eqn 1- 71.

$$\frac{\Delta T_{Mean(S)}}{\Delta T_{Mean(B)}} = \frac{P_S}{P_B} = \left(\frac{L_S}{\kappa_S}\right) \div \left(\frac{L_B}{\kappa_B}\right) = \frac{\kappa_B L_S}{\kappa_S L_B} \qquad 1\text{- }71$$

Their experiments confirmed that boiling of the sample zone could occur in conditions of sample stacking if high conductivity electrolytes were used. If as reported by Knox amd McCormack [53], the increase in electrolyte temperature is dependent on P/L, Eqn 1- 72 gives a simpler relationship for the relative temperature increases.

$$\frac{\Delta T_{Mean(S)}}{\Delta T_{Mean(B)}} = \frac{P_S / L_S}{P_B / L_B} = \frac{\kappa_B}{\kappa_S} \qquad 1\text{- }72$$

Watzig [114] introduced the use of thermochromic solutions for temperature measurement in CE in 1992. The method was based on the change to the absorption spectrum of cobalt(II)chloride solution that occurs with temperature. This could be monitored using the diode array detector of the CE instrument at 495 nm. Watzig

acknowledged that the temperature being determined was only that of the electrolyte in the bare section of the capillary inside the cassette which was under thermostat control, so that the average temperature increase for the electrolyte would be somewhat larger.

Davis et al. [105] introduced the use of Raman thermometry in CE in 1993. Their method of temperature measurement was based on the dependence of the oxygen-hydrogen stretching frequency on temperature. They calibrated their Raman microprobe using external thermocouples and the variation in conductivity. They reported an accuracy of 1 ºC and a precision of ± 0.1 ºC.

In 1994, Knox and McCormack [53] used κ, μ_{EOF}, μ_{ep} as temperature probes. Like Burgi et al. [102], they assumed that the product $\varepsilon\zeta$ was independent of temperature. The temperatures that they determined from the electroosmotic mobility and electrophoretic mobility were consistently higher than those based on conductivity measurements. Unlike Burgi et al. [102], Knox and McCormack [53] assumed that viscosity alone was responsible for variations in conductivity. Despite these approximations, the electrolyte temperatures calculated for the three different methods agreed within ± 2 ºC.

Based on their experimentally-determined temperature values, they came to the conclusion that for passively-cooled capillaries, the rise in the mean temperature of the electrolyte is approximately proportional to the power per unit length and inversely proportional to the diameter of the capillary.

$$\Delta T_{Mean} = \frac{1.273}{d_o^{0.3}} \bullet \frac{P}{L} \qquad 1\text{- }73$$

where d_o is the external diameter in metres and P/L is measured in Wm^{-1}.

Nishikawa and Kambara [84] used very thin thermocouples to measure the external temperatures of capillaries during CE in 1996. They were able to calculate the electrolyte temperature by subtracting the calculated temperature differences across the electrolyte and the walls from the external temperature (see Eqns 1- 11 and 1- 12). They calibrated their thermocouples by using the temperature-dependence of resistivity (resisitivity is the reciprocal of conductivity).

In 1998, Cross and Cao [108] used five sulfonamides to investigate the effect of ionic strength of the electrolyte on the degree of ionisation and electrophoretic mobility during CE. They used similar methods to those of Knox and McCormack[53] to measure electrolyte temperature but found that the increases they observed were about four times

smaller than expected using Eqn 1- 73. They attributed this to the use of forced air-cooling rather than the passive air-cooling employed by Knox and McCormack [53]. In 2000, Tallarek et al. [98] also used the variation of μ_{EOF} with E to determine temperature. Like Burgi et al. [102] and Knox and McCormack [53], they assumed that $\varepsilon\zeta$ was constant so that any variation in μ_{EOF} was associated with changes to the viscosity.

In 2002, Rathore et al. [112] measured internal electrolyte temperatures during CE and CEC using electrical conductivity as a temperature probe for electrolytes containing 80 % acetonitrile. Their method of temperature determination was different to that of Burgi et al. [102] in that they took into account the autothermal parameter using the approach of Bello and Righetti [89] (see Eqns 1- 24 to 1- 30).They found that, to a good approximation, electrical conductivity is proportional to the cube of the electrical field strength. The maximum increase in temperature recorded was 35 ºC at P/L = 5.5 Wm^{-1}. Smaller increases were recorded for the packed capillaries.

In 2003, Porras et al. [49] used a similar approach to Rathore et al. [112] to predict the increase in temperature for a range of solvents including water, methanol and acetonitrile. They attempted to verify their predictions experimentally by using conductivity as a temperature probe; however they used a quadratic fit for the variation of conductivity with temperature. They attributed the large deviation between their predicted and experimental results to the considerable fraction of the capillary not subject to thermostat control. It would also appear that the values of h that they used were unrealistically high for the instruments that were employed (still air h = 130 $Wm^{-2}K^{-1}$; forced air h = 4000 $Wm^{-2}K^{-1}$ and circulating liquid h = 10 000 $Wm^{-2}K^{-1}$). The assumption, that the mean electrolyte temperature is half the sum of T_{Wall} and T_{Axis}, also contributed to the deviation between the predicted and measured radial temperature gradients. The discrepancy becomes more significant for organic solvents due to their lower thermal conductivities (see Eqn 1- 11).

Since the work of Cross and Cao [108], a number of methods different to the mainstream approaches of using viscosity, conductivity or electroosmotic mobility as temperature probes have been investigated. These are listed below for completeness but often involve considerable additional expense in the experimental set-up.

In 1998, Chaudhari et al. [109] employed thermochromic liquid crystals (TLCs) to measure temperatures in miniaturised devices, used for the polymerase chain reaction, with a precision of 0.1 ºC. The reflectivity of TLCs is strongly temperature-dependent. Ross et al. [113] pointed out that the size of the TLCs (typically tens of micrometers)

would make them problematic for separating media with narrow channels as encountered in CE and chip CE.

In 2000, Lacey et al. [103] used the strong temperature-dependence of the proton resonance frequency for water during nuclear magnetic resonance (NMR) to monitor the temperature of aqueous electrolytes during CE. They reported an accuracy of > 98 % and a precision of ± 0.2 ºC, however, the expense and practical considerations associated with this method make it unsuitable for routine use. In his review article of 2004, Rathore [99] compared the theoretical increase in electrolyte temperature using Gobie and Ivory's [60] model with those measured independently by Lui et al [81] using Raman thermometry and Lacey, Webb and Sweedler [103] using NMR. He found that the values agreed to within 2 ºC for $P/L < 2.8$ Wm^{-1} and that the agreement was better for lower values of P/L.

In 2001, Swinney and Bornhop [110] introduced the quantitative determination of temperature to CE planar microfluidic devices (chips). Their method was based on the temperature-dependence of the shift of the 3rd interference fringe which is highly sensitive to changes in refractive index (n). Although dn/dT is relatively small ~ $-1 \times 10^{-4} K^{-1}$ [115], the interferometry signal from the shift in the 3rd fringe is strongly temperature-dependent (7.75 % per ºC at 25 ºC) enabling a resolution of 0.001 ºC in a volume of less than 0.2 nL to be achieved [110]. It should be noted however, that while this technique is amenable to use in microfluidic devices, its incorporation into commercial CE instruments would not only be expensive but also experimentally challenging.

Ross et al. [113] used the temperature-dependence of the fluorescence signal of Rhodamine B to measure electrolyte temperatures in chips. The quantum yield of Rhodamine B changes by about 2.3 % per ºC [116]. The technique involved the use of a fluorescence microscope coupled to a charge coupled device (CCD) to measure fluorescent intensity, once again adding considerable instrumental expense. By employing signal averaging, Ross et al. [113] were able to achieve a resolution which varied from 0.03 ºC at room temperature to 0.07 ºC at a temperature of about 85 ºC.

In 2004, Berezovski and Krylov [104], introduced a non-spectroscopic approach to determining temperature in CE. It was based on measuring a temperature-dependent rate constant of complex dissociation by means of a kinetic CE method known as non-equilibrium capillary electrophoresis of equilibrium mixtures (NECEEM). First, a calibration curve of "the rate constant versus temperature" was established using

NECEEM and a CE instrument with a reliable temperature control. The calibration curve was then used to find the temperature during CE in the same buffer but with another CE apparatus or under otherwise different conditions (cooling efficiency, length and diameter of the capillary). Unfortunatley, the method only allows for temperature determination in CE with a precision of 2 °C.

Recently Giordano et al. [65] used a similar technique to Ross et al. [113] to measure bulk electrolyte and sample zone temperatures in capillaries rather than in chips, based on the decreasing fluorescent quantum yield of Rhodamine B that occurs with increasing temperature. Giordano et al.'s approach [65] was similar to that of Vinther and Soeberg [61], however their equations to predict the temperature increase of the sample were different in two ways. Firstly, they gave a different meaning to the symbol *a* used by Vinther and Soeberg: ($a^* = 1/a$) and secondly they assigned different values of a^* for the sample and the bulk electrolyte.

$$\Delta T_{Mean(B)} = a^*_B P_B \qquad 1\text{- }74$$

$$\Delta T_{Mean(S)} = a^*_S P_S \qquad 1\text{- }75$$

The corresponding equation for Eqn 1- 71 becomes:

$$\frac{\Delta T_{Mean(S)}}{\Delta T_{Mean(B)}} = \frac{a^*_S P_S}{a^*_B P_B} = \left(a^*_S \frac{L_S}{\kappa_S} \right) \div \left(a^*_B \frac{L_B}{\kappa_B} \right) = \frac{a^*_S \kappa_B L_S}{a^*_B \kappa_S L_B} \qquad 1\text{- }76$$

The great advantage of Giordano et al.'s [65] temperature measurement method was that they could distinguish the temperatures of sample zones from the bulk electrolyte whereas the method used by Vinther and Soeberg [61] only determined the average temperature. Giordano et al. [65] found that the temperature increase in the sample zones was typically four times greater than in the bulk electrolyte. They noted a 15.5 % discrepancy between the predicted increase in sample zone temperature using Eqn 1- 75 and that from their Rhodamine B response which gave a lower temperature. They hypothesized that the discrepancy was due to the lack of active liquid cooling at the detection window, although this would appear to be inconsistent with a decrease in the observed sample temperature because a reduction in cooling efficiency should result in an increase in temperature. If, as described above, the increase in temperature

relates to the power per unit length in the zone rather than the power, Eqn 1- 76 simplifies to Eqn 1- 77.

$$\frac{\Delta T_{Mean(S)}}{\Delta T_{Mean(B)}} = \frac{a^*_S P_S / L_s}{a^*_B P_B / L_B} = \left(\frac{a^*_S}{\kappa_S}\right) \div \left(\frac{a^*_B}{\kappa_B}\right) = \frac{a^*_S \kappa_B}{a^*_B \kappa_S} \qquad 1\text{- }77$$

Even more recently, Patil and Narayanan [117] used infra-red thermography in a pressure-driven microfluidic device to measure the temperature of the fluid near the wall with an uncertainty of 0.6 ºC or more at lower flow-rates. To date, the method does not appear to have been used in electrically-driven microfluidic devices.

In summary, a number of methods have been employed to measure temperatures inside capillaries. The most precise of these methods have involved additional instrumentation, such as an NMR spectrometer, which is not routinely applicable for use in commercial CE instruments. Alternative, less expensive methods, such as the use of external thermocouples or the use of bulk properties, have been limited to a precision of ≥ 1 ºC.

1.6. Project Aims

The preceeding review of the literature has revealed that an accurate knowledge of electrolyte temperature in CE is essential for reproducibility, method robustness and separation efficiency. Calculation of theoretical plate heights relies on an accurate knowledge of the radial temperature profile in the electrolyte and how the mean electrolyte temperature compares with the temperature at the inner wall and at the central axis. The literature review has also shown that discrepancies exist between temperatures measured using different probes and that there is a need for a better understanding of these discrepancies.

The general aim of this work is to develop a robust and inexpensive method of measuring the mean electrolyte temperature of electrolytes, with this method being suitable for use in commercial instruments with a precision of ± 0.1 ºC.

The specific aims are:

- to develop a theoretical understanding of the relationship between the temperatures of the electrolyte at the central axis (T_{Axis}), near the inner wall (T_{Wall}) and the mean temperature of the electrolyte in the cross-section (T_{Mean})
- to develop the use of conductance as a temperature probe for T_{Mean} free from the influence of Joule heating.

- to develop the use of electroosmotic mobility as a complimentary temperature probe for T_{Wall}.
- to measure the variation in zeta-potential with temperature for a fused-silica capiilary.
- to compare the increase in electrolyte temperature for a number of different polymer capillaries with similar dimensions to those of a fused-silica capillary.
- to develop a method of determining electrophoretic mobilities free from the influence of Joule heating

2 Experimental

This section describes the instrumentation, chemicals and procedures used throughout this work unless specified otherwise in the particular chapter.

2.1 Instrumentation

Experiments were performed on an HP^{3D} CE, (Agilent, Palo Alto USA) capillary electrophoresis instrument equipped with a UV absorbance detector using Chemstation software (Hewlett Packard). The temperature of the vial tray was set to 25.0 ºC using a Messegerate-Werk waterbath (Lauda, Königshofen, GDR). The internal temperature of the CE instrument where the sample vials were located during the run was monitored using a digital thermometer. A small fan powered by an external 12 V power supply was also introduced to circulate the air in this region.

Fused-silica capillaries with an internal diameter of 74.0 μm and an outer diameter of 362.8 μm and a total length of 33.2 cm were purchased from Polymicro Industries (Phoenix USA). Capillary made from a copolymer of tetrafluoroethene and hexafluoropropene (FEP), with an unknown internal diameter (~75 μm) and an external diameter of (~365 μm) and total length of 33.2 cm were obtained from Dr. P. Schuman (OPRI, Gainesville, USA). PEEK capillaries with stated internal and external diameter of 75 μm and 360 μm, respectively, were obtained from Upchurch Scientific (Oak Harbour, USA). Poly(methyl methacrylate) (PMMA) capillaries with stated internal and external diameter of 66 μm and 366 μm respectively were obtained from Dr I. Koev (Biogeneral, San Diego, USA). All capillaries were flushed with 0.1 M sodium hydroxide (BDH, Sydney, Australia) and then flushed with 18.2 MΩcm water (obtained using a Millipore (Bedford, MA USA) Milli-Q water purification system) at a pressure of 95 kPa for 5 min before use. The external temperature of the capillary was set using the active-cooling supplied by the CE instrument. The external diameters of the capillaries were measured using a digital electronic micrometer screw-gauge, Mitutoyo 601-906 (Takatsu-ku, Kawasaki, Japan). Measurements were made at 2 cm intervals along the length of the capillaries before averaging the results.

2.2 Reagents

All solutions were prepared using Milli-Q (18.2 MΩ cm) water. The buffer electrolyte (BGE) was prepared using AR grade orthophosphoric acid (BDH, Sydney, Australia) and AR grade sodium hydroxide (BDH, Sydney, Australia). LR grade acetone (BDH, Sydney, Australia) and LR grade thiourea (AJAX, Sydney, Australia) were used as neutral EOF markers. The 10 mM phosphate electrolyte (pH 7.21, ionic strength = 22mM) was produced by titrating 10.0 mM phosphoric acid solution with 12 M sodium hydroxide until the required pH was achieved. The EOF markers were produced by making a 20 % solution by volume of acetone in the BGE or by adding thiourea to the BGE to a concentration of ca. 1 gL^{-1}.

2.3 Conductance Measurements

The current and voltage were monitored at intervals of 0.01 min throughout each run using the Chemstation software. Conductance values were calculated for each point in time up until the appearance of the EOF peak and were then averaged.

$$G = \frac{I}{V} \qquad 2\text{- }1$$

Similarly the current and voltage readings were used to find the power per unit length *P/L* at each point in time using Eqn 2- 2 before averaging.

$$\frac{P}{L} = \frac{VI}{L} \qquad 2\text{- }2$$

The Agilent CE instrument's current and voltage readings were verified by connecting a 100 MΩ resistor in series with the electrodes and sweeping the voltage from 0-5 kV. The gradient of the voltage versus current plot was compared with the resistance of the 100 MΩ resistor.

2.4 Electroosmotic Mobility Measurements

Each capillary was flushed with the BGE (95.0 kPa) for 1 min before injecting the EOF marker at a pressure of 2.0 kPa for 3 s. Alternatively, an electrokinetic injection at 10 kV for 5 s was used. Measurements were made using separating voltages in

increments of 5.0 kV with a total of five runs for each voltage. The EOF marker was detected using UV detection at 280 nm for acetone and at 250 nm for thiourea. Calculation of the electroosmotic mobility was performed using Eqn 2- 3 [118]

$$\mu_{EOF} = \frac{L_{tot} L_{\det}}{t_{EOF} V} \qquad 2\text{- }3$$

where L_{tot} and L_{det} refer to the total length of the capillary (32.2 cm) and the length to the detector (23.7 cm), respectively, t_{EOF} is the migration time of the neutral marker and V is the applied voltage.

2.5 Temperature Measurements

Voltage and current data were collected digitally using a commercial instrument at time intervals of 0.01 min until the EOF was detected. Electroosmotic mobility and conductance data were collected during the same run.

Conductance was calculated using the voltage and current data collected from the instrument at a set temperature of 25.0 ºC. G_0 was extrapolated from a plot of G versus P/L. The relationship expressed in Eqn 2- 4 was used to find T_{Mean}.

$$T_{Mean} = 25.0^0 C + \frac{\left\{\frac{G_T}{G_0} - 1\right\}}{0.0205^\circ C^{-1}} \qquad 2\text{- }4$$

Similar to the approach described for conductance, the linear variation in the electroosmotic mobility was plotted as a function of the power per unit length and the value of μ_{EOF} at zero power dissipation ($\mu_{EOF}{}^0$) was found by extrapolation. Two methods to find the internal temperature using the electroosmotic mobility were employed. The first method assumed that $\varepsilon\zeta$ was constant so that the variation of μ_{EOF} with T was due only to changes in viscosity. μ_{EOF} was determined at different power levels with the external temperature set at 25 ºC and was extrapolated to give the value at zero power. Electroosmotic mobilities at higher power levels were used to calculate the viscosity of the electrolyte using Eqn 2- 5.

$$\eta(T) = \frac{\mu_{EOF}{}^0(25\,^\circ\mathrm{C})}{\mu_{EOF}} \bullet \eta(25\,^\circ\mathrm{C}) \qquad 2\text{- }5$$

In Eqn 2- 5, $\eta(T)$ and $\eta(25\ ^{o}C)$ are the viscosities of the electrolyte at the elevated temperature as a result of Joule heating and at 25 ºC, respectively, and μ_{EOF} and $\mu_{EOF}^{0}(25\ ^{o}C)$ are the electroosmotic mobilities at the elevated temperature and for zero Joule heating at 25 ºC, respectively. The temperature was calculated by interpolation using known values of viscosity [119].

In the second method, the temperature coefficient of electroosmotic mobility was first found by preparing a calibration curve for μ_{EOF} *versus* $T_{Effective}$ (the average electrolyte temperature taking into account axial variations associated with the instrument).

This enabled the temperature of the electrolyte near the inner wall (T_{Wall} see **Figure 1- 4**) to be found using Eqn 2- 6.

$$T_{Wall} = \frac{\left(\frac{\mu_{EOF}}{\mu_{EOF}^{0}(25\ ^{o}C)} - 1 \right)}{0.0222} + 25\ ^{o}C \qquad 2\text{- }6$$

The details of this method are discussed in Section 4.3.

3 The Radial Temperature Profile of the Electrolyte During CE

In this section, new equations are developed from first principles to demonstrate how the radial temperature difference depends on *P/L* and to show the interrelationships between T_{Mean} over the cross-section of the capillary, T_{Wall} and T_{Axis} (see **Figure 1- 4**).

3.1 Modeling the Radial Temperature Profile

The rate at which heat is dissipated in capillaries has been modeled by Knox [52] and independently by Jones and Grushka [80] who suggested that a parabolic temperature profile would exist inside the capillary with a maximum along its central axis. Computer modeling by Bello and Righetti [93] showed that even if the electrolyte temperature increases by as much as 30 ºC, the temperature profile is still essentially parabolic. This conclusion was supported by the Raman thermomicroscopic measurements made by Liu et al. [81].

It may be shown that the radial temperature difference can be calculated from the thermal conductivity of the electrolyte (λ) and *P/L* by modifying Knox's equation (Eqn 3- 1).

$$\Delta T_{Radial} = \frac{Q d_i^{\,2}}{16\lambda} = \frac{Q r_i^{\,2}}{4\lambda}$$

$$Q = \frac{P}{Vol} = \frac{P}{\pi r_i^{\,2} L}$$

$$\therefore \Delta T_{Radial} = T_{Axis} - T_{Wall} = \frac{P}{\pi r_i^{\,2} L} \bullet \frac{r_i^{\,2}}{4\lambda} = \frac{1}{4\pi\lambda} \bullet \frac{P}{L} \qquad \text{3- 1}$$

where $\lambda \approx 0.605$ $Wm^{-1}K^{-1}$ for dilute aqueous electrolytes. Based on Eqn 3- 1, the radial temperature difference is expected to increase linearly with the power per unit length at a rate of approximately 0.13 ºC W^{-1} m.

A quadratic equation to model the parabolic temperature profile of the electrolyte inside the capillary is given in Eqn 3- 2.

$$\Delta T(r) = (T_{Axis} - T_{Wall}) \bullet \left(\frac{r_i^{\,2} - r^{\,2}}{r_i^{\,2}} \right) \qquad \text{3- 2}$$

where $\Delta T(r)$ is the difference in temperature between the inner wall and the electrolyte at a distance r from the central axis and r_i is the internal radius of the capillary.

To visualise the radial temperature profile within the electrolyte, it is convenient to plot the fractional temperature difference ($\Delta T(r)$ / ΔT_{Radial}) against the dimensionless radial position (r / r_i) shown in **Figure 3- 1**, as the shape of this graph will be identical for all capillaries no matter what the size of the radial temperature difference or the internal radius.

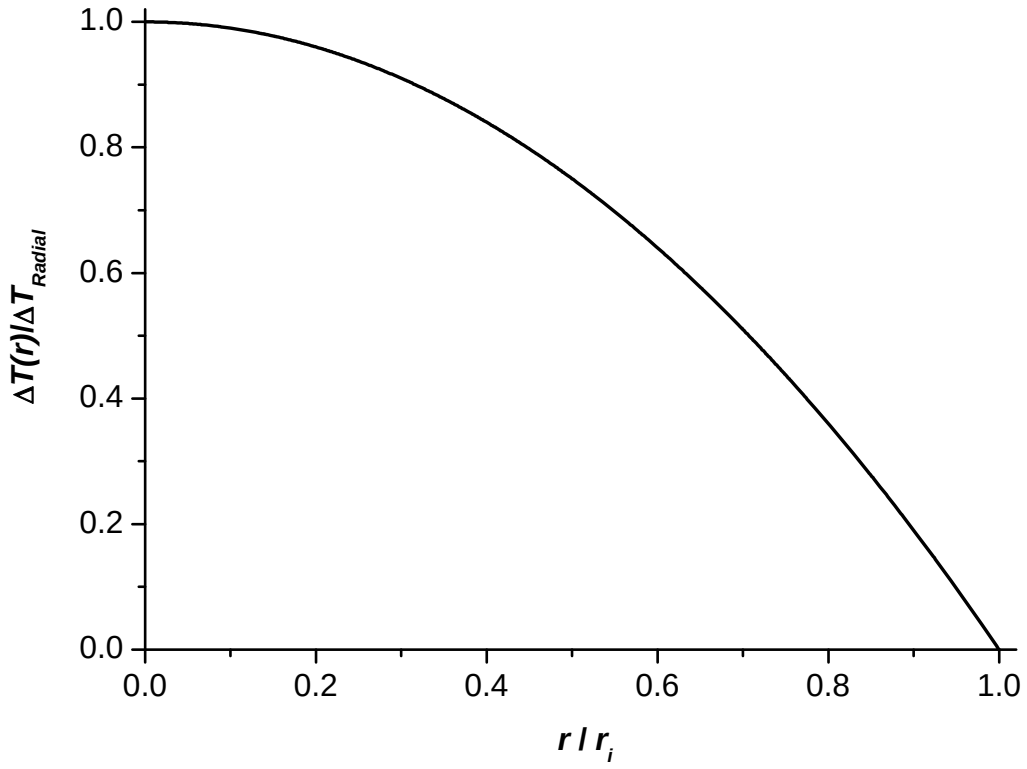

Figure 3- 1: Variation of fractional temperature difference with dimensionless radial position.

Inspection of **Figure 3- 1** shows that the fractional temperature difference exceeds 0.5 for more than 70 % of radial positions. This appears to be at odds with Equation 5 of Porras et al. [49] who gave the relationship shown in Eqn 3- 3.

$$T_{Mean} = T_{Wall} + \tfrac{1}{2}\Delta T_{Radial} \qquad 3\text{- }3$$

Intuitively, it would seem that Eqn 3- 3 underestimates T_{Mean}, however Eqn 3- 3 can be validated by summing contributions over area rather than the model used by Evenhuis et al. [5], which gave each radial position an equal weighting.

T_{Mean} can be calculated for a parabolic temperature profile by summing the temperature contributions of concentric rings of area $2\pi rdr$ and dividing by the internal area of the capillary.

$$\int_0^{r_i} \Delta T(r) 2\pi r.dr = \int_0^{r_i} \Delta T_{Radial} \bullet \left(\frac{r_i^2 - r^2}{r_i^2} \right) \bullet 2\pi r.dr$$

$$= \frac{\Delta T_{Radial}}{r_i^2} \bullet \int_0^{r_i} (2\pi r_i^2 r - 2\pi r^3).dr$$

$$= \frac{\Delta T_{Radial}}{r_i^2} \bullet (\pi r_i^4 - \tfrac{1}{2}\pi r_i^4)$$

$$= \tfrac{1}{2}\Delta T_{Radial} \bullet \pi r_i^2 \qquad \text{3- 4}$$

The average temperature difference (ΔT_{Mean}) between the electrolyte and the inner wall is found by dividing the integral by πr_i^2.

$$\Delta T_{Mean} = \tfrac{1}{2}\Delta T_{Radial} \qquad \text{3- 5}$$

$$\therefore T_{Mean} = T_{Wall} + \tfrac{1}{2}\Delta T_{Radial} \qquad \text{3- 2}$$

Obviously Eqn 3- 2 can be rearranged to give Eqn 3- 6 and used to determine T_{Wall} of the capillary when T_{Mean} and ΔT_{Radial} are known.

$$T_{Wall} = T_{Mean} - \tfrac{1}{2}\Delta T_{Radial} \qquad \text{3- 6}$$

Similarly if T_{Mean} and ΔT_{Radial} are known, Eqn 3- 7 can be used to find T_{Axis}.

$$T_{Axis} = T_{Mean} + \tfrac{1}{2}\Delta T_{Radial} \qquad \text{3- 7}$$

The radial position (r_{Mean}) in the electrolyte for which $T = T_{Mean}$ can be found by solving Eqn 3- 2 for $\Delta T(r) = {}^1/_2\, \Delta T_{Radial}$ which leads to Eqn 3- 8.

$$\therefore r_{Mean} = \frac{r_i}{\sqrt{2}} \approx 0.71 r_i \qquad \text{3- 8}$$

3.2 Conclusions

If the conductance and the power per unit length are known, it is possible to calculate the mean temperature of the electrolyte in the capillary (Eqn 2- 4), the radial temperature difference (Eqn 3- 1), the electrolyte temperatures near the inner wall (Eqn 3- 6) and at the axis of the capillary (Eqn 3- 7).

4. Using Conductance and Electroosmotic Mobility as Temperature Probes for the Mean Electrolyte Temperature

4.1 Introduction

In their pioneering work, Burgi, Salomon and Chien [102] used the temperature-dependence of electroosmotic mobility (μ_{EOF}) and conductivity (κ) to determine the mean electrolyte temperature as a function of the separating voltage. To relate the conductivity measurements to temperature, the approximation that κ increases with temperature at a rate of 2.05 % per ^{o}C was used. The temperature of the electrolyte in the 100 cm long capillaries with internal diameter (d_i) 75 µm increased by 11 ^{o}C per W for passively-cooled capillaries and by 6 ^{o}C per W when active-cooling was employed. At lower power levels (< 3 Wm^{-1}), good agreement was obtained between the internal temperatures calculated using both μ_{EOF} and. κ. At higher power levels, however, the temperatures obtained from measurements of electroosmotic mobility would be expected to become unreliable, as changes in the electrical permittivity and the zeta-potential were not taken into account. A small error was introduced in the determination of the mean electrolyte temperature (T_{Mean}) since the measurements at ambient temperature based on μ_{EOF} and κ were performed in the presence of Joule heating at 5.0 kV. Porras et al. [49] attempted to reduce this error by using the conductivity measured at 1.0 kV as an estimate of G at ambient temperature. Kok [120] described a method to eliminate the effects of Joule heating altogether by plotting the conductivity (κ) as a function of P/L and extrapolating to zero power.

4.2 Calibrating Conductance as a Temperature Probe

4.2.1 Experimental

The general details are given in Chapter 2. Detailed conditions are given in each figure caption.

The work presented here uses a simple method similar to that of Kok [120] to find ΔT_{Mean} in CE capillaries but uses conductance (G), which is more straightforward to calculate than conductivity as the only requirements are measurements of current and

voltage (see Eqn 2- 1). The power per unit length is calculated using the same data using Eqn 2- 2.

If conductance is measured for a range of voltages, a plot of *G versus P/L* is linear and can be used to find the conductance free of Joule heating (G_0). By applying Eqn 4- 1, the ratio of *G* at higher power levels to G_0 (i.e. G_T/G_0) can be used to find the mean temperature of the electrolyte in the device (T_{Mean}).

$$T_{Mean} = 25.0^0 C + \frac{\left\{\frac{G_T}{G_0} - 1\right\}}{\gamma} \qquad 4\text{- }1$$

Clearly, the accuracy of the method depends on the how accurately the thermal coefficient of electrical conductivity (γ) is known. Its value was checked using a number of different methods.

Firstly, the value of *G* was calculated from first principles using tabulated data and a modified form of the Debye-Hückel-Onsager (DHO) (Eqn 4- 2) with the approximation for 1:1 electrolytes over the temperature range 15 ºC – 35 ºC.

$$G = \frac{1}{\eta}\left(\frac{cA}{L}\right) \bullet \left\{\eta\Lambda_0 - \left(\frac{z^2 eF^2}{3\pi}\right)\left(\frac{2c}{\varepsilon RT}\right)^{1/2} - q^*\eta\Lambda_0\left(\frac{z^3 eF}{24\pi\varepsilon RT}\right)\left(\frac{2c}{\varepsilon RT}\right)^{1/2}\right\} \qquad 4\text{- }2$$

where *z* is the valency of the ions, Λ_0 is the specific conductivity at infinite dilution *e* is the charge on an electron, *F* is Faraday's constant, η is the viscosity, ε is the electrical permittivity of the electrolyte and *q** is a parameter relating to the mobility of the ions and the stoichiometry of the electrolyte. A plot of G / G(25 ºC) versus temperature was plotted from the values of G and the gradient of the graph used to estimate γ. (A complete derivation of Eqn 4- 2 is shown in Appendix 1)

Secondly, a conductivity cell calibrated with 0.01000 M KCl using a Philips PW9504/00 resistance meter (North Ryde, NSW, Australia) was used to measure the variation of conductivity with temperature for the phosphate electrolyte for the same range of temperatures. The conductance was calculated from the conductivity (κ) at each temperature using Eqn 4- 3:

$$G = \frac{\kappa A}{L_{tot}} \qquad 4\text{- }3$$

where *A* is the cross-sectional area of the capillary and L is its length. Once again a plot of *G* / *G(25 ºC)* versus *T* was employed to find γ.

The third method of determining γ used current and voltage data collected from the CE instrument using different set temperatures. Conductance was averaged until the EOF peak was detected for a range of values of *P/L*. These graphs were extrapolated to *P/L* = 0 to obtain conductance values at the set temperature, free of Joule heating effects. A correction factor was introduced to take into account the contribution from those parts of the capillary for which the temperature was measured (see **Figure 1- 10**) but not controlled. For the capillary used, the effective temperature, $T_{Effective}$ of the electrolyte at zero power was found using Eqn 4- 4.

Length of non-regulated capillary	= 6.6 cm →	20.5 % of total
Length of set temperature capillary	=25.6 cm →	79.5 % of total

$$T_{Effective} = 0.795T_{Set} + 0.205T_{Cavity} \qquad 4\text{- }4$$

where T_{Set} is the set temperature in the actively-cooled cassette and T_{Cavity} is the measured, but not controlled, temperature in the cavity of the instrument.

A modification of the last method was made to minimise the influence of the cavity temperature. Instead of waiting for the EOF, conductance was only measured for a period of 1.00 min at each voltage for each temperature. Once again the plots of conductance were extrapolated to zero power to eliminate the effects of Joule heating.

Finally, the experimentally-determined values of γ were compared with values from the literature for 1:1 and 2:1 electrolytes.

4.2.2 Results and Discussion

The results of the Debye-Hückel-Onsager calculations are shown in **Figure 4- 1.** Values of G were calculated from 15 ºC to 35 ºC in increments of 2.5 ºC. The temperature coefficient of electrical conductance is the gradient of the plot suggesting $\gamma = 0.0212\ K^{-1}$. This value is significantly larger than the value used by Burgi, Salomon and Chien [102] and may reflect a slight error in q* which was based on the approximation for 1:1 electrolytes. At this pH = pK_{A2}, the buffered electrolyte contains approximately equal amounts of $H_2PO_4^-$(aq) and HPO_4^{2-}(aq) so that the electrolyte

contains approximately equal amounts of a 1:1 electrolyte and a 2:1 electrolyte. The conductivity cell was used to find values of κ in the temperature range 25 ºC – 45 ºC (see **Figure 4- 2**). The value obtained from the conductivity cell data, $\gamma = 0.0201\ K^{-1}$ is in good agreement with the previously published value.

Obtaining a value of γ using data from the CE instrument (see **Figure 4- 3**) is not as straightforward as values used for the calibration are obtained by extrapolation of *G* to *P/L* = 0 at each temperature. In the interests of clarity only 5 of the 9 plots are shown. A summary of the complete data set is shown in **Table 4- 1**.

Table 4- 1: Conductance Values Free of the Effects of Joule Heating (G_0) vs Effective Temperature.
Conditions: 32.2 cm fused-silica capillary, d_i = 74.0 µm, d_o = 362.8 µm, BGE 10.0 mM phosphate electrolyte at pH 7.21, EOF marker 20 % v/v acetone in BGE, pressure injection 2.0 kPa for 3.0 s, range of effective temperatures 18.4 ºC to 32.9 ºC

T_{Set} (ºC)	T_{Cavity} (ºC)	$T_{Effective}$ (ºC)	G_0 (x10^{-9}S)
17.5	22.0	18.4	1.632
20.0	24.8	21.0	1.819
22.5	28.4	23.7	1.890
25.0	24.9	25.0	1.957
25.0	29.5	25.9	1.941
27.5	26.4	27.3	2.049
27.5	28.6	27.7	1.973
30.0	26.6	29.3	2.093
35.0	24.9	32.9	2.176

A plot of relative conductance versus effective temperature (see **Figure 4- 4**) was prepared using the data from **Table 4- 1**. The value of γ obtained using data from the CE instrument (**Figure 4- 4**), $\gamma = 0.0184\ K^{-1}$ was significantly lower than the previous values. The discrepancy may reflect uncertainty in the temperature of the cavity and may also be due to a gradual change of temperature in the electrolyte vials which are not under thermostat control during electrophoresis.

The extrapolated data collected from the 1 min conductance runs showed better linearity than the conductance data collected with the EOF data shown in **Table 4- 1** and illustrated in **Figure 4- 4**. This improvement supports the hypothesis that there was a significant variation in the temperature of the electrolyte in the vials during the longer runs.

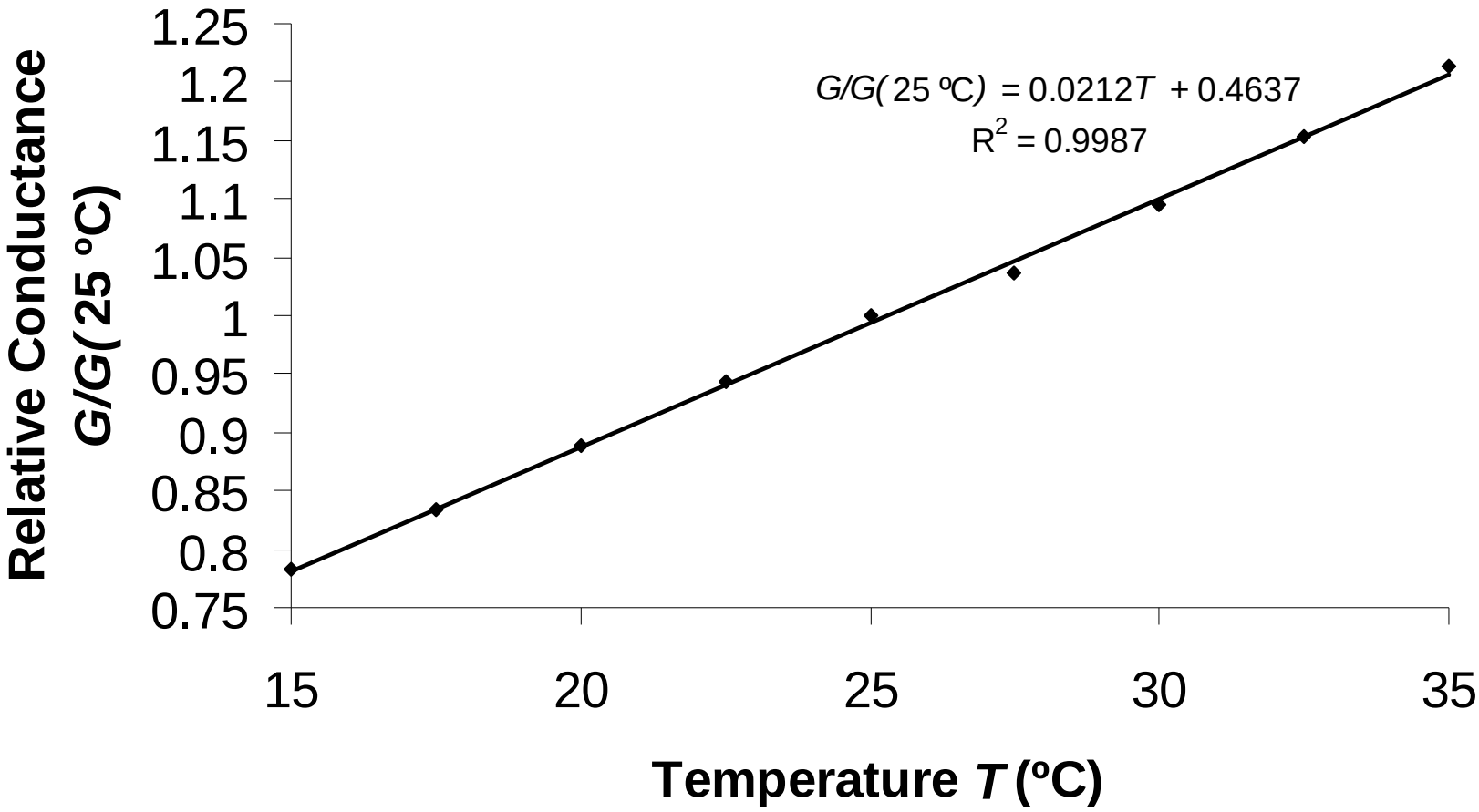

Figure 4- 1: Calculated values of relative conductance for 10mM phosphate electrolyte (pH = 7.21) using the modified form of the DHO equation (Eqn 4- 2)

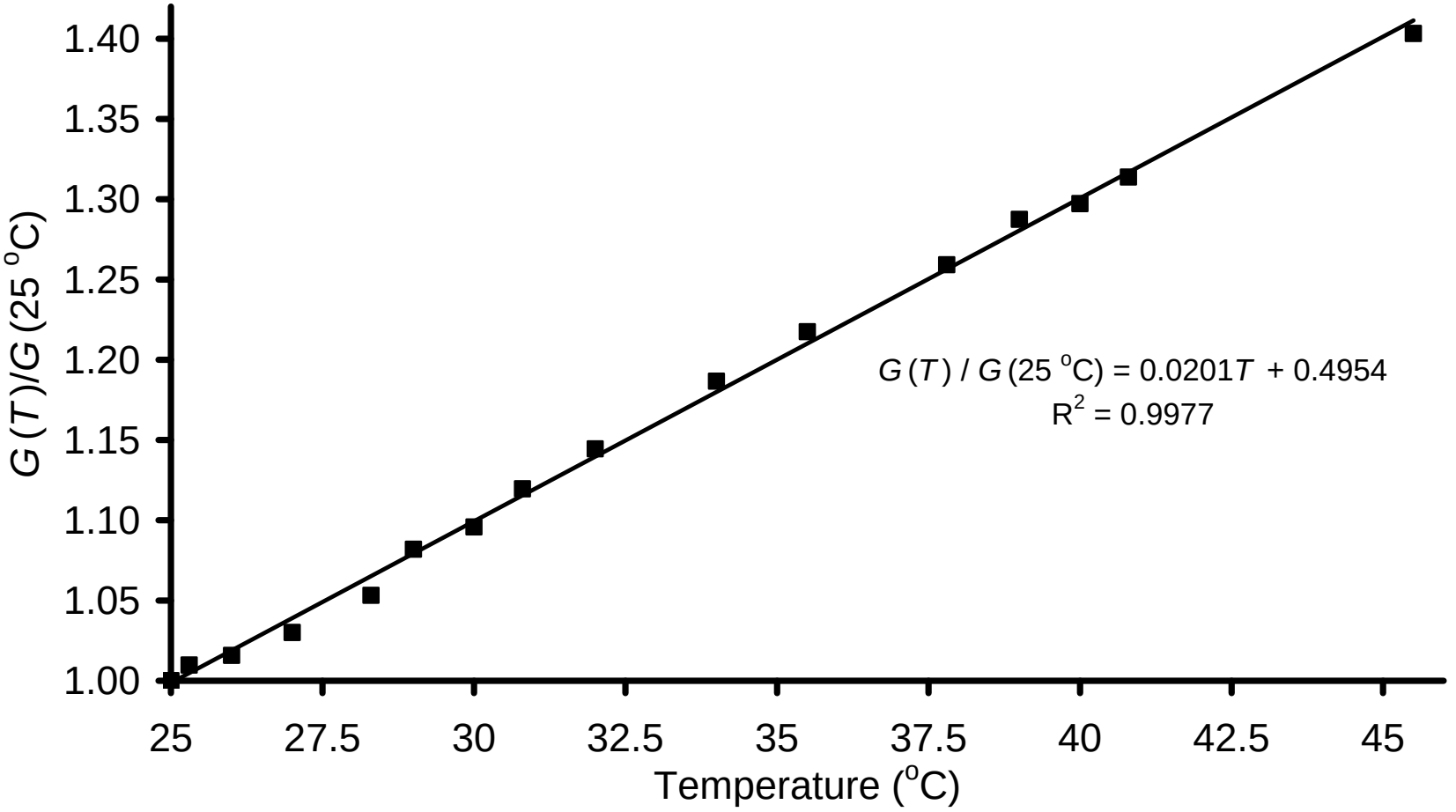

Figure 4- 2: Calculated values of relative conductance for 10mM phosphate electrolyte (pH = 7.21) using data collected from a conductivity cell.

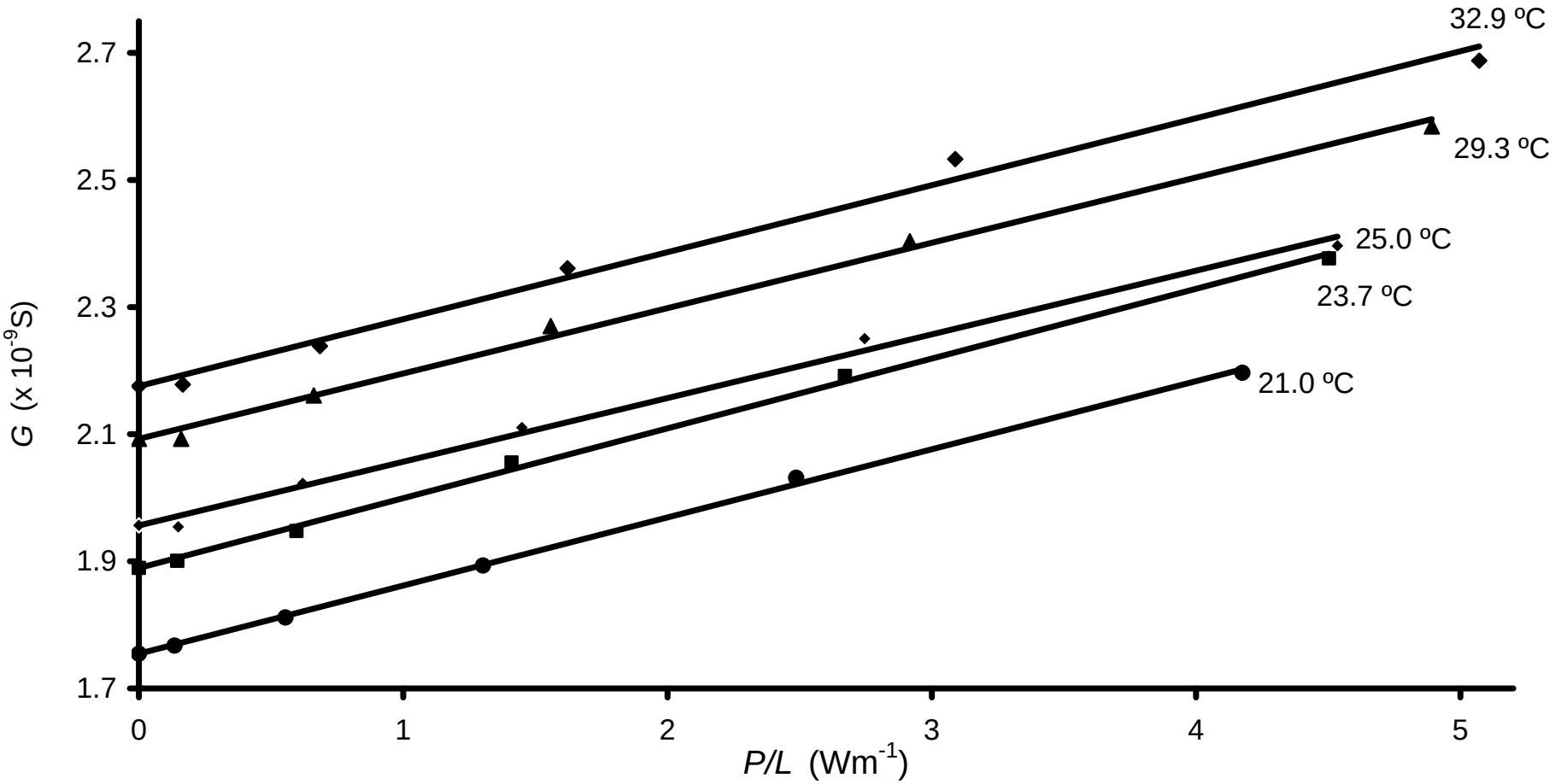

Figure 4- 3: Conductance values taken from the CE instrument for a range of effective temperatures.

Conditions: 32.2 cm fused-silica capillary, d_i = 74.0 µm, d_o = 362.8 µm, BGE 10.0 mM phosphate electrolyte at pH 7.21, EOF marker 20 % v/v acetone in BGE, pressure injection 2.0 kPa for 3.0 s, range of effective temperatures 21.0 ºC to 32.9 ºC

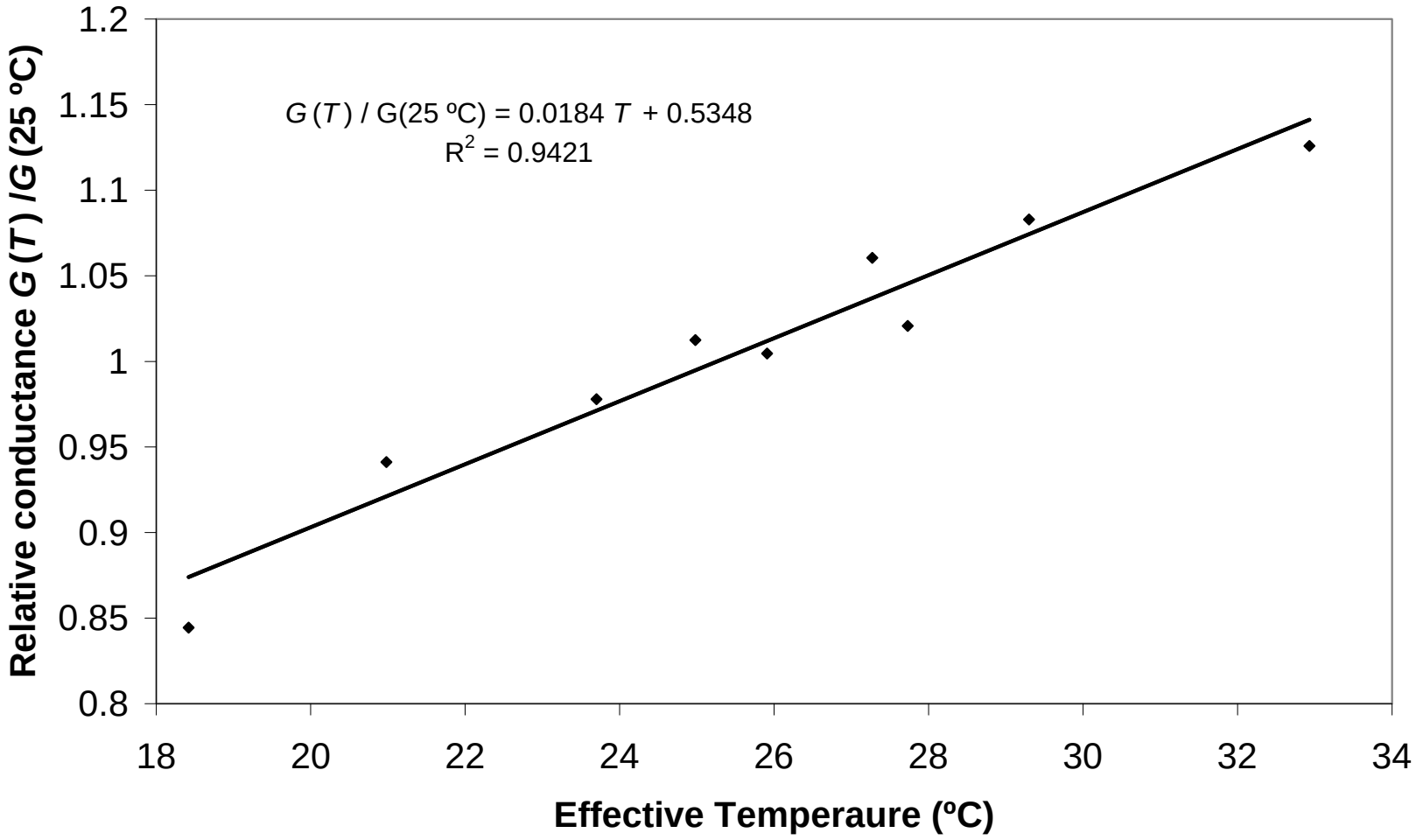

Figure 4- 4: Variation of Relative Conductance with Effective Temperature from CE Conditions: As in **Figure 4- 3**

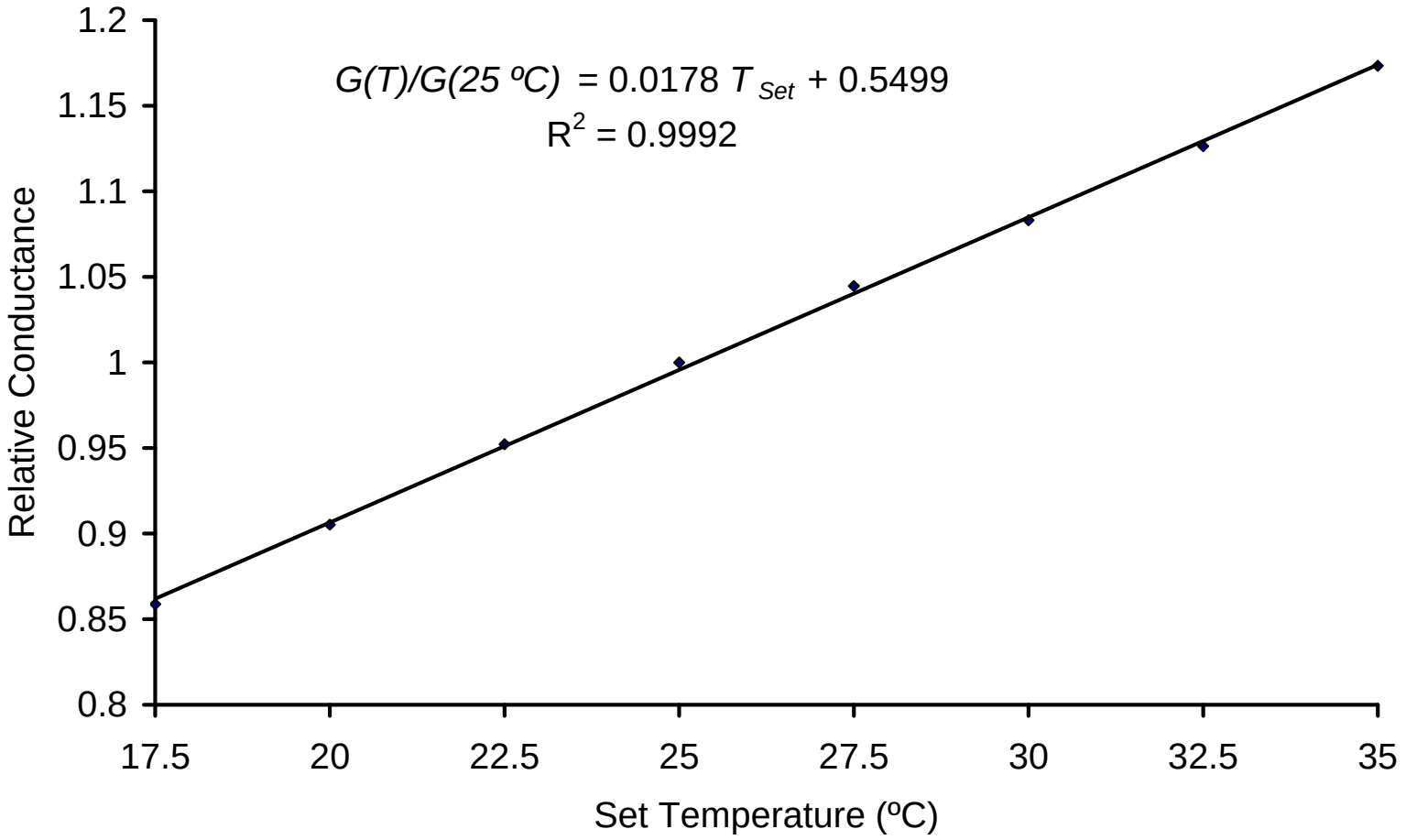

Figure 4- 5: Variation in relative conductance with set temperature using data collected from the CE instrument.

Conditions: 32.2 cm fused-silica capillary, d_i = 74.0 µm, d_o = 361.0 µm, BGE 10.0 mM phosphate electrolyte at pH 7.21, no injection

The gradient of **Figure 4- 5** is an estimate of γ (the temperature coefficient of conductance). The large discrepancies between the values of γ obtained from the DHO equation or conductivity cell and the values of γ obtained from conductance measurements using the CE instrument clearly demonstrate that a systematic error in measurement of current and/or voltage exists. This idea is explored further in Section 4.7 of this thesis.

Isono [90] determined γ experimentally for a wide range of electrolytes and found average values of γ = 2.02 % per ^{o}C for 1:1 electrolytes and 2.08 % per ^{o}C for 2:1 electrolytes. As the electrolyte used in this experiment contained approximately equal amounts of NaH_2PO_4 and Na_2HPO_4 (1:1 and 2:1 electrolytes), it is reasonable to assume γ=2.05 % per ^{o}C.

4.2.3 Conclusions

Eqn 4- 5 can be used to find the mean increase in temperature of the electrolyte (ΔT_{Mean}) from the set temperature.

$$\Delta T_{Mean} = \frac{G(T) - G_0}{\gamma G_0} = \frac{G(T) - G_0}{0.0205 G_0} \qquad 4\text{- }5$$

where *G(T)* is the conductance that results from Joule heating and G_0 is the conductance extrapolated to zero power at the set temperature [3] As a rule of thumb using γ =0.020 K^{-1} gives values of ΔT_{Mean} to within 5 %, but for more accurate values a calibration process is necessary. Given the complexity of the Debye-Hückel-Onsager equation, and the time taken to collect conductance data free from Joule heating effects over a range of temperatures from the CE instrument and the errors associated with these values, a reliable value of γ for a particular electrolyte is best obtained by preparing a calibration curve using a conductivity meter or by consulting the literature.

4.3 Calibrating Electroosmotic Mobility as a Temperature Probe

4.3.1 Experimental

The general details are given in Chapter 2. Detailed conditions are given in each figure caption. A similar approach to that used for measuring the variation of G_0 with $T_{Effective}$ was used to find the temperature coefficient for electroosmotic mobility (μ_{EOF})

using data collected from the CE instrument. The electroosmotic mobility was measured over a range of *P/L* values, and the graph of μ_{EOF} vs *P/L* extrapolated to *P/L* = 0 Wm^{-1} to obtain values of μ_{EOF} free from the effects of Joule heating (μ_{EOF}^{0}) at each effective temperature. The relative electroosmotic mobility was calculated by dividing the value of μ_{EOF}^{0} at the effective temperature by the value obtained at 25 ºC.

4.3.2 Results and Discussion

Figure 4- 6 shows the variation of electroosmotic mobility with *P/L* at each effective temperature. In the interests of clarity of presentation, only 5 of the 9 plots are shown. The graphs are essentially parallel and can be extrapolated to find the electroosmotic mobility free of Joule heating at each effective temperature. These data are summarised in **Table 4- 2**.

The values of μ_{EOF}^{0} at each effective temperature were divided by $\mu_{EOF}^{0}(25\ ºC)$ *to* find the relative electroosmotic mobility. A graph of $\mu_{EOF}^{0}(T)$ / $\mu_{EOF}^{0}(25\ ºC)$ versus the effective temperature is shown in **Figure 4- 7**. The gradient of this graph 0.0222 K^{-1} is equal to the temperature coefficient of electroosmotic mobility.

Table 4- 2: Electroosmotic Mobility Values Free of the Effects of Joule Heating ($\mu_{EOF}^{0}(T)$) vs Effective Temperature ($T_{Effective}$)
Conditions: 32.2 cm fused-silica capillary, d_i = 74.0 µm, d_o = 362.8 µm, BGE 10.0 mM phosphate electrolyte at pH 7.21, EOF marker 20 % v/v acetone in BGE, pressure injection 2.0 kPa for 3.0 s, range of effective temperatures 21.0 ºC to 32.9 ºC

T_{Set} (ºC)	T_{Cavity} (ºC)	$T_{Effective}$ (ºC)	μ_{EOF}^{0} ($x10^{-9}m^2s^{-1}V^{-1}$)
17.5	22.0	18.4	51.54
20.0	24.8	21.0	55.41
22.5	28.4	23.7	60.72
25.0	24.9	25.0	62.25
25.0	29.5	25.9	65.64
27.5	26.4	27.3	65.41
27.5	28.6	27.7	64.25
30.0	26.6	29.3	68.56
35.0	24.9	32.9	72.06

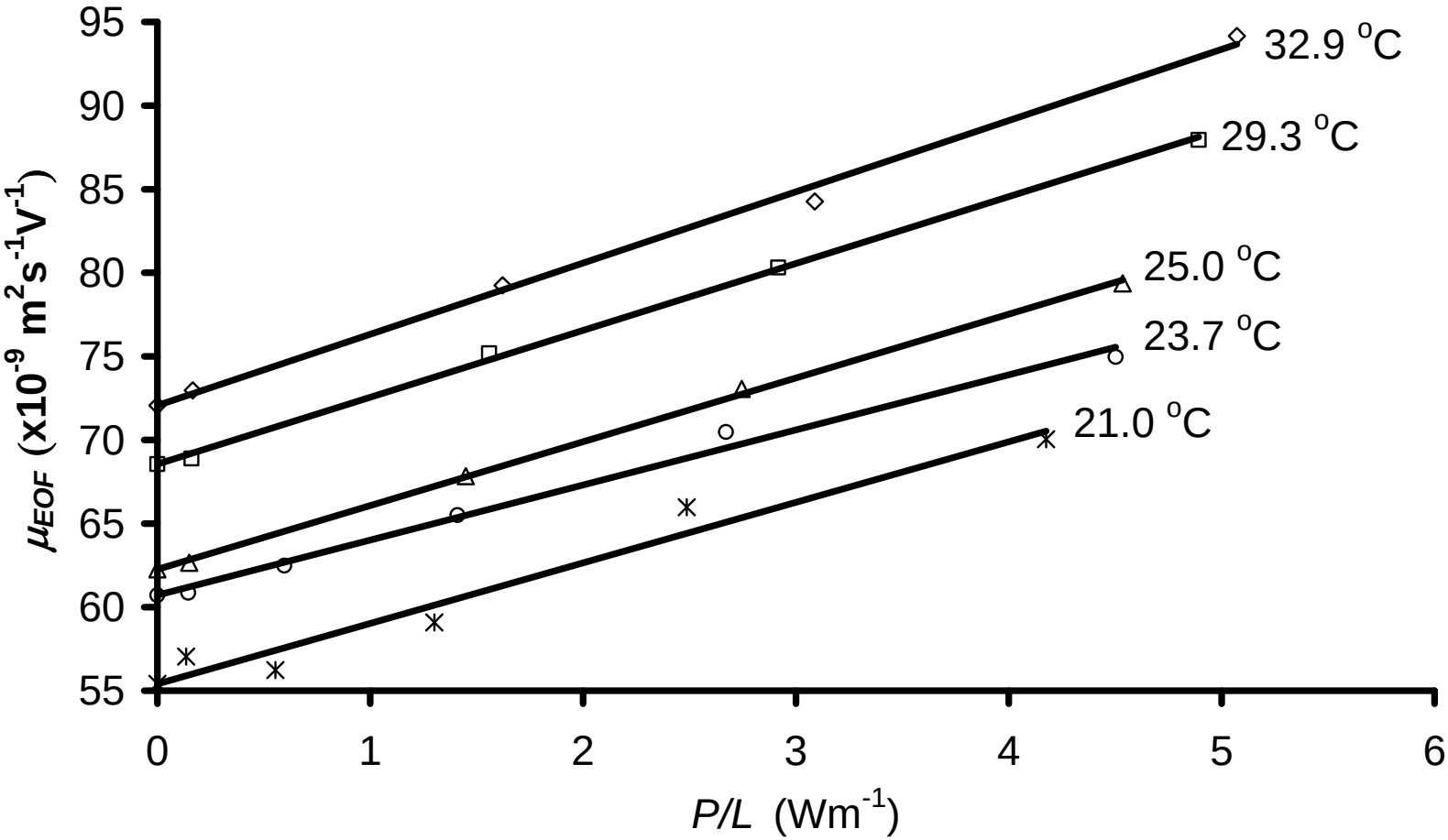

Figure 4- 6: Variation of electroosmotic mobility with power per unit length at a range of effective temperatures

Conditions**:** As in **Figure 4- 3**

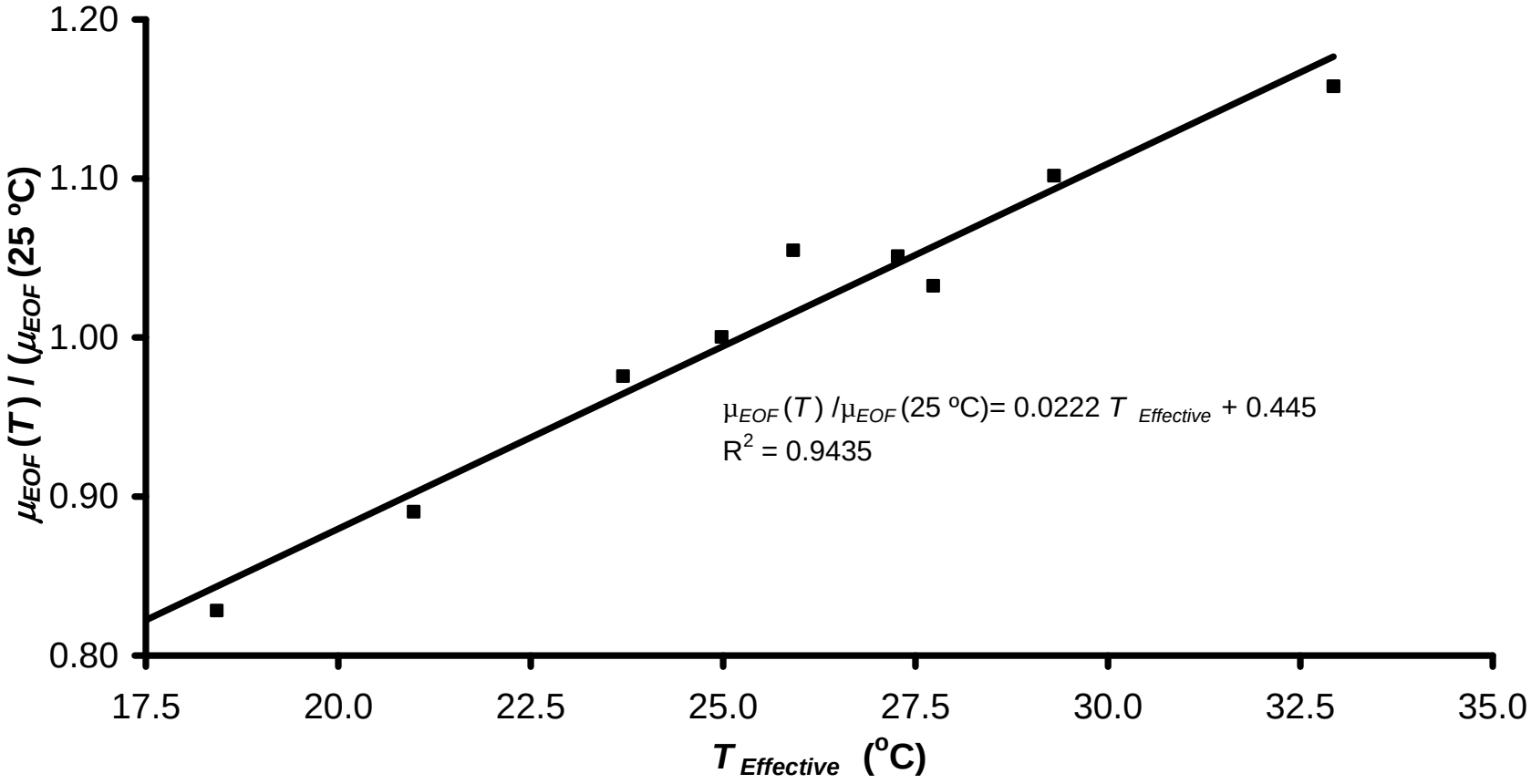

Figure 4- 7: Variation of Relative Electroosmotic Mobility with Effective Temperature

Conditions: As in **Figure 4- 3**

As the EOF is generated at the sheer plane (see **Figure 1- 2**), μ_{EOF} reflects the mean temperature a few nanometres from the inner wall of the capillary (T_{Wall}) rather than the mean temperature of the bulk electrolyte.

4.3.3 Conclusions

For the 10 mM phosphate electrolyte at pH =7.21, the average temperature of the electrolyte near the inner wall of the capillary during CE can be found by applying Eqn 4- 6.

$$T_{Wall} = \frac{\left(\frac{\mu_{EOF}}{\mu_{EOF}{}^{0}(T_{Set})} - 1 \right)}{0.0222} + T_{Set} \qquad 4\text{- }6$$

For other electrolytes, the procedure described in Section 4.3.1 can be performed to produce a calibration curve of relative electroosmotic mobility versus effective temperature and its gradient determined to find the temperature coefficient of μ_{EOF}. In practice, this is a rather time-consuming process. Section 4.5 demonstrates that T_{Wall} can be determined using the straightforward calculation shown in Eqn 3- 6.

4.4 Comparison of μ_{EOF} and *G* as temperature probes

4.4.1 Introduction

Knox and McCormack [53] found that the temperatures estimated from μ_{EOF} were consistently higher than that obtained from *G*. If as suggested above, *G* reflects the mean temperature of the bulk electrolyte (T_{Mean}) and μ_{EOF} the temperature of the electrolyte near the inner wall (T_{Wall}) we would expect *G* to yield higher temperatures. The discrepancy in Knox and McCormack's results comes from using the assumption that μ_{EOF} and *G* depend on the inverse of viscosity only.

4.4.2 Results and Discussion

A summary of the data averaged over 6 runs collected at a set temperature of 25.0 ºC is shown in **Table 4- 3**.

$T_{EOF(\eta)}$ is the temperature determined from interpolation of viscosity data assuming μ_{EOF} depends on $1/\eta$ only. $T_{EOF\ (0.0222\ K^{-1})}$ and $T_{G\ (0.0205\ K^{-1})}$ are determined using Eqn 4- 6 and Eqn 4- 1 respectively.

Table 4- 3: Raw data collected from CE for temperature determination

V (kV)	I (μA)	P/L (Wm^{-1})	G ($x10^{-9}$ S)	μ_{EOF} ($x10^{-9}m^2s^{-1}V^{-1}$)	$T_{EOF(\eta)}$ (ºC)	T_{EOF} $_{(0.0222\ K^{-1})}$ (ºC)	T_G $_{(0.0205\ K^{-1})}$ (ºC)
0.000	0.000	0.000	1.935	72.09	25.00	25.00	25.00
4.953	9.627	0.148	1.943	72.40	25.19	25.19	25.20
9.902	19.829	0.612	2.002	74.60	26.52	26.57	26.69
14.793	31.118	1.441	2.101	78.61	28.90	29.07	29.18
19.666	43.945	2.714	2.229	83.24	31.60	31.97	32.41
24.436	59.935	4.625	2.441	91.79	36.43	37.31	37.76
29.147	80.489	7.444	2.739	103.42	42.75	44.58	45.27

Conditions: As in **Figure 4- 3**

Superficially, it might appear that both methods of using μ_{EOF} are appropriate for finding the temperature of the electrolyte near the wall T_{Wall} as both methods consistently have $T_{Wall} < T_{Mean}$ as expected from the radial temperature profile (see **Figure 1- 4**). The predictions only appear to differ markedly at elevated power levels.

To demonstrate which of the two methods is superior for predicting T_{Wall}, a simple verification is performed by calculating the radial temperature difference (ΔT_{Radial}). This may be done by rearranging Eqn 3- 6 and comparing values with theoretical values from Eqn 3- 1.

$$\Delta T_{Radial} = 2(T_{Mean} - T_{Wall}) \qquad 4\text{- }7$$

Substituting λ =0.605 $Wm^{-1}K^{-1}$ for the thermal conductivity of the aqueous electrolyte at 25 ºC in Eqn 3- 1 generates Eqn , which can be used to find the theoretical radial temperature difference for any value of P/L.

$$\Delta T_{Radial} = 0.1315\frac{P}{L} \qquad 4\text{- }8$$

Figure 4-8 compares the predicted values of ΔT_{Radial} from the two methods of using μ_{EOF} to determine T_{Wall}. If one assumes that μ_{EOF} = k/η, where k is a constant, the predicted values of ΔT_{Radial} are too large by a factor of almost 5, however if Eqn 4- 6 is used to find the error in predicting ΔT_{Radial} is reduced by more than 71%.

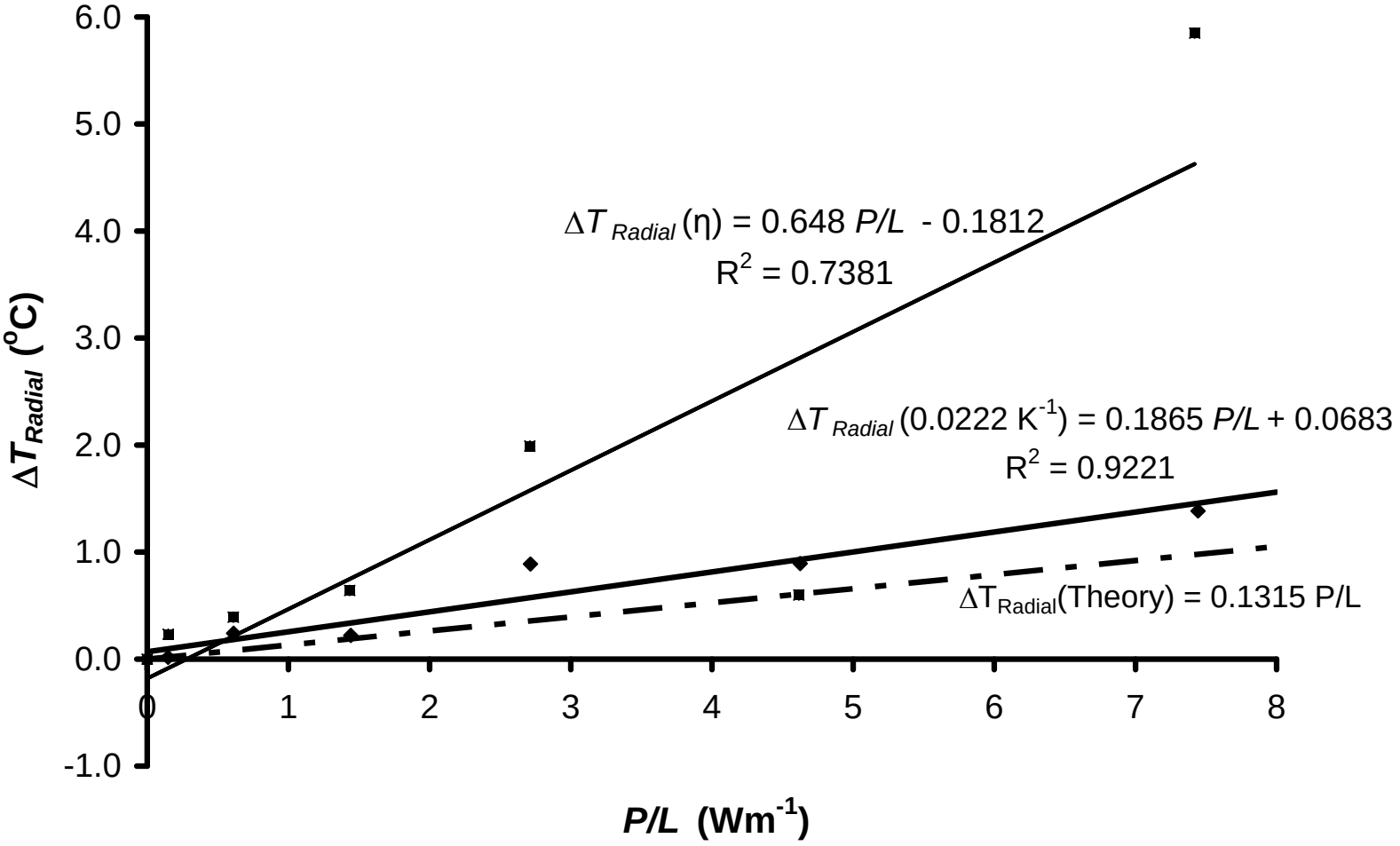

Figure 4- 8 Predicted radial temperature differences from theory and experiment

Conditions: As in **Figure 4- 3**

The approach that uses Eqn 4- 6 based on the calibration process described in Chapter 4.3 gives much better agreement with the theoretical values. The maximum deviation was ~0.5 ºC and most predictions were significantly more accurate.

4.4.3 Conclusions

The assumption that the product $\varepsilon\zeta$ is independent of temperature has been shown to be erroneous and leads to determinations of T_{Wall} that are smaller than expected. Unlike conductance which is a fairly rugged temperature probe, the electroosmotic mobility is well-known to be sensitive to many parameters, including changes to the surface charge and surface properties, electrolyte composition and the presence of impurities. Therefore, in principle, μ_{EOF} cannot generally be expected to be a robust probe for T_{Wall}. Another factor making μ_{EOF} unsuitable as a routine temperature probe is the need for a separate calibration curve for the variation of μ_{EOF} with temperature for each electrolyte as the gradient of the curve will vary. This time-consuming process is necessary as the electroosmotic mobility is affected by variations in the zeta-potential, dielectric constant and electrolyte composition, not just viscosity as was assumed previously.

Nevertheless, in this work a new method has been introduced to use μ_{EOF} as a temperature probe in order to validate the previously introduced method of temperature measurement based on conductance. The new method has demonstrated that if sufficient experimental care is exercised, temperatures can be determined accurately using measurements of either μ_{EOF} or G.

4.5 Using *G* to find T_{Wall}

4.5.1 Introduction

The previous sections have demonstrated that G and μ_{EOF} can be used as probes for T_{Mean} and T_{Wall} but the calibration process for the μ_{EOF} was highly time-consuming. Eqn 4- 9 illustrates an alternative approach for determining T_{Wall} from G.

$$T_{Wall} = T_{Mean} - \frac{1}{2}\Delta T_{Radial} \qquad \text{4- 9 (previously 3- 6)}$$

Substituting Eqn 2- 4 for T_{Mean} and Eqn 4- 8 for ΔT_{Radial} gives an expression for aqueous electrolytes if the set temperature is 25.0 ºC

$$T_{Wall} = 25.0\ ^{0}C + \frac{\left\{\frac{G_T}{G_0} - 1\right\}}{0.0205\ ^{\circ}C^{-1}} - 0.0658\frac{P}{L} \qquad 4\text{- }10$$

4.5.2 Results and Discussion

Figure 4- 9 illustrates predicted values of T_{Wall} using μ_{EOF} (Eqn 4- 6) and G (Eqn 4- 10). Both equations gave very similar results, with the gradients differing by less than 0.2 %. The maximum difference in predicted temperatures was 0.2 ºC; most predictions were within 0.1 ºC.

4.5.3 Conclusions

Eqn 4- 10 appears to be a simple and effective means for determining T_{Wall}. The clear advantage of using G over μ_{EOF} is the ease and speed with which calibration can be performed.

4.6 Calculation of a complete temperature profile for a fused-silica capillary

4.6.1 Introduction

A combination of the equations governing the radial temperature gradient in the electrolyte, the wall and the coolant surrounding the electrolyte and the variation of T_{Mean} with P/L enables the construction of a semi-quantitative temperature profile for a fused-silica capillary at any value of P/L.

A simplified model to describe the dissipation of heat energy from the capillary to the surroundings is that a thin cylindrical layer of static air surrounds the capillary, through which heat is transferred only by conduction (see **Figure 4- 10** for schematic diagram). This model makes the assumptions that the temperature at the outer edge of the layer is equal to the ambient temperature and that the air velocity at this location is zero. These simplifications are shown by the dotted line. In reality, heat energy is dissipated by a combination of conduction and convection when active-cooling is employed and unless the external capillary wall is porous or has a roughened surface, the air velocity only reaches zero at the surface.

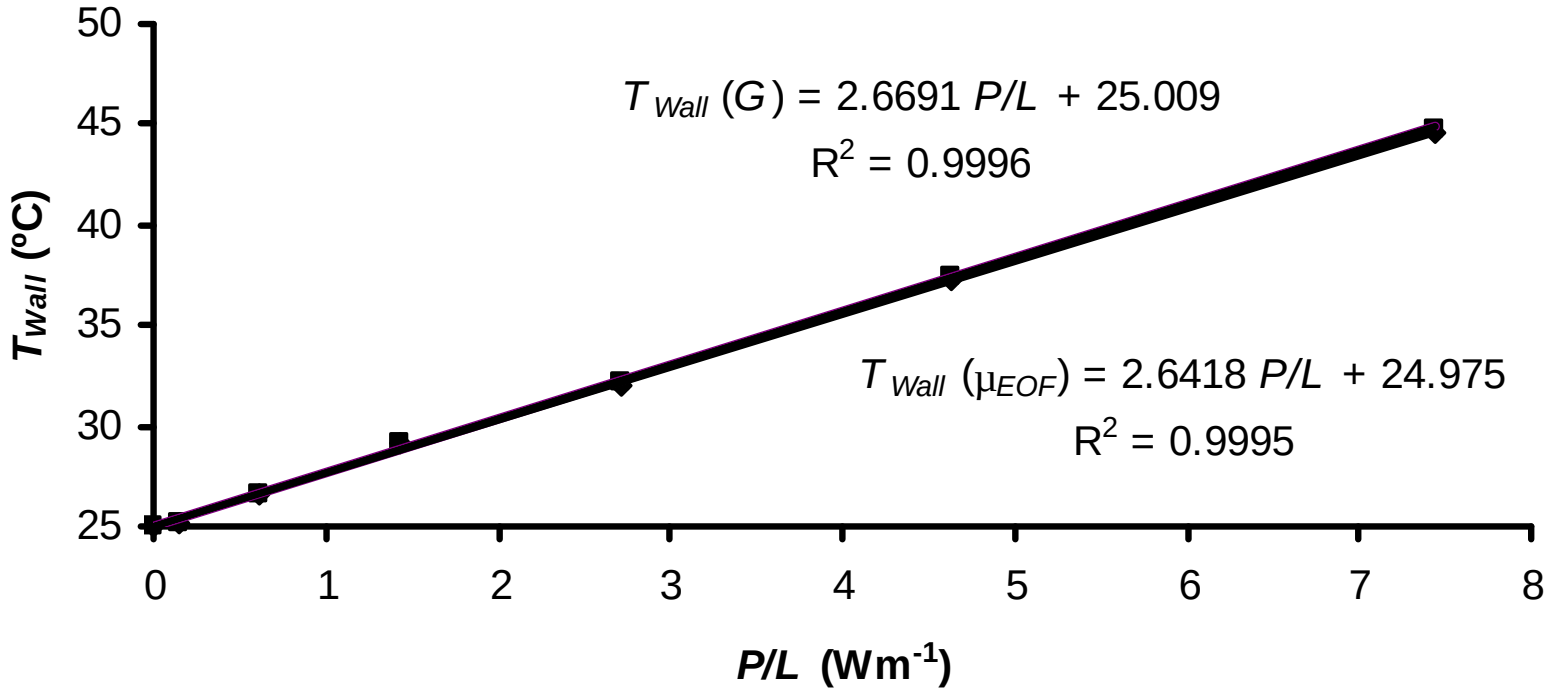

Figure 4- 9: Predicted wall temperatures using μ_{EOF} (♦)and G (■)as probes.
Conditions: As in **Figure 4- 3**

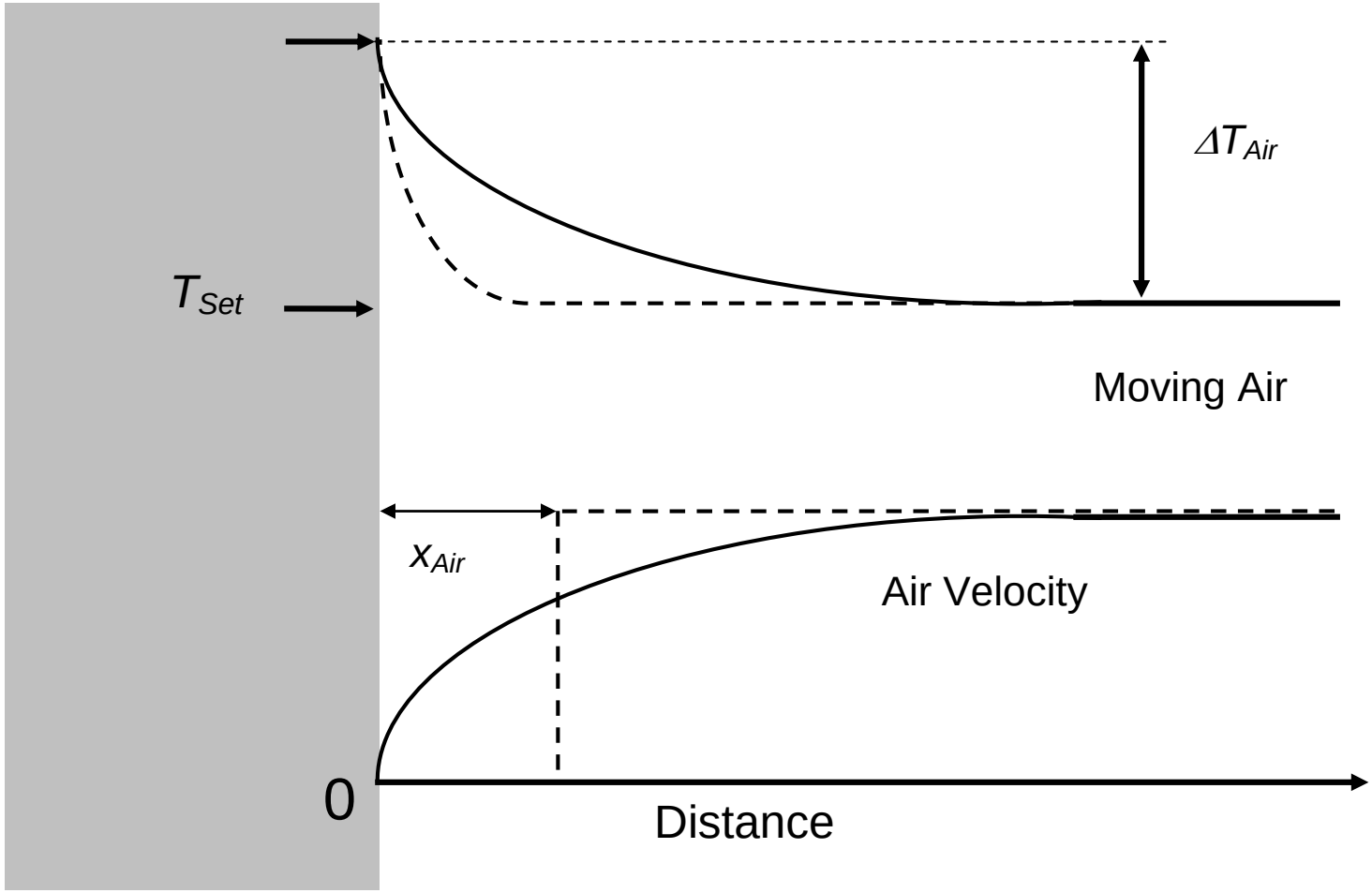

Figure 4- 10: Schematic diagram showing the temperature profile and velocity profile for the moving air and the static air layer model.

Key: Dashed line shows the simplified model and solid line shows expected variations in air temperature and velocity.

4.6.2 Theory

By rearranging Newton's Law of Cooling (Eqn 1- 17), it is possible to derive Eqn 4- 11 to give an expression for ΔT_{Air} in terms of h the heat transfer coefficient or x_{Air} the thickness of the static air layer. It should be noted that in this form, the equation is more appropriate to rectangular slabs [83] rather than the cylindrical capillaries encountered in CE, nevertheless, this approach does allow estimation of the thickness of the static air layer (x).

$$\Delta T_{Air} = \frac{P}{hA} = \frac{Px}{\lambda_{Air} A} \qquad 4\text{- }11$$

where A is the surface area through which the heat is conducted. As one would expect, the larger the heat transfer coefficient, the smaller will be the thickness of the static air layer. It may be shown by rearranging 4- 11 that the thickness of this layer is independent of the material from which the capillary is made and depends only on its heat transfer coefficient and the thermal conductivity of the air (λ_{Air}) [55, 83]

The thickness of the static air layer can be approximated by using Eqn 4- 12.

$$x = \frac{\lambda_{Air}}{h} \qquad 4\text{- }12$$

An accurate knowledge of the heat transfer coefficient is required to enable a complete temperature profile of the capillary to be calculated. As demonstrated in Section 1.3.2.3, h can be calculated if the velocity of the coolant and the external diameter of the capillary are known via calculation of the Reynolds number and the Nusselts number. An alternative approach for calculating h is suggested by Eqn 4- 13, which enables h to be calculated from ΔT_{Air}.

$$h = \frac{1}{\pi d_o \Delta T_{Air}} \bullet \frac{P}{L} \qquad 4\text{- }13 \text{ (previously 1- 18)}$$

Section 3.1 demonstrated the relationship between T_{Mean}, T_{Wall} and T_{Axis}, which can all be determined experimentally. It follows that by rearranging Eqn 1- 15 and using the relationship between T_{Mean} and T_{Axis} (see Eqn 3- 7), ΔT_{Air} can be calculated by subtracting half of the radial temperature difference across the electrolyte (ΔT_{Radial}) and the temperature difference across the wall of the capillary (ΔT_{Wall}) from ΔT_{Mean}, as shown in Eqn 4- 14.

$$\Delta T_{Air} = \Delta T_{Mean} - \tfrac{1}{2}\Delta T_{Radial} - \Delta T_{Wall} \qquad 4\text{- }14$$

This method of finding ΔT_{Air} allows the heat transfer coefficient to be calculated for the instrument using Eqn 4- 14 without knowing the actual velocity of the actively-cooled air.

The linear relationship between ΔT_{Radial} and P/L was previously demonstrated in Eqn 3- 1. By rearranging Eqns 4- 14 and 1- 12, it may be shown that ΔT_{Air} and ΔT_{Wall} depend linearly on the power per unit length.

$$\Delta T_{Wall} = \frac{Q d_i^{\,2}}{8\lambda_{Wall}} \ln\left(\frac{d_o}{d_i}\right) = \frac{4P d_i^{\,2}}{\pi d_i^{\,2} 8\lambda_{Wall}} \ln\left(\frac{d_o}{d_i}\right) = \frac{1}{2\pi\lambda_{Wall}} \ln\left(\frac{d_o}{d_i}\right) \bullet \frac{P}{L} \qquad 4\text{- }15$$

4.6.3 Experimental

The data collected for **Table 4- 3** were used to plot the increase in the mean electrolyte temperature (ΔT_{Mean}) with P/L. The calculated increase in temperature of the electrolyte near the inner wall of the capillary ($\Delta T_{At\ Wall}$) and at the axis of the capillary ($\Delta T_{At\ Axis}$) using Eqn 3- 6 and Eqn 3- 7 are shown for comparison.

Microsoft Excel was used to calculate a complete temperature profile for the fused-silica capillary for increasing distance (r) from the central axis in increments of 0.1 µm until the temperature reached the set temperature. Eqn 1- 16 was modified so that the temperature in the electrolyte was calculated as a function of P/L for $0 \le \pm r \le 37.0$ µm using 4- 16.

$$T(r) = T_{Set} + \frac{1}{2\pi}\left(\frac{1}{\lambda_{FS}} \ln\left(\frac{d_{FS}}{d_i}\right) + \frac{1}{\lambda_{PI}} \ln\left(\frac{d_{PI}}{d_{FS}}\right) + \frac{2}{d_{PI} h} + \frac{1}{2\lambda}\left(1 - \frac{r^2}{R^2}\right)\right) \bullet \frac{P}{L} \qquad 4\text{- }16$$

For the capillary under investigation, the temperature at the inner wall (T_{Wall}) is essentially equal to T(37.0µm). Eqn 4- 17 was used to find the temperature within the fused-silica itself for 37.0 µm ≤ r ≤.160.4 µm where $|r|$ denotes the absolute value of r.

$$T(r) = T_{Wall} - \frac{1}{2\pi\lambda_{FS}} \ln\left(\frac{|r|}{R}\right) \bullet \frac{P}{L} \qquad 4\text{- }17$$

The temperature within the poly(imide) layer was calculated for 160.4 µm ≤ $\pm r$ ≤ 181.4 µm using Eqn 4- 18.

$$T(r) = T(160.4) - \frac{1}{2\pi\lambda_{PI}} \ln\left(\frac{|r|}{160.4}\right) \bullet \frac{P}{L} \qquad 4\text{- }18$$

Lastly, the temperature inside the stagnant air layer was calculated for 181.4 µm < *r* using Eqn 4- 19. The process was continued till $T(r) = T_{Set}$.

$$T(r) = T(181.4) - \frac{1}{2\pi\lambda_{Air}} \ln\left(\frac{|r|}{181.4}\right) \bullet \frac{P}{L} \qquad 4\text{- }19$$

4.6.4 Results and Discussion

For the instrument used in this work, the velocity of the air stream is reported to be 10 ms^{-1} and the fused silica capillary has an external diameter of 362.8 µm. The corresponding values for the Reynolds number and the Nusselts number are R_e = 231 and N_u =7.77, which predict h = 561 $Wm^{-2}K^{-1}$ for the part of the capillary under active-cooling.

Figure 4- 11 demonstrates that ΔT_{Mean} (calculated from the conductance) depends linearly on the power per unit length and increases at the rate of 2.715 ºC for each additional Wm^{-1}. As all of the temperature changes in Eqn 4- 14 depend linearly on *P/L*, it is simple to calculate ΔT_{Air} for a fused-silica capillary at P/L = 1.000 Wm^{-1} using Eqn 4- 20. The thermal conductivity data are found in **Table 1- 1** and the radial dimensions of the capillary are d_i = 74.0 µm, d_{FS} =320.8 µm, d_{PI} =362.8 µm for the internal diameter of the capillary, the external diameter of the fused-silica and the external diameter of the poly(imide) coating, respectively.

$$\begin{aligned}\Delta T_{Air} &= \Delta T_{Mean} - \tfrac{1}{2}\Delta T_{Radial} - \Delta T_{FS} - \Delta T_{PI} \\ &= \Delta T_{Mean} - \left[\frac{1}{8\pi\lambda} + \frac{1}{2\pi\lambda_{FS}} \ln\left(\frac{d_{FS}}{d_i}\right) + \frac{1}{2\pi\lambda_{PI}} \ln\left(\frac{d_{PI}}{d_{FS}}\right)\right] \bullet \frac{P}{L}\end{aligned} \qquad 4\text{- }20$$

Substitution of the data into Eqn 4- 20 gives ΔT_{Air} = 2.356 ºC.

By substituting ΔT_{Air} = 2.356 ºC into Eqn 1- 18, the value obtained for the heat transfer coefficient is h = 372 $Wm^{-2}K^{-1}$, which is significantly less than the value of h = 561 $Wm^{-2}K^{-1}$ calculated from the Nusselts number and an air velocity of 10 ms^{-1}. There are two reasons for this apparent discrepancy. Firstly, ΔT_{Air} yields an average value of h for the whole capillary, of which less than 80 % was under active-cooling, so that a lower value of h is inevitable using this technique.

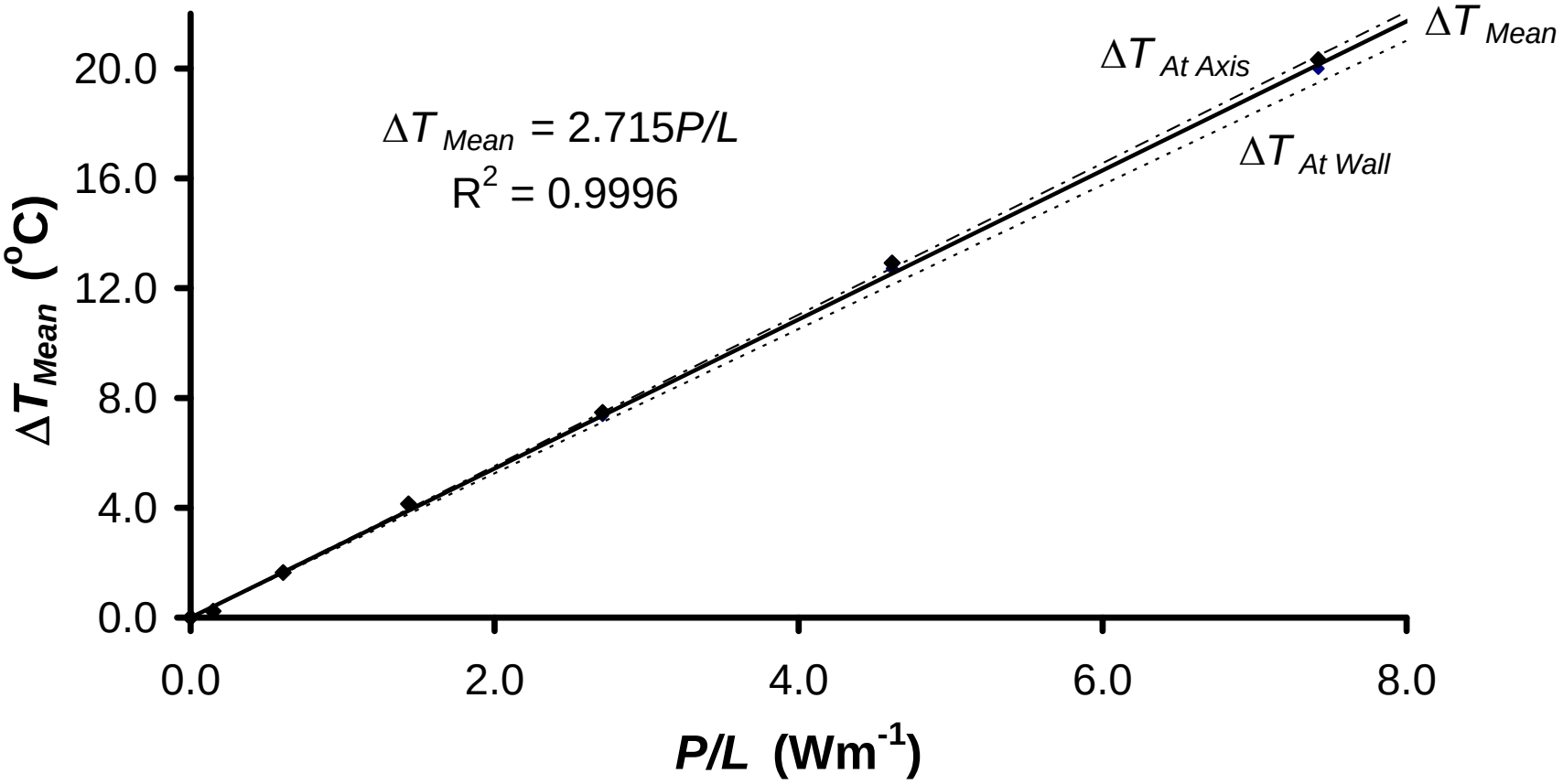

Figure 4- 11: Change in the mean electrolyte temperature and change in electrolyte temperature at the axis and near the inner wall of the capillary.

Conditions: As in **Figure 4- 3**.

Secondly, it would appear that the actual air velocity experienced by the capillary within the actively-cooled cassette was less than 10 ms^{-1}. It is possible to estimate the actual velocity of the air used in active cooling by assuming that the measured value of *h* is a weighted average of *h* for the passively cooled and actively cooled sections of the capillary (see Eqn 4- 4)

$$h_{Measured} = 0.205h_{Passive} + 0.795h_{Active} \qquad 4\text{- }21$$

A small computer fan was used to circulate the air in the cavity in which the passively cooled part of the capillary was housed. An estimate of $h_{Passive}$ based on **Table 1- 2** is 130 $Wm^{-2}K^{-1}$; rearrangement of Eqn 4- 21 suggests that h_{Active} = 435 $Wm^{-2}K^{-1}$. Working backwards using Eqns 1- 22 to 1- 24 suggests an average air speed of approximately 5.8 ms^{-1}.

An approximation for the thickness of the stagnant air layer (*x*) can be found by substituting λ_{Air} = 0.0266 $Wm^{-1}K^{-1}$ and *h* = 372 $Wm^{-2}K^{-1}$ into Eqn 4- 12 to give *x* = 70.7 µm for this capillary. This is an approximation as this equation is more appropriate for rectangular blocks than for concentric cylinders.

It is also possible to calculate x_{Air} by treating the static air layer as a cylindrical wall made of air for which the temperature difference is known.

$$\Delta T_{Air} = \frac{1}{2\pi\lambda_{Air}} \ln\left(\frac{d_{Air}}{d_{PI}}\right) \bullet \frac{P}{L} \qquad 4\text{- }22$$

where d_{Air} is the external diameter of the static air layer. Rearrangement of Eqn 4- 22 enables d_{Air} to be calculated.

$$d_{Air} = d_{PI} e^{\frac{2\pi\lambda_{Air}\Delta T_{Air} L}{P}} \qquad 4\text{- }23$$

Substitution of ΔT_{Air} = 2.356 ºC into Eqn 4- 23 yields d_{Air} = 537.9 µm (see **Figure 4- 12**). As the capillary and the stagnant air layer are concentric cylinders, the thickness of the air layer *x* is half the difference in their external diameters.

$$x = \frac{d_{air} - d_{PI}}{2} \qquad 4\text{- }24$$

This second approach to finding x_{Air} gives a slightly larger value than that from Eqn 4- 12; $x_{Air} \approx$ 87.5 µm.

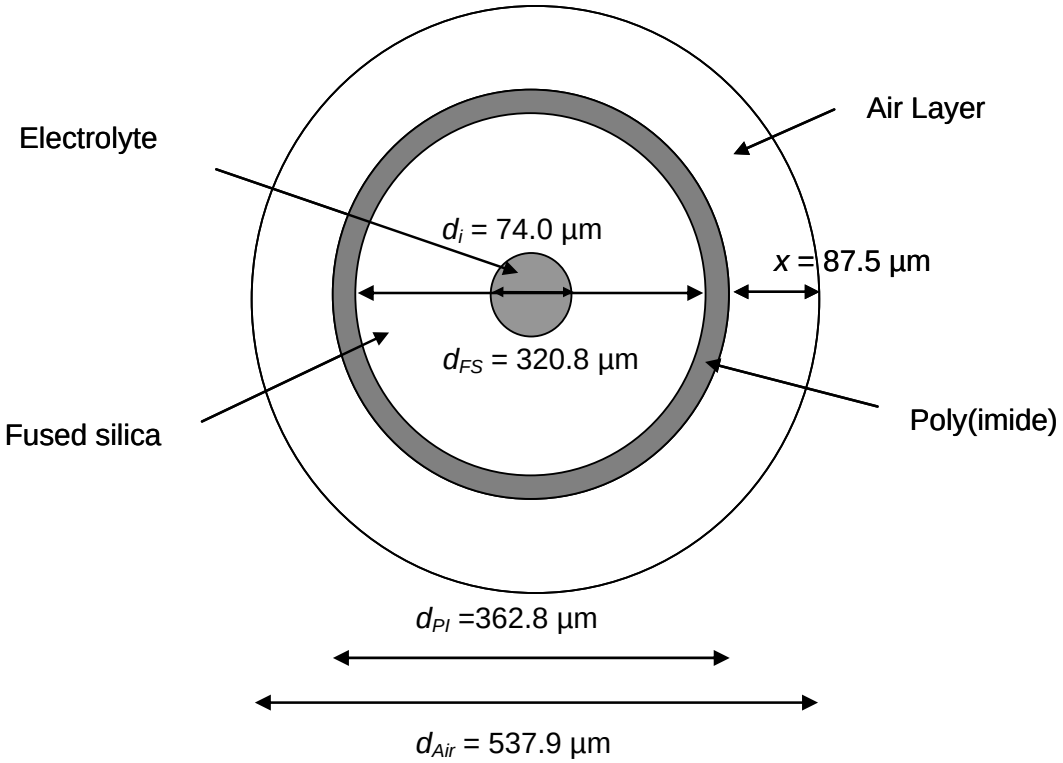

Figure 4- 12: Schematic diagram of the fused-silica capillary

A plot of the calculated temperature excess at P/L = 1.00 Wm^{-1} versus radial distance is shown in **Figure 4- 13**. For higher values of P/L each section of the graph would be correspondingly steeper as each of the temperature changes increases linearly with P/L. It is interesting to note that the temperature differences across the electrolyte and across the fused-silica and poly(imide) walls are approximately equal, but are dwarfed by the temperature difference across the stagnant air layer. It would appear that the increase in temperature of the electrolyte could be minimised by excluding the stagnant air layer by means of liquid or solid-state cooling.

4.6.5 Conclusions

The shape of the graph in **Figure 4- 13** is an approximation of the average temperature profile over the whole length of the capillary; for this reason the profile is semi-quantitative. In reality, the thickness of the static air layer will tend to be smaller in the section of the capillary under thermostat control and larger in the passively-cooled sections. Obviously, the temperature excesses in the thermostat-controlled part of the capillary will be lower than those parts with no temperature control. The calculations of *h*

illustrated in Section 4.6.4 will agree better with *h* calculated using empirical calculations in longer capillaries for which the fraction of the capillary with no temperature control will be significantly smaller.

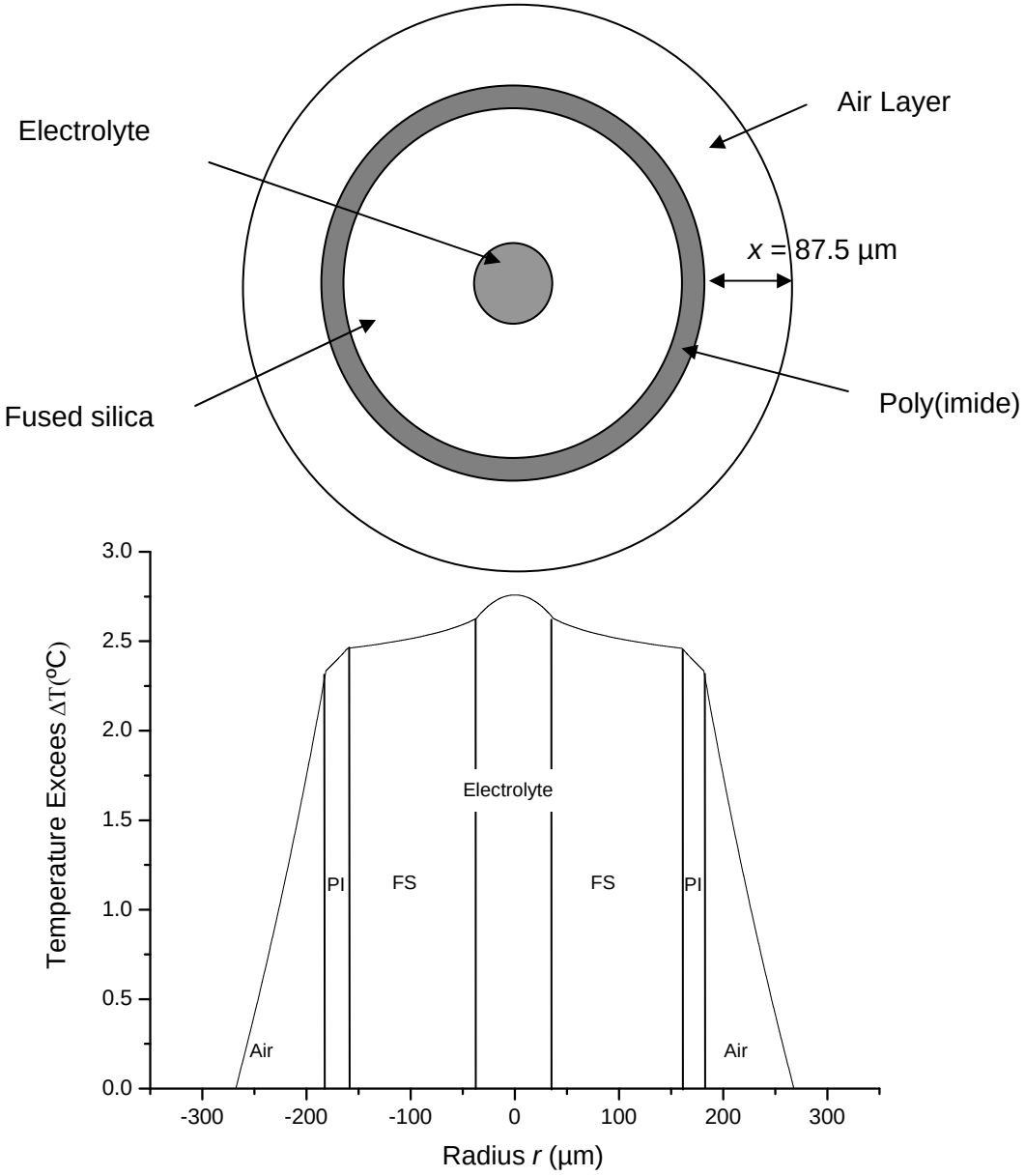

Figure 4- 13: Calculated temperature excess for a fused-silica capillary.
Conditions: As in **Figure 4- 3** with *P/L* = 1.00 Wm^{-1} and h = 372 $Wm^{-2}K^{-1}$.

4.7 Investigation of an alternative method for determining *h*.

4.7.1 Introduction

Section 4.2 suggested that there may be systematic errors in measuring current and or voltage. These errors become apparent at low voltages when the calculated conductance values deviate significantly from values extrapolated to zero power.

The purpose of this section is to introduce a novel method, based on curve-fitting of plots of conductance versus voltage, to calculate several important parameters including the systematic errors in the current and the voltage, the mean increase in temperature of the electrolyte, the heat transfer coefficient, the conductance free of Joule heating effects the voltage that causes autothermal runaway to occur, and the overall heat transfer coefficient.

4.7.2 Theory

To use the variation in conductance with voltage to determine *h* requires rearrangement of Eqns 1- 24 to 1- 26 and 1- 29 to be rewritten in terms of *G* and *V*. Rearrangement of 1- 26 results in Eqn 4- 25 which shows how conductance varies with the mean temperature of the electrolyte.

$$G = G_0 + \gamma G_0 \Delta T_{Mean} \qquad \text{4- 25}$$

Eqn 1- 25 is rewritten as Eqn 4- 26.

$$\Delta T_{ref} = \frac{\kappa_0 E^2 r_i^{\,2}}{\lambda} = \frac{G_0 L_{tot}}{\pi r_i^{\,2}} \bullet \frac{V^2 r_i^{\,2}}{\lambda L_{tot}^{\,2}} = \frac{G_0 V^2}{\pi \lambda L_{tot}} \qquad \text{4- 26}$$

Eqn 1- 24 becomes Eqn 4- 27.

$$k^* = \sqrt{\gamma \Delta T_{ref}} = \sqrt{\frac{\gamma G_0 V^2}{\pi \lambda L_{tot}}} \qquad \text{4- 27}$$

Eqn 1- 29 may be rearranged to produce Eqn 4- 28.

$$\Delta T_{Mean} = \frac{G_0 V^2}{2\pi L_{tot} h_{OA} r_i - \gamma G_0 V^2} \qquad \text{4- 28}$$

Substituting ΔT_{Mean} into Eqn 4- 25 leads to Eqn 4- 29.

$$G = G_0\left(\frac{1}{1-\frac{\gamma G_0 V^2}{2\pi r_i h_{OA} L_{tot}}}\right) = \frac{G_0}{1-k_1 V^2} \qquad 4\text{- }29$$

where $k_1 = \gamma G_0 / 2\pi r_i h_{OA} L_{tot}$.

Complete derivations of Eqn 4- 28 and Eqn 4- 29 are shown in Appendix 3.

Autothermal runaway occurs when the denominator in Eqn 4- 29 equals zero. It follows that the voltage that causes autothermal runaway V_{max} can be predicted if k_1 is known.

$$V_{\max} = \sqrt{\frac{1}{k_1}} \qquad 4\text{- }30$$

4.7.3 Experimental

Apparatus

Experiments were performed on an HP^{3D} CE, (Agilent, Palo Alto USA) capillary electrophoresis instrument at Charles University (Prague, Czech Republic). Similar fused-silica capillaries were used to those previously described, however, the outer diameter was 361.0 µm (including the 19.0 µm thick poly(imide layer), the total length was 33.3 cm and no cooling was available for the vial-tray. Preparation of the capillaries was similar to that described previously. Experiments were repeated at the University of Tasmania where cooling of the vial tray was also possible.

Chemicals

All solutions were prepared using Milli-Q (18 MΩ-cm) water. The buffer electrolyte (BGE) was prepared using AR grade NaH_2PO_4 2 H_2O and AR grade Na_2HPO_4 (Sigma). The 10 mM phosphate buffer (pH 7.21), by weighing out the two salts to prepare the electrolyte composed of 4.00 mM NaH_2PO_4 and 6.00 mM Na_2HPO_4.

Procedure

The current and voltage were monitored at a sampling-rate of 20 Hz throughout each run for a period of 1.00 min with set voltages of 0.5, 1.0, 1.5, 2.0, 2.5, 3.0, 3.5, 4.0, 5.0, 6.0, 7.0, 8.0, 12.0, 18.0, 24.0 and 30.0 kV using the Chemstation software. Values of conductance and the power per unit length were calculated for each point in time before averaging. The procedure was carried out for a range of set temperatures from 17.5 ºC to 35.0 ºC in increments of 2.5 ºC

4.7.4 Results and Discussion

A typical conductance versus voltage graph is shown in **Figure 4- 14**. On first viewing its shape is somewhat puzzling. While Joule heating explains the approximately parabolic shape of the graph for $V > 4.0$ kV, the increase of conductance with decreasing voltage is nonsensical, as at low voltages, it should plateau. It appears that systematic errors in the current and/or voltage measurement do exist. Obviously for G to be too high, the measured current must be too high or the measured voltage too low. The error in the measured current is referred to as the offset current (I_0) and the error in voltage as the offset voltage (V_0). These errors have a negligible influence at high voltages but exert a substantial effect as the size of the error approaches the parameter being measured.

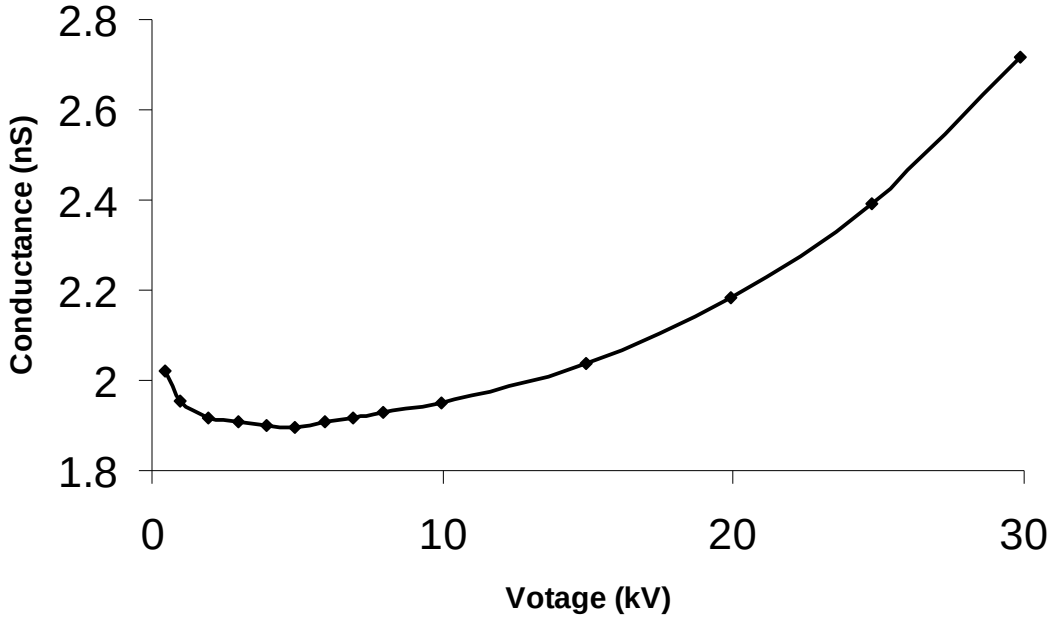

Figure 4- 14: Variation of conductance with voltage at a set temperature of 25 ºC
Conditions: As in **Figure 4- 5**

The data were fitted using ”Origin” software. The relationship used for curve-fitting was similar to Eqn 4- 29, but also included the influences of I_0 and V_0 (the error in the voltage).

$$G = \frac{I_0}{V - V_0} - \frac{G_0}{1 - \frac{k_1}{(V - V_0)^2}} \qquad 4\text{- }31$$

The analysis suggested that the recorded values of the current were consistently too high; the systematic error in the current I_0 averaged 0.08 µA. Voltage readings were usuallly too low, the average systematic error was -100 V.

Table 4- 4 compares the two methods of calculating G_0: extrapolation of a plot of G vs P/L to zero power, and curve-fitting using Eqn 4- 31. Generally speaking, there was good agreement between the values of G_0 predicted from the two methods.

Table 4- 4: Variation of Conductance Free of Joule Heating with Temperature.

G_0 Values Generated by Extrapolation of Data from 5 – 30kV plots and G_0* values were generated using Eqn 4- 31. Conditions as in **Figure 4- 5**.

T (°C)	G_0 (nS)	R^2	G_0*(nS)	R^2	I_0 (µA)	V_0 (kV)	k_1 x 10^{-6} kV^{-2}	V_{Max} (kV)
17.5	1.608	0.9997	1.609	0.9995	0.05	-0.36	316.0	56.3
20.0	1.617	0.9995	1.697	0.9995	0.06	0.01	327.0	55.3
22.5	1.708	0.9997	1.782	0.9994	0.07	0.05	339.0	54.3
25.0	1.884	0.9999	1.870	0.9996	0.09	-0.11	350.9	53.4
27.5	1.879	0.9999	1.885	0.9921	0.11	-0.18	298.9	57.8
30.0	1.946	1.0000	1.944	0.9992	0.00	0.45	350.8	53.4
32.5	2.022	0.9994	1.999	0.9979	0.19	-0.58	332.9	54.8
35.0	2.110	1.0000	2.100	0.9999	0.07	-0.03	349.5	53.5

Both techniques gave a more reliable estimate of the conductance at a particular temperature free of the effects of Joule heating than selecting data from say 1 kV (as was previously advocated by Porras et al. [49]) due to the significant error in measuring conductance at low voltage, as illustrated in **Figure 4- 14**. There appears to be no clear trend in the values of k_1 (which relate to the cooling efficiency) or in the values of V_{max}, suggesting that the cooling efficiency was not influenced greatly by the set temperature.

A clear advantage of using curve-fitting is illustrated in the plot of G vs P/L shown in **Figure 4- 15**. As one would expect from the previous discussion, the raw data are

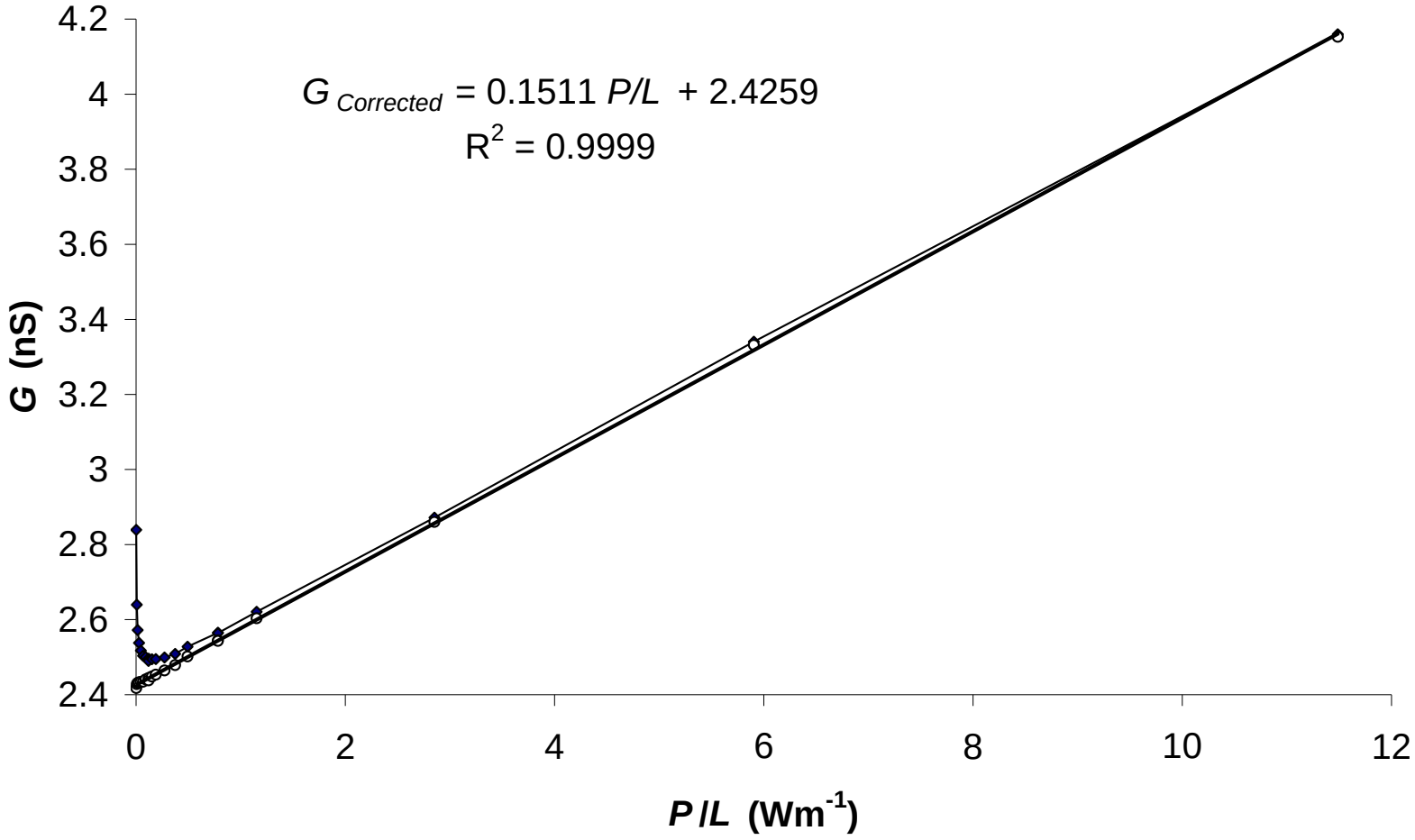

Figure 4- 15: Plot of conductance vs power per unit length for data collected from V = 0.5 kV to 30.0 kV at set temperature 25.0 ºC Conditions: Fused-silica capillary, d_i ~ 75 µm, d_o ~ 375 µm, L_{tot} = 32.3 cm, Electrolyte 6.00 mM Na_2HPO_4 and 4.00 mM NaH_2PO_4.

linear at power levels associated with *V* greater or equal to 5 kV but show increasing values for lower power values. Curve-fitting using Origin software enabled the error in the current to be subtracted from each point and conductance values to be corrected. The corrected conductance data showed excellent linearity. The higher value of G_0 reflected the slightly larger internal diameter of the capillary used and the lack of temperature control for the vial tray. (These measurements were performed in a similar instrument, but at a different university in collaboration with Vlastmil Hruška).

It is of interest to compare the elevation in mean electrolyte temperature and the heat transfer coefficient calculated from the extrapolated value of G_0 (using data from 5 - 30 kV) with the values calculated from the curve-fitting data (0.5 – 30 kV, which predicted an error in the current of 0.207 μA).

Table 4- 5: Comparison of ΔT_{Mean} calculated from Eqn 4- 5 using extrapolation of raw data and corrected data* from curve-fitting using Origin software. Conditions: As in **Figure 4- 15**.

V (kV)	*P/L* (Wm^{-1})	*G* (nS)	ΔT_{Mean} (ºC)	*P/L** (Wm^{-1})	*G** (nS)	ΔT_{Mean}^{*} (ºC)
0.000	0.000	2.454	0.00	0.000	2.426	0.00
4.982	0.192	2.495	0.81	0.189	2.453	0.55
5.976	0.276	2.499	0.89	0.273	2.464	0.78
6.980	0.378	2.509	1.08	0.374	2.479	1.07
7.971	0.497	2.528	1.46	0.492	2.502	1.53
9.971	0.790	2.565	2.21	0.783	2.545	2.39
11.959	1.161	2.621	3.32	1.153	2.604	3.58
17.944	2.863	2.872	8.30	2.852	2.860	8.74
23.926	5.921	3.341	17.62	5.905	3.332	18.22
29.890	11.505	4.160	33.90	11.486	4.153	34.72

Table 4- 5 suggests that even at voltages of 5 kV, a small error in *G* leads to overestimation of the rise in temperature if the raw data are used. This is evident when a graph of ΔT_{Mean} vs *P/L* is plotted; a better estimate for ΔT_{Mean} at 5 kV would be about 0.56 ºC. Analysis of the data from **Table 4- 5** indicated that the predicted elevation in T_{Mean} at 1.00 Wm^{-1} using extrapolation of raw data was 2.96 ºC and was 3.04 ºC for the corrected data. These values are about 10 % greater than the value of 2.715º C from

Figure 4- 11 and reflect the lack of cooling of the electrolyte in the vials for this particular experimental set-up.

Values of the surface heat transfer coefficient were calculated using the approach of Chapter 4.6 and by rearranging the expression for k_1. The first approach predicted ΔT_{Air} ~ 2.59 ºC at P/L = 1.00 Wm^{-1} and h = 328 $Wm^{-2}K^{-1}$.

Curve-fitting gave a value of k_1 =456.6 x 10^{-6} kV^{-2} and a value for the overall heat transfer coefficient of h_{OA} = 1431 $Wm^{-2}K^{-1}$. Rearrangement of Eqn 1- 28 gave a value of h = 317 $Wm^{-2}K^{-1}$ in good agreement with the previously calculated value for the same instrument.

4.7.5 Conclusions

Measuring conductance over an extended range of voltages including V < 5 kV demonstrates the peril of using values of G from relatively low voltages to estimate G_0 so that temperature can be determined. Errors in the determination of G_0 can be minimized by using data from 10-30 kV for extrapolation or by using an extended voltage range and curve-fitting conductance with voltage employing 4- 31. This second technique can also yield information that enables the heat transfer coefficient to be determined.

5 The Variation of Zeta-Potential with Temperature

5.1 Introduction

Controlling the electroosmotic flow (EOF) is central to obtaining reproducible results from electrokinetic separations in capillaries and microfluidic devices [40, 121]. Factors that influence the EOF include the electrical field strength (*E*), the viscosity (η) the electrical permittivity (ε) of the electrolyte and the zeta-potential (ζ). A definition of the zeta-potential and the location at which it is determined is described in Section 1.2.1

In the absence of changes to the temperature of the electrolyte, Eqn 1- 8 predicts that μ_{EOF} would be independent of *E*. In practice, Joule heating is unavoidable and μ_{EOF} increases linearly with the power per unit length (*P/L*) due to the increase in temperature (*T*) of the electrolyte [99].

Most authors have attributed these changes to μ_{EOF} to well-documented variations in η and ε that occur with *T*, but the influence of ζ has received less attention [40, 102, 122-124]. It has been accepted for many years that the product $\varepsilon\zeta$ is independent of *T* [53, 55] but as was demonstrated in Section 4.4, there is strong evidence to refute this claim. In his early review on free zone electrophoresis, Hjerten [48] did acknowledge that this was an approximation.

A theoretical relationship between ζ and *T* for 1:1 electrolytes is given in Eqn 5-1 [125].

$$\zeta = -\frac{2RT}{F}\sinh^{-1}\left(\frac{\sigma_w}{8RT\varepsilon_0\varepsilon_r c^{1/2}}\right) \qquad 5\text{-}1$$

where *R* is the ideal gas constant, *T* is the absolute temperature, *F* is Faraday's constant, σ_w is the charge density on the inner surface of the capillary, ε_0 is the electrical permittivity of a vacuum, ε_r is the dielectric constant of the electrolyte assumed to equal that of water for dilute solutions and *c* is the concentration of the electrolyte [125]. Increasing the temperature has two effects on ζ. Obviously $2RT/F$ increases with temperature; at 25 ºC, it increases at the rate of 0.335 % per ºC.

The influence of $\sinh^{-1}\left(\frac{\sigma_w}{8RT\varepsilon_0\varepsilon_r c^{1/2}}\right)$ on temperature is less straightforward.

At pH values exceeding 3, a negative charge arises on the fused-silica surface as a result of ionisation of silanol groups. The charge density is expected to increase with temperature due to increased ionisation [122]. ΔG^0 for the deprotonation of silanol groups was determined by Hiemstra and Van Riemsdeijk [126] to be 42.8 kJmol^{-1} in quartz, enabling the dissociation constant (K_{diss}) to be calculated at any temperature using Eqn 5- 2.

$$\ln K_{diss} = \frac{-\Delta G^0}{RT} \qquad 5\text{- }2$$

Over the temperature range 15-35 ºC, K increases from 1.71 x 10^{-8} to 5.46 x 10^{-8} so that increased ionisation would be expected to play a significant part in an increase in zeta-potential with temperature.

The charge on the surface is due not only to silanol groups but is influenced also by adsorbed counterions. Clearly, any model that attempts to quantify the change in ζ with T must also take into account adsorption equilibria between counter-ions and the silica surface. Kirby and Hasselbrink [46] found that for monovalent counter-ions, the zeta-potential was proportional to -log c where c is the molar concentration of counter-ions.

It is well known that the dielectric constant decreases as the temperature increases. Using tabulated values of ε_r, it may be shown that in the temperature range 15-35 ºC the product $\varepsilon_r T$ decreases at the rate of 0.12 % per ºC [127]. At a temperature of 25 ºC and a concentration of monovalent counterions of 15 mM, Kirby and Hasselbrink's analysis of measurements from several different authors suggests that ζ ~ -51.8 mV at pH 7.0, although it should be noted that values from -30 mV to -100 mV were recorded for the same concentration of counter-ions using different electrolytes [40]. At the same temperature, the quotient $-2RT/F$ = -51.4 mV. It follows that under these conditions,

$$\sinh^{-1}\left(\frac{\sigma_w}{8RT\varepsilon_0\varepsilon_r c^{1/2}}\right) = 1.00_8$$

and increases at a rate of just 0.087 % per ºC if changes to σ_w are ignored. At 25.00 ºC, $2RT/F$ increases at the rate of 1/298.15 K ≈ 0.335 % K^{-1}. Thus, taking into account both terms in Eqn 5- 1, but neglecting the effect of increasing charge density with

temperature, at 25 ºC one would expect ζ to increase with T at a rate of 0.336 % K^{-1} + 0.087 % K^{-1} = 0.423 % K^{-1}.

Most of the experimental data available for the influence of T on ζ arise from measurements of streaming potentials in ground minerals. Ishido and Mizutani [128] and Samasundaran and Kulkarni [129] found independently that for ground quartz, ζ increased at a rate of 1.75 % K^{-1}. Their streaming potential measurements using 1 mM and 10 mM KNO_3 at pH 7.0 as electrolytes showed large experimental variations.

Using thermodynamic calculations based on the increased ionisation of silanol groups with temperature and taking into account the adsorption of counter-ions, Revil et al. [122] predicted that ζ of quartz would increase linearly with T at a rate of 1.9 % K^{-1}. However, it is questionable whether either the previous experimental findings based on ground minerals or the theoretical predictions are an accurate reflection of the situation in fused-silica capillaries or microfluidic devices constructed from glass.

In the present study, values of electroosmotic mobility μ_{EOF} obtained at different temperatures but corrected for the effects of Joule heating, are used to find the variation of ζ with T in fused-silica capillaries. The correction for Joule heating is important not only for accuracy, but also for sufficient precision of the acquired data, so that a relatively small effect of T on ζ can be evaluated precisely on a much larger background of changes to the viscosity and electrical permittivity.

5.2 Experimental

The linear variation in μ_{EOF} was plotted as a function of the power per unit length (P/L) and the value of μ_{EOF} at zero power dissipation (μ_{EOF}^{0}) was then found by extrapolation. Values of μ_{EOF}^{0} were plotted as a function of effective temperature see Eqn 4- 4 [5] to produce a calibration graph free of the effects of Joule heating (see **Figure 5- 1**). Eqn 1- 8 was rearranged to given an expression for ζ.

$$\zeta = \frac{-\eta\mu_{EOF}^{0}}{\varepsilon} = \frac{-\eta\mu_{EOF}^{0}}{\varepsilon_r\varepsilon_0} \qquad 5\text{- }3$$

Values of ζ and the charge density were calculated from measurements of μ_{EOF}^{0} using tabulated values of η and ε_r for each effective temperature.

5.3 Results and Discussion

Plots of μ_{EOF} vs P/L were extrapolated to zero power to obtain values of μ_{EOF}^{0}. **Figure 5- 1** shows how these values were used to produce a calibration graph.

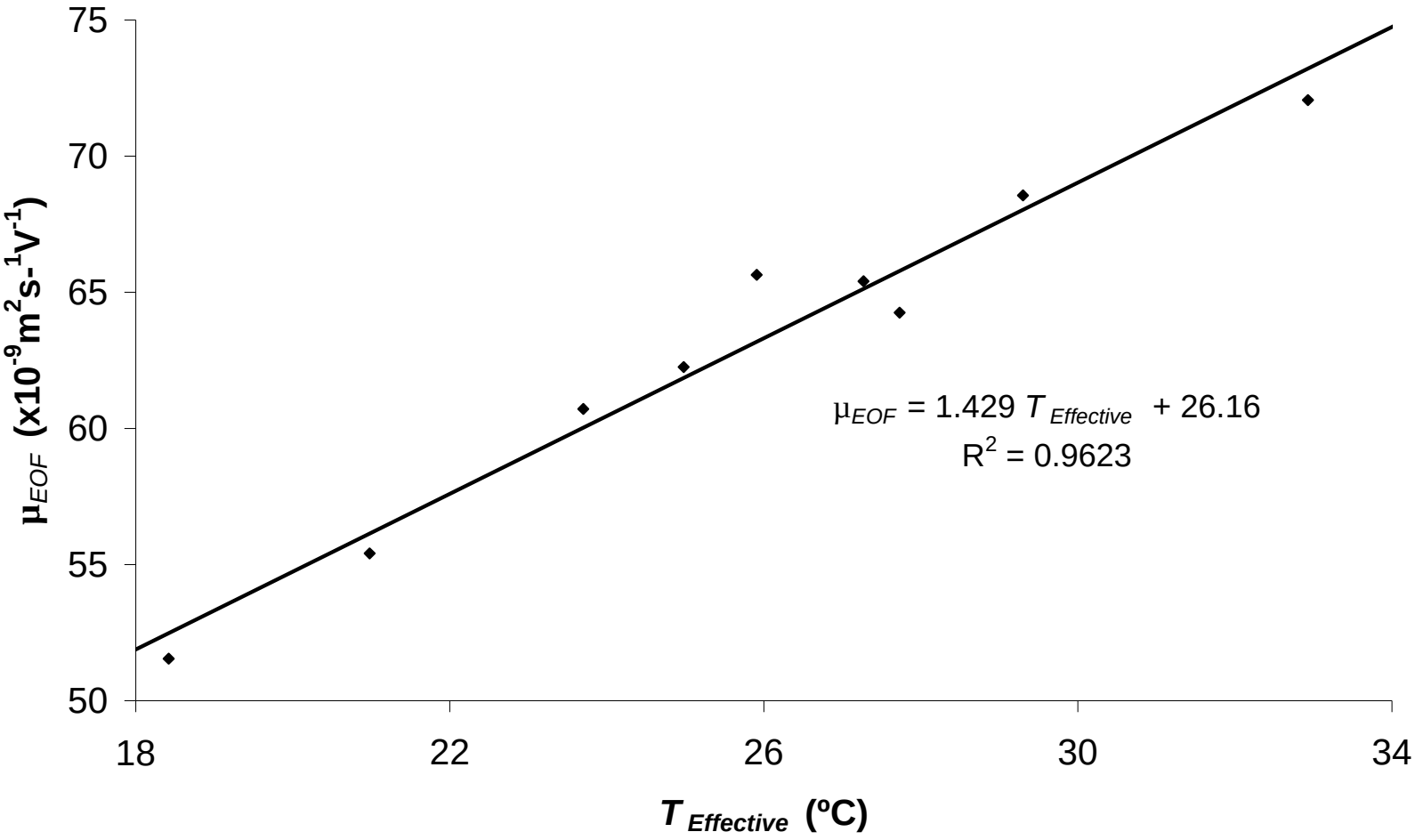

Figure 5- 1: Variation of μ_{EOF} free of Joule heating effects with temperature.
Conditions: As in **Figure 4- 3**

Eqns 5- 3 and 5- 4 were used to calculate ζ and σ_w.

$$\sigma_w = 8RT\varepsilon_0\varepsilon_r c^{1/2} \bullet \sinh\left(\frac{-F\xi}{2RT}\right) \qquad 5\text{- }4$$

Values of μ_{EOF}^0 interpolated from **Figure 5- 1** for a range of temperatures and corresponding values of the dielectric constant of water, its viscosity and the calculated zeta-potentials are shown in **Table 5- 1** [4]. (By using the raw μ_{EOF} data the trend in ζ vs T was less obvious.)

The change of $\zeta(T)$ /ζ(25 ºC) with T is shown in **Figure 5- 2**, together with the geophysical data of Somasundaran et al. [129] based on measuring streaming potentials in ground quartz and Revil's prediction based on thermodynamic calculations [122].

Table 5- 1: Variation of electroosmotic mobility, zeta-potential and charge density with temperature.

T (ºC)	μ_{EOF}^0 ($\times 10^{-9}$ $m^2V^{-1}s^{-1}$)	η (cp)	$\varepsilon_r(H_2O)$	ε ($\times 10^{-10}$ Fm^{-1})	$\zeta=\mu\eta/\varepsilon$ (mV)	ζ / ζ(25 ºC)	σ_w ($\times 10^{-6}$ Cm^{-2})
18.3	52.16	1.0452	80.763	7.1394	-76.36	0.9708	3.697
20.9	55.69	0.9803	79.785	7.0530	-77.41	0.9842	3.715
23.3	58.96	0.9261	78.955	6.9796	-78.23	0.9946	3.720
25.7	62.22	0.8765	78.108	6.9047	-78.98	1.004	3.718
26.4	63.17	0.8628	77.860	6.8828	-79.19	1.007	3.717
27.9	65.21	0.8346	77.326	6.8356	-79.62	1.012	3.713
29.4	67.25	0.8079	76.796	6.7888	-80.03	1.018	3.707
33.2	72.42	0.7461	75.472	6.6717	-80.99	1.050	3.686

The charge density calculated using Eqn 5- 4 was found to be temperature-independent ($\overline{\sigma_w}$ = 3.71 x 10^{-6} Cm^{-2}, RSD = 0.35 %).

5.4 Conclusions

Examining Eqn 5- 1 and the data in **Table 5- 1** reveals that most of the variation in ζ can be attributed directly to an increase in the absolute temperature rather than an increase in the surface charge density. The stable value of charge density as temperature increases, suggests that the increase in charge that results from the ionization of silanol groups is completely neutralized by the adsorption of additional counter-ions.

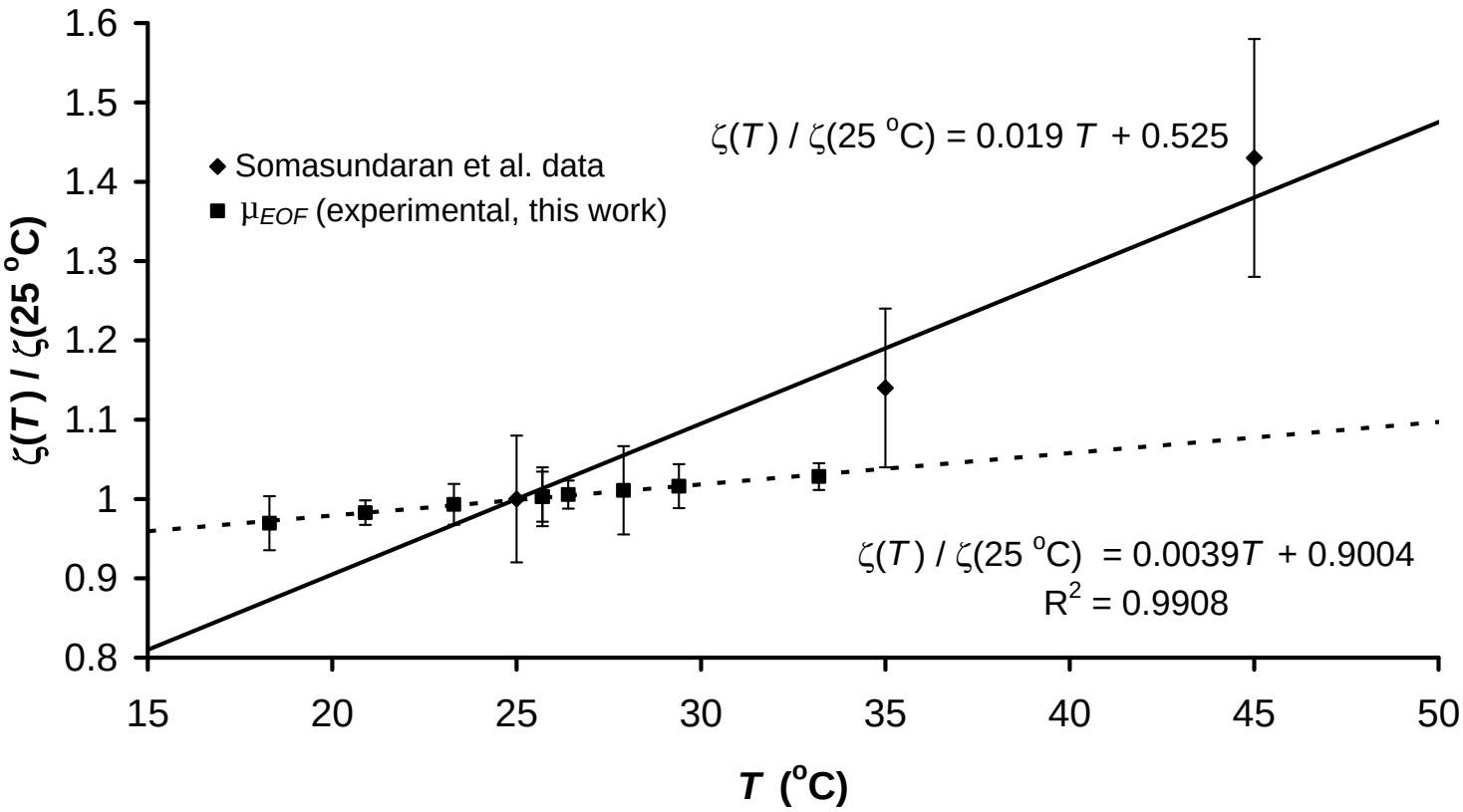

Figure 5- 2 Variation of relative zeta-potential, $\zeta(T) / \zeta(25\ ^{o}C)$ with temperature.

■ Variation of relative zeta-potential, ζ (T) / ζ(25 ºC) with temperature based on μ_{EOF} measurements with least squares line of best fit. – – – -

For comparison, data available from the literature have been included in this figure.♦, Experimental data from Somasundaran et al. obtained from streaming potential measurements in quartz.

Revil's prediction based on thermodynamics calculations. ——

Conditions: As in **Figure 4- 3**.

Figure 5- 3 illustrates that the contributions to μ_{EOF} of ζ and ε are dwarfed when compared to the effect of changing viscosity. The subtle influence of T on ζ could be detected only by correcting for the effects of Joule heating on μ_{EOF} and by exercising great care to minimise experimental error.

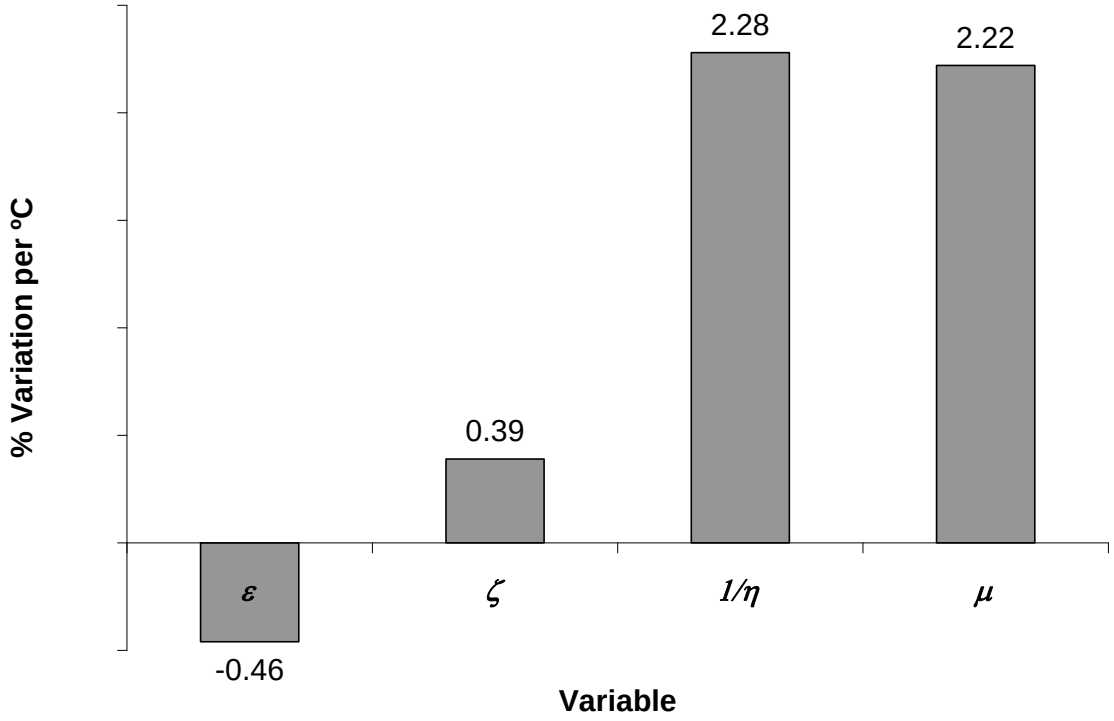

Figure 5- 3: Schematic of the contributions to electroosmotic mobility (μ_{EOF}) from the electrical permittivity of the BGE (ε), the zeta potential (ζ) and the reciprocal of viscosity ($1/\eta$)
Conditions: As in **Figure 4- 3**.

6 Temperature Increases in Polymer Capillaries

6.1 Introduction

Introduced in the late 1970s, fused-silica (FS) capillaries with a poly(imide) (PI) coating were immensely successful in improving the robustness of capillary gas chromatography (CGC) and improving the performance of gas phase separations relative to the packed columns that were used previously [130-132]. Due to its favourable mechanical properties, its high thermal conductivity and its high precision in manufacture, PI-coated FS tubing is now accepted widely as the standard material for CGC columns and is also used in a variety of other analytical applications including CE, capillary liquid chromatography and CEC [133]. Fused-silica also has the advantage that it is optically transparent in the UV and visible spectral regions. Polymeric materials have also been studied as materials for CE capillaries since they offer a variety of different surface physical properties. Examples include: poly(methylmethacrylate (PMMA) [134, 135], fluorinated ethylene-propylene copolymer (FEP) [136], poly(propene) [137], poly(butylene-terephthallate) [137], poly(tetrafluoroethene) (PTFE) [71, 133, 138, 139] and poly(etherether ketone) (PEEK) [140]. Recently a patent was published describing the use of poly- and copoly(n-vinylamide)s in CE capillaries for the separation of biomolecules [141]. In comparison to fused-silica, polymers generally have inferior optical, mechanical and thermal properties so it is not surprising that polymer capillaries have remained something of a rarity in capillary-based CE. In microfluidic devices, in contrast, polymer materials are becoming increasingly popular as a result of the low fabrication costs. In this work, the simple and regular geometry of capillaries is used to investigate the relationship between thermal conductivity and heat dissipation in electro-driven separations.

The thermal conductivities (λ) of the materials used in this study are shown in **Table 6- 1**. Also included are values of λ for a range of other materials employed in CE chips. In polymer capillaries, the low thermal conductivities of materials typically used result in a less efficient transfer of the heat generated by Joule heating of the electrolyte to the outside of the capillary. In CE chips made from polymer materials, Joule heating continues to be problematic despite the large thermal mass of the chips and their relatively small channel dimensions [142].

Table 6- 1: Thermal Conductivity of Various Substances

Material	Thermal Conductivity (λ) at 25 ^{o}C ($Wm^{-1}K^{-1}$)*	Reference
Acetonitrile	0.188	[49]
Air	0.025	[52]
Alumina	36	[62]
Aluminium	237	[77]
Borosilicate Glass	1.0	[52]
Cyclic olefin copolymer (COC)	0.12-0.15	[143]
Diamond	2000	[144]
Fluorinated ethylene-propylene copolymer (FEP)	0.209	[145]
Fused-silica (FS)	1.40	[52]
Iron	80.4	[77]
Methanol	0.202	[77]
Poly(dimethylsiloxane) (PDMS)	0.18	[146]
Poly(etherether ketone (PEEK)	0.252	[3]
Poly(fluoroethene)	0.1	[147]
Poly(imide)	0.155	[54]
Poly(iminohexamethylene-iminohexamethlyene) (Nylon-6,6)	0.23	[148]
Poly(methyl methacrylate) (PMMA)	0.193	[149]
Poly(phenylethene) (Polystyrene)	0.11	[150]
Poly(tetrafluoroethene) (PTFE)	0.265	[151]
Silicon	149	[77]
Teflon AF	0.116	[152]
Water	0.605	[52]

*To convert from $Wm^{-1}K^{-1}$ to $cals^{-1}m^{-1}K^{-1}$ divide by a factor of 4.184

The work presented here uses the conductance method described in Chapter 2.5 to find the mean temperature of the electrolyte in the device (T_{Mean}).

The aim of this work was to investigate the influence of thermal conductivity of different materials on heat dissipation in electrodriven separations. The average

temperature of the electrolyte free of Joule heating effects was determined using a commercial CE instrument. The average temperature increase of the electrolytes for polymer capillaries was compared with that of a fused-silica capillary. The effects of capillary dimensions and the thermal conductivity of the capillary material as well as the importance of active-cooling are discussed. This study is the first step towards the longer-term objective of the study of heating effects occurring in polymeric microfluidic devices.

6.2 Theory

Conductance, employed in this work as a temperature probe for the mean electrolyte temperature in the capillary (T_{Mean}), is defined in Eqn 6- 1 as the inverse of resistance (R) where *I* is the electric current and *V* is the voltage.

$$G = \frac{1}{R} = \frac{I}{V} = \frac{\pi \kappa d_i^2}{4L} \qquad 6\text{- }1$$

Eqn 6- 1 also demonstrates how the conductance depends on the electrical conductivity of the electrolyte, the internal diameter of the capillary and its length.

G may be used to find the internal diameter of different capillaries of equal length if they contain the same electrolyte at the same temperature. Eqn 6- 2 applies where G_{01} and G_{02} refer to the conductance in the first and second capillaries free from Joule heating effects and d_{i1} and d_{i2} are their respective internal diameters. G_0 values cannot be measured directly but can be extrapolated from plots of *G* versus *P/L* as described in Section 2.5) [3].

$$\frac{d_{i1}}{d_{i2}} = \sqrt{\frac{G_{01}}{G_{02}}} \qquad 6\text{- }2$$

It cannot be assumed that as the speed of the airflow in the cooling system is constant, that the temperature difference across the air layer (ΔT_{Air}) will be constant because R_e depends linearly on the outer diameter of the capillary (see Eqn 1- 22).

Substituting Eqn 1- 22 into the appropriate form of Eqn 1- 23, the equation for the Nusselts number for the instrument that was used for this work is:

$$N_u = 0.615(R_e)^{0.466} = c' d_o^{\,0.466} \qquad 6\text{- }3$$

where *c'* is a constant. By substituting Eqn 6- 3 into Eqn 1- 20; it is possible to deduce how *h* depends on the external diameter of the capillary.

$$h = \frac{N_u \lambda_{Coolant}}{d_o} = c'' d_o^{-0.534} \qquad 6\text{- }4$$

where c" is another constant. Substitution of Eqn 6- 4 into Eqn 4- 13 (previously 1- 18) leads to 6- 5 and reveals how ΔT_{Air} depends on the external diameter of the capillary.

$$\Delta T_{Air} = \frac{1}{\pi d_o h} \bullet \frac{P}{L} = \frac{1}{\pi d_o c'' d_o^{-0.534}} \bullet \frac{P}{L} = c''' d^{-0.466} \qquad 6\text{- }5$$

where c'" is another constant. Eqn 6- 6 shows how ΔT_{Air} can be calculated for capillaries of equal length with different external diameters used in the same instrument.

$$\Delta T_{Air\,2} = \left(\frac{d_{o\ 1}}{d_{o\ 2}} \right)^{0.466} \bullet \Delta T_{Air\,1} \qquad 6\text{- }6$$

6.3 Experimental

The general details are given in Chapter 2. The details of the polymer capillaries are discussed below. FEP capillaries, with an unknown internal diameter (~75 μm) and an external diameter of (~365 μm) and total length of 33.2 cm were obtained from Dr. P. Schuman (OPRI, Gainesville, USA). PEEK capillaries with stated internal and external diameter of 75 μm and 360 μm, respectively, were obtained from Upchurch Scientific (Oak Harbour, USA). PMMA capillaries with stated internal and external diameter of 66 μm of 366 μm, respectively, were donated by Dr I. Koev (Biogeneral, San Diego, USA). The external temperatures of the capillaries were set using the active-cooling supplied by the CE instrument. The external diameters of the polymer capillaries were measured using a digital electronic micrometer screw-gauge, Mitutoyo 601-906 (Takatsu-ku, Kawasaki, Japan). Measurements were made at 2 cm intervals along the length of the capillaries before averaging the results.

Current and voltage measurements from the CE instrument were used to calculate the mean conductance and power dissipated per unit length for each run. G_o was obtained by extrapolation from a plot of *G* versus *P/L* for each of the capillaries, which

were of equal length. Eqn 6- 2 was used to find their internal diameters employing a 74.0 µm internal diameter fused-silica capillary as the standard.

Mean electrolyte temperatures were determined using Eqn 2- 4, as described in Section 2.5. The wall temperature difference for the fused-silica capillary was calculated using the modified form of Eqn 1- 12 shown below.

$$\Delta T_{Wall} = \frac{1}{2\pi\lambda_{Wall}} \ln\left(\frac{d_o}{d_i}\right) \bullet \frac{P}{L} \qquad 6\text{- }7$$

where λ_{Wall} is the thermal conductivity of the capillary material. The temperature difference across the conducting air layer (ΔT_{Air}) was calculated using Eqn 6- 8.

$$\Delta T_{Air} = \Delta T_{Mean} - \Delta T_{FS} - \Delta T_{PI} - \tfrac{2}{3}\Delta T_{Radial} \qquad 6\text{- }8$$

For the polymer capillaries, ΔT_{Air} was calculated using Eqn 6- 7 and the fused-silica data and ΔT_{Wall} was calculated using Eqn 6- 9.

$$\Delta T_{Wall} = \Delta T_{Mean} - \Delta T_{Air} - \tfrac{2}{3}\Delta T_{Radial} \qquad 6\text{- }9$$

For each polymer capillary, its effective thermal conductivity $\lambda_{Wall\ (Effective)}$ was calculated by using Eqn 6- 10.

$$\lambda_{Wall\,(Effective)} = \frac{1}{2\pi\Delta T_{Wall}} \ln\left(\frac{d_o}{d_i}\right) \qquad 6\text{- }10$$

6.4 Results and Discussion

The linear increase of G with *P/L* was confirmed experimentally for each of the different capillary materials studied (see **Figure 6- 1**); R^2 values for the dependence on conductance on the power per unit length in polymer capillaries ranged from 0.9991 to 0.9995. The intercepts on the vertical axis were employed to calculate the internal diameters of each of the capillaries using Eqn 6- 2 and are given in **Table 6- 2**. The differences between the specified and determined effective internal diameters illustrate the benefits of using Eqn 6- 2.

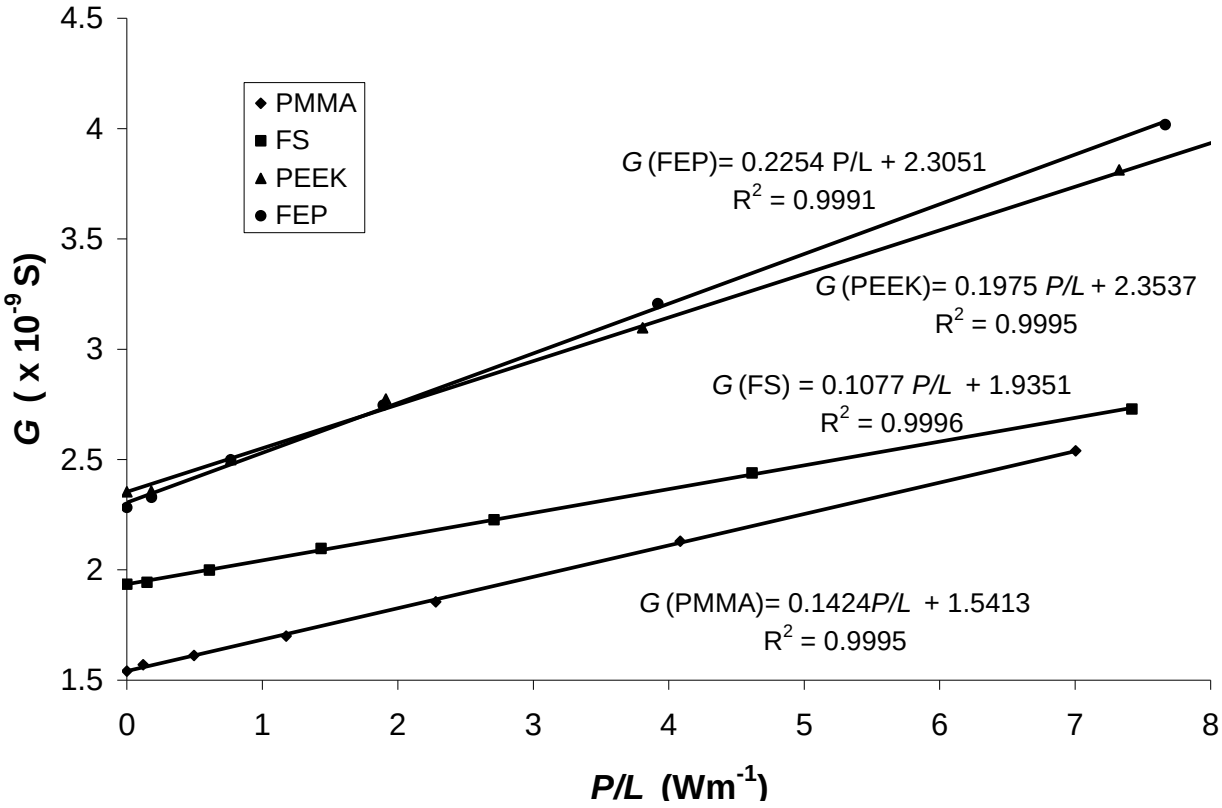

Figure 6- 1: Variation of *G* with *P/L* for a number of capillaries with similar dimensions made from different materials (d_i, d_o)

- ● Fluorinated ethylene-propylene copolymer (FEP) *(*82.3 µm, 365 µm)
- ▲ Poly(etheretherketone) (PEEK) (81.8 µm, 360 µm)
- ■ Fused-silica (FS) (74.0 µm, 362.8 µm)
- ♦. Poly(methylmethacrylate) (PMMA) (66.0 µm, 365 µm)

Conditions: 32.2 cm capillaries, BGE 10.0 mM phosphate electrolyte at pH 7.21, set temperature 25.00 ºC. EOF marker, ●, ▲, ■ 20 % v/v acetone in BGE, ♦ ca. 1 gL^{-1} thiourea in BGE, pressure injection 2.0 kPa for 3.0 s

The differences in gradients ranging from 0.1077 x 10^{-9} SmW^{-1} for fused-silica to 0.2254 x 10^{-9} SmW^{-1} for the fluoropolymer capillary relate to differences in the electrolyte temperatures in the different capillaries. The larger the gradient, the greater is the increase in conductance (and therefore temperature) for a particular *P/L* value. In practice a combination of the gradient and intercept are used to determine the increase in temperature of the electrolyte at a particular power level. The increase in the mean electrolyte temperature with the power per unit length is plotted in **Figure 6- 2**. It **Figure 6- 2**demonstrates that the increase in the mean electrolyte temperature was significantly greater for polymer capillaries than for the fused-silica capillary. The thermal conductivity of the capillary wall makes a significant contribution to ΔT_{Mean}. The rises in electrolyte temperature associated with a power per unit length of 1.0 Wm^{-1} for different capillaries of similar dimensions are shown in **Table 6- 2**.

It could be argued that to measure T_{Mean}, data should only be taken after the initial ramping of the electric current when a steady-state has been achieved. Although this is justified for fused-silica capillaries for which a steady-state is usually established in a matter of seconds [89], there are good reasons for collecting conductance data from the whole run in polymer capillaries. Firstly, the ramping of the current may continue throughout the run (see **Figure 6- 3**) particularly if the power per unit length exceeds 3 Wm^{-1} so that the selected period over which data are analyzed could be rather arbitrary. Secondly, the apparent electrophoretic mobility of analytes reflects the average temperature of the electrolyte during the complete run rather than the maximum temperature determined from the steady-state data. In the interests of reproducibility of CE measurements, the method used in this study finds the average temperature of the electrolyte up until detection of the EOF peak. Clearly, the method can be altered to find the steady-state temperature of the electrolyte by taking data only from the latter part of the run.

Values of ΔT_{Mean} measured using conductance as a temperature probe are larger than would be expected using published values for the thermal conductivities of polymers. Each of the polymer capillaries was behaving as if its thermal conductivity was significantly lower. These differences could be due partly to variations in surface morphologies giving rise to differences in the thickness of the static air layer or due to the simplifications used in the model itself.

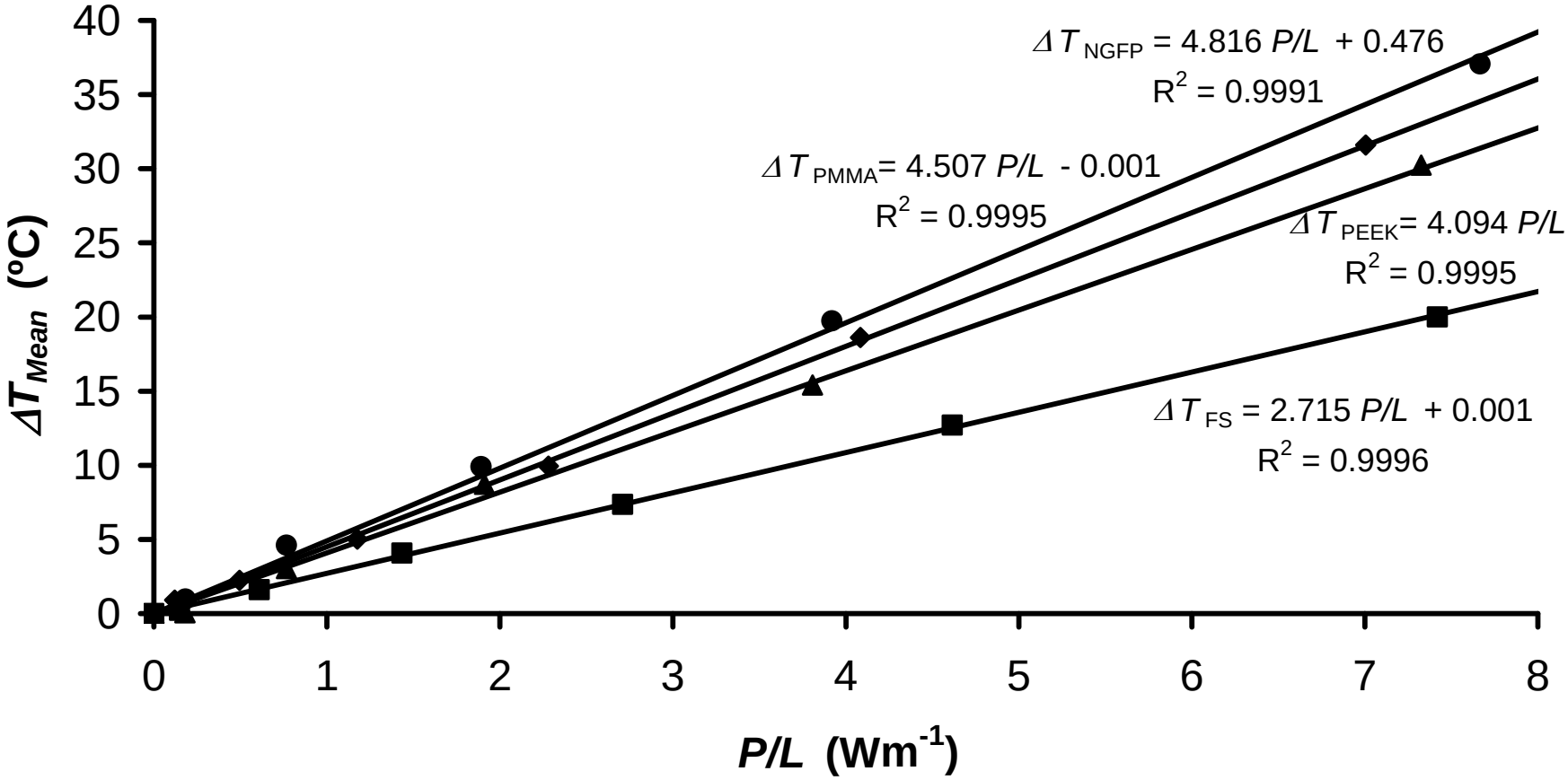

Figure 6- 2: Variation of *G* with *P/L* for a number of capillaries with similar dimensions made from different materials (d_i, d_o)

- ● Fluorinated ethylene-propylene copolymer (FEP) *(*82.3 µm, 365 µm)
- ▲ Poly(etheretherketone) (PEEK) (81.8 µm, 360 µm)
- ■ Fused-silica (FS) (74.0 µm, 362.8 µm)
- ♦. Poly(methylmethacrylate) (PMMA) (66.0 µm, 365 µm)

Conditions as in **Figure 6- 1**

However, the main influence was from sections of the capillary not under thermostat control. These sections contributed to a larger increase in ΔT_{Mean} measured over the whole capillary than that which occurred in the cooled section. It follows that the calculated values of ΔT_{Wall} using Eqn 6- 9 are larger than expected and the resulting effective thermal conductivities are lower than expected.

Table 6- 2: Calculated internal diameters (d_i) and measured external diameters (d_o), increase in mean electrolyte temperature (ΔT_{Mean}) and temperature differences across capillary walls (ΔT_{Wall})

Material	d_i (µm) $RSD_{(n=5)}$	d_i (µm) $RSD_{(n=5)}$	λ_{Wall} (Published) ($Wm^{-1}K^{-1}$)	λ_{Wall} (Effective ($Wm^{-1}K^{-1}$)	ΔT_{Mean} (ºC) (P/L=1Wm^{-1})	ΔT_{Wall} (ºC) (P/L=1Wm^{-1})	ΔT_{Air} (ºC) (P/L=1Wm^{-1})
FS/PI	74.0 0.99 %	362.8 0.29 %	0.863†	0.863	2.71	0.29	2.35*
FEP	80.8 1.95 %	369.9 0.71 %	0.209	0.100	4.82	2.42	2.33
PEEK	81.6 5.72 %	368.0 0.63 %	0.252	0.142	4.09	1.69	2.33(5)
PMMA	66.0 5.89 %	366.1 1.69 %	0.193	0.130	4.51	2.10	2.34

† $\lambda_{Wall\ (FS/PI)}$ is a composite based on d_o(FS) =320.8 µm and d_o(PI) =362.8 µm

* If P/L= 1.0 Wm^{-1}, $\Delta T_{Air} \cong \Delta T_{Mean} - \Delta T_{Wall} - \frac{1}{2}\Delta T_{Radial}$

$$= \Delta T_{Mean} - \Delta T_{Wall} - 0.06(5)^{o}C \qquad 6\text{- }11$$

For comparison, plots of ΔT_{Mean} *versus* the reciprocal of the published thermal conductivity of the capillary wall ($1/\lambda_{Wall\ Published}$) and ΔT_{Mean} *versus* the reciprocal of the effective thermal conductivity of the capillary wall ($1/\lambda_{Wall\ Effective}$) are shown in **Figure 6- 4**.

As expected, both plots in are linear, demonstrating an inverse relationship between ΔT_{Mean} and λ_{Wall}, however if the capillaries had similar dimensions (d_i = 75 µm and d_o = 365 µm), one would expect the gradient of each graph to equal $\ln(d_o/d_i)/2\pi \approx 0.25$ Wm^{-1} and the vertical intercept to equal $\Delta T_{Radial} + \Delta T_{Air} \approx 2.40$ ºC. Clearly using the effective thermal conductivities gives better linearity and agrees much better with the expected gradient and intercept.

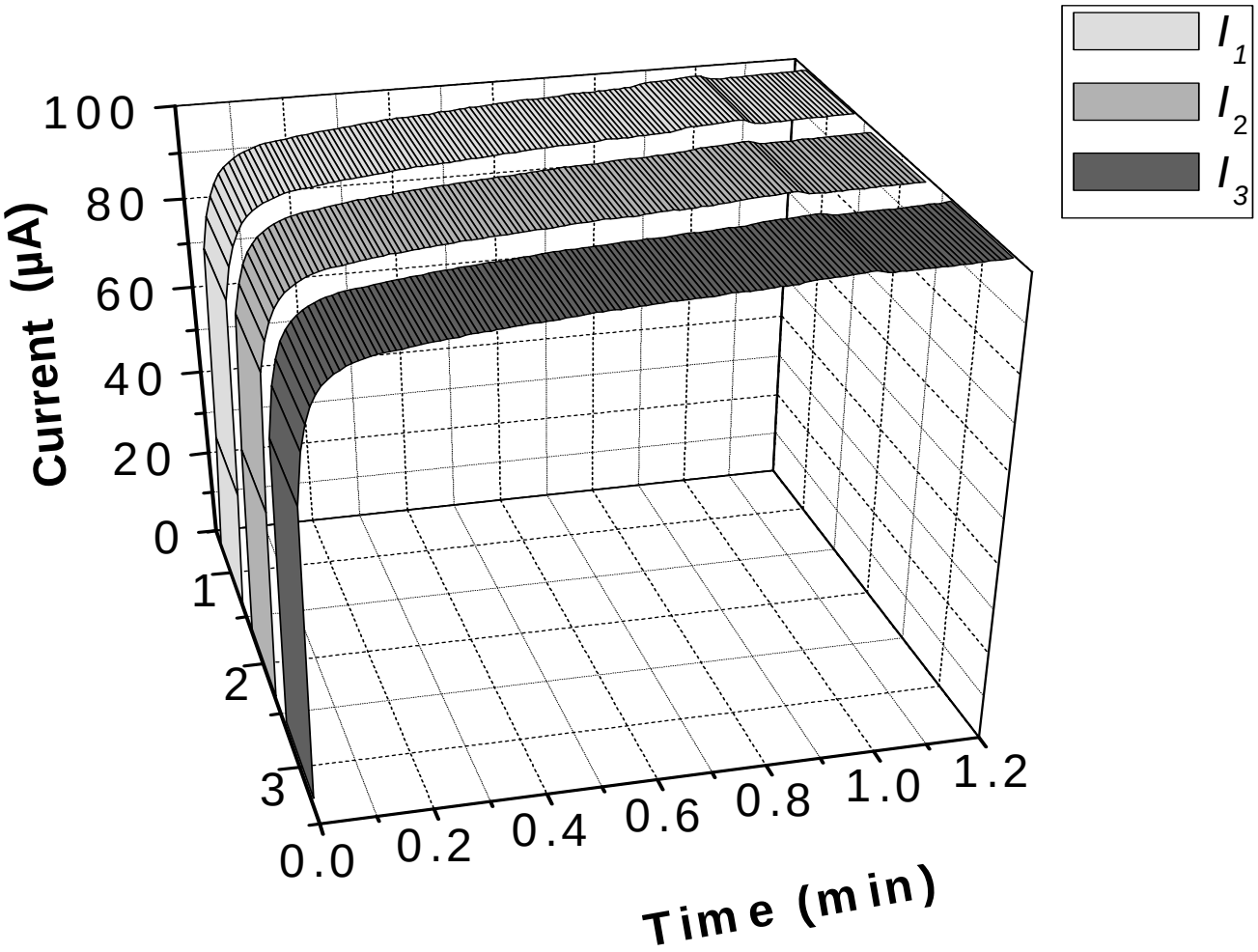

Figure 6- 3: Variation of current with time for 3 consecutive runs in FEP capillary.

Conditions: L_{tot}= 32.2 cm, L_{det} = 23.7 cm, electrolyte 10mM phosphate pH=7.21, V = 30 kV, P/L ≈10 Wm^{-1}

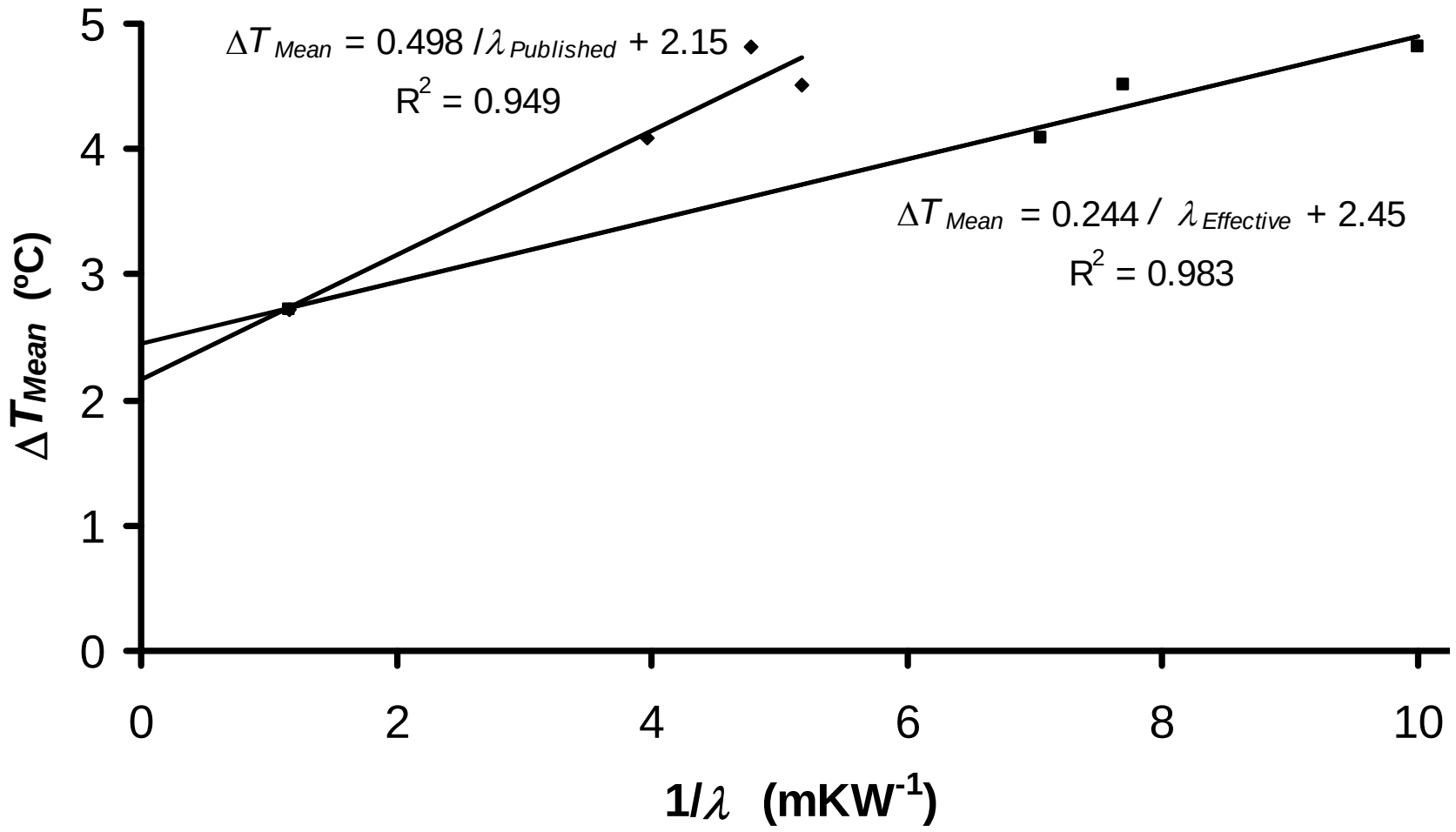

Figure 6- 4: Variation of ΔT_{Mean} with $1/\lambda_{Wall}$:

♦ Published values of λ_{Wall}
■ Effective values of λ_{Wall}
Conditions: As in **Figure 6- 1**

Knox[52] pointed out that ΔT_{Radial} and ΔT_{Wall} were relatively small compared to ΔT_{Air} for fused-silica but **Table 6- 2** shows that. ΔT_{Wall} is far more significant for polymer capillaries and that the lower effective thermal conductivity of polymers is the main factor influencing variations in ΔT_{Mean}. As one would expect, the greater the thermal conductivity of the wall, the lower the temperature difference across it and the smaller the ratio of ΔT_{Wall} to ΔT_{Mean}.

Values of ΔT_{Wall} ranged from 11 % of ΔT_{Mean} for the fused-silica capillary to 51 % of ΔT_{Mean} in the NGFP capillary. Clearly, the static air layer has a major impact on the rise in temperature of the electrolyte but its significance is less for polymer capillaries. Although its effects may be reduced by employing a high velocity of actively-cooled air over the capillary, an even better solution is to exclude air from around the capillary wall by using liquid or solid state cooling.

The findings of this work have significant implications for electrokinetic separation performed in polymer based microfluidic devices. The thermal conductivity of the chip material plays a significant part in the rise in temperature of the electrolyte during electrokinetic separations. This was clearly demonstrated by the work of Erickson, Sinton and Li [142] comparing heat dissipation in PDMS chips with that in hybrid PDMS/ glass chips with similar dimensions. As is the case for capillaries, heat dissipation is made more effective by limiting the thickness and/or increasing the thermal conductivity of the substrates surrounding the channel containing the electrolyte.

The present study has demonstrated that the air layer surrounding the capillary was a limiting factor in heat dispersion and that a great improvement in heat dispersion could be made by excluding this air layer. In chips this could be achieved by attaching a highly conductive temperature-controlled solid, such as a heat sink, above and/or below the device. This approach was recently implemented by Zhang et al. [153], who demonstrated that heat dissipation in their poly(dimethylsiloxane) (PDMS) chip was greatly improved by attaching a heat sink to the cover (ie. above the channel). Erickson, Sinton and Li [142] showed that most of the heat was transferred through the lower layer of the chip when this layer was in contact with a relatively large flat surface at ambient temperature.

Because of the large differences in geometry between chips and capillaries, great care should be taken before using the equations for heat dissipation proposed here for studying Joule heating effects on microfluidic devices.

6.5 Conclusions

For polymers, the experimentally determined thermal conductivities are decreased relative to published values during active-cooling. The autothermal effect is particularly noticeable for polymer capillaries. The rate at which a steady-state (constant current when a constant voltage is applied) can be established depends on the rate at which the heat is conducted through the capillary wall, and therefore on its thickness and thermal conductivity. Unless low power levels are used, establishment of a steady state takes significantly longer for polymer capillaries than for fused-silica capillaries, which have higher thermal conductivity under identical experimental conditions. For reproducible CE experiments in materials with low thermal conductivity, the use of voltage and current data collected from the start of the CE run is recommended for calculation of the mean electrolyte temperature. In this way, arbitrary decisions on achievement of a steady state can be avoided since the autothermal effect is a reproducible effect.

Although polymers are inferior to glass, ceramics and diamond for heat dissipation (see **Table 6- 1**) their lower cost of manufacture continues to drive the use of polymers for microfluidic devices. Their relatively low thermal conductivity can be enhanced if thin layers of the polymers are used in the chips and the air layer is excluded by surrounding the device with a temperature-controlled highly thermally conductive solid as has recently been demonstrated [153].

7 Measurement of Electrophoretic Mobilities Free from the Effects of Joule Heating

7.1 Introduction

The basic theory of electrophoresis including the definition of electrophoretic mobility μ_{ep} is described in Chapter 1.1.

$$\mu_{ep} = \frac{v_{ep}}{E} = \frac{q}{6\pi r_h \eta} \qquad \text{7- 1 (previously 1- 2)}$$

Eqn 7-1 suggests that calculated values of electrophoretic mobility should be independent of the capillary dimensions or the voltage used but in reality Joule heating causes significant variations in μ_{EOF} and μ_{ep}, mainly through a decrease in the viscosity. For aqueous electrolytes at 25 ºC, η decreases at a rate of about 2.28 % per ^{o}C [127]. It follows that μ_{ep} would be expected to increase at a similar rate [53].

For inorganic ions, electrophoretic mobility values vary from about 40 - 80 x 10^{-9} m^2 V^{-1} s^{-1} for cations and –30 to –120 x 10^{-9} m^2 V^{-1} s^{-1} for anions. Organic ions tend to have lower mobilities, typical values are 10 to 60 x 10^{-9} m^2 V^{-1} s^{-1} for aliphatic cations and -10 to –60 x 10^{-9} m^2 V^{-1} s^{-1} for aliphatic anions [154].

There have been two major approaches to measuring electrophoretic mobilities based on conductivity and isotachophoresis [155]. The first approach uses the relationship between the limiting ionic equivalent conductance (λ_{equiv}) and the limiting ionic mobility μ_{ep}^{0}. Eqn 7- 2 enables theoretical values of electrophoretic mobilities at zero ionic strength (also known as limiting ionic mobility) to be calculated from the limiting ionic equivalent conductance (λ_{equiv}) [156].

$$\mu_{ep}^{\ 0} = \frac{\lambda_{equiv}}{F} \qquad \text{7- 2}$$

where F is Faraday's constant, F = 96 487 $Cmol^{-1}$.

The second approach is based on the fact that during isotachophoresis, zones containing ions all travel at the same speed [157] but differ in the electrical field strength (E) according to their mobility, as illustrated in Eqn 7- 3.

$$v = E_L \mu_L = E_A \mu_A = E_B \mu_B = E_T \mu_T$$ 7- 3

where the subscripts L, A, B and T refer to the co-ions of the leading electrolytes, analytes A and B and the terminating electrolyte, respectively. Provided that A and B are fully dissociated, their effective mobilities can be simply calculated by comparing the electrical field strength in their zone with that measured in the leading electrolyte [158]. As mobilities are temperature-dependent, measurements of μ_{ep} are usually carried out with low currents to minimize Joule heating effects. Under these conditions there is good agreement between the values of μ_{ep} calculated using Eqns 7- 2 and 7- 3.

If electrophoretic mobilities are determined using CE, the magnitude of μ_{ep} obtained by an operator varies according to the composition of the electrolyte used, the dimensions of the capillary, the electrical field strength and the efficiency of the cooling system associated with the instrumentation.

Eqn 7- 4 describes how μ_{ep} for an analyte can be determined from experimental measurements of migration times.

$$\mu_{ep\,A} = \frac{L_{\det} L_{tot}}{V}\left(\frac{t_{EOF} - t_A}{t_{EOF} t_A}\right)$$ 7- 4 (previously 1- 6)

where $\mu_{ep\,A}$ is the effective electrophoretic mobility of the analyte, L_{det} is the distance from the inlet to the detector, L_{tot} is the length of the capillary, V is the voltage, t_{EOF} and t_A are the times taken for a neutral species and the analyte to be detected. ($\mu_{ep\,A}$ is known as the *effective mobility* as it only applies to the particular conditions of that separation). Apart from the charge to radius ratio and viscosity of the medium, a significant influence on the size of μ_{ep} is the ionic strength of the electrolyte.

As early as 1932, Onsager and Fuoss [159] described how interactions (known as the “relaxation effect” and as the “electrophoretic effect’) between the migrating ions of the analyte and the counter-ions of the electrolyte reduced their mobilities. These interactions are described below.

In the absence of an electrical field, each cation is surrounded by a number of anions to form a spherically symmetrical ionic atmosphere (see **Figure 7- 1**a).

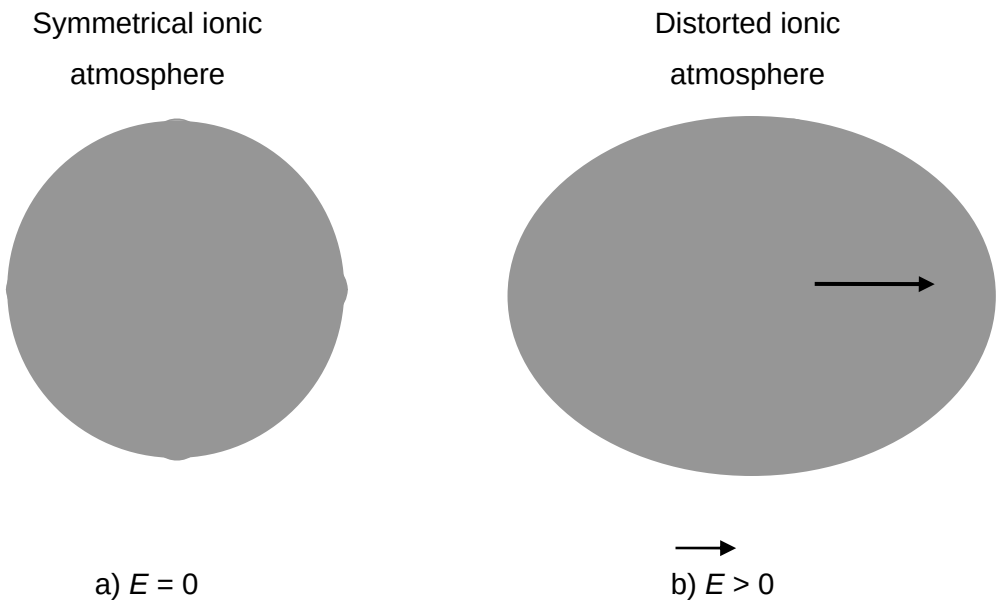

Figure 7- 1: Schematic diagram showing the ionic atmosphere of a cation in a) the absence and b) the presence of an electric field. Diagram adapted from Atkins [160]

Figure 7- 1b) shows that when an electrical field is applied, the cation migrates in the direction of *E*. There is a time delay before the anions adjust to the moving cation so that the ionic atmosphere is incompletely formed in front of the cation and incompletely decayed behind the cation. The overall effect is a displacement of the centre of charge of the ionic atmosphere behind the ion. The attraction of the anions for the cation reduces its mobility. This is known as the relaxation effect. As the ionic atmosphere formed by the anions moves in the opposite direction to the cations it adds to the viscous drag experienced by the cations; this is known as the electrophoretic effect [160]. As one would expect, the decrease in mobility becomes less apparent as the ionic strength of the electrolyte decreases due to a reduction in the attractive forces between the analyte and the counter-ions.

The Debye-Hückel-Onsager Equation (Eqn 4- 2) shows how the molar conductivity (Λ_m) of a 1:1 electrolyte decreases with increasing concentration (c).

$$\Lambda_m = \Lambda_0 - (A + B\Lambda_0)c^{1/2} \qquad 7\text{- }5$$

where Λ_0 is the conductivity at infinite dilution and A and B are known as Debye-Hückel-Onsager coefficients. For electrolytes composed of monovalent ions (1:1 electrolytes) dissolved in water at 25 ºC, A and B take the values 6.021 x 10^{-3} $Sm^2mol^{-1}M^{-1/2}$ and 0.2289 $M^{-1/2}$ respectively [161]. Since conductivity and mobility are linearly related, there is a corresponding expression for the variation of electrophoretic mobility with ionic strength.

Eqn 7- 6 shows how values of electrophoretic mobility for dilute solutions of strong electrolytes can be adjusted for ionic strength to obtain values comparable to those obtained from limiting ionic conductance [162].

$$\mu_{epA} = \mu_{epA}{}^{0} - \left[\mu_{epA}{}^{0} B_1 \left(\frac{q^*}{1+\sqrt{q^*}} \right) + zB_2 \right] \frac{\sqrt{I_s}}{1+1.5\sqrt{I_s}} \qquad 7\text{- } 6$$

where B_1 and B_2 are constants, which for aqueous solutions at 25 ºC have the values B_1 = 7.8171 x 10^{-8} $(molm^{-3})^{-1/2}$ and B_2 =3.138 x 10^{-8} $m^2s^{-1}V^{-1}(molm^{-3})^{-1/2}$. I_s is the ionic strength of the electrolyte and q* is defined in Eqn 7- 7.

$$q^* = \left(\frac{z_+ |z_-|}{z_+ + |z_-|} \right) \left(\frac{\mu_{ep}{}^{0}{}_{+} + \mu_{ep}{}^{0}{}_{-}}{|z_-| \mu_{ep}{}^{0}{}_{+} + z_+ \mu_{ep}{}^{0}{}_{-}} \right) \qquad 7\text{- } 7$$

where z_- and z_+ are the charge numbers for the analyte ion and counter ion and the $\mu_{ep}{}^{0}{}_{-}$ and $\mu_{ep}{}^{0}{}_{+}$ are their limiting ionic mobilities. For symmetrical electrolytes q^* is assigned a value of 0.5. In Eqn 7- 7, the first bracketed term relates to the relaxation effect and the second bracketed term to the electrophoretic effect.

For weak electrolytes it is also necessary to take into account the mole fraction for each of the species present. The calculation of effective mobilities from limiting ionic mobilities has been well described by Jaros et al. [163] and ionic strength corrections are very conveniently performed using their freely available software “Peakmaster 5.1” available at http://www.natur.cuni.cz/~gas/.

In summary, ionic strength corrections to find limiting ionic mobilities from experimentally obtained effective electrophoretic mobilities can be performed from first principles using Debye–Fuoss Theory or rather more simply by using the Peakmaster 5.1 software.

Unfortunately the values of $\mu_{ep}{}^{0}$ obtained after taking into account the ionic strength of the electrolyte tend to be higher than those calculated from Eqn 7- 6**,** particularly at the high field strengths used for optimum separation efficiency. Joule

heating has a significant influence on the experimentally-determined electrophoretic mobilities; increases in μ_{ep} of 20 % are common even when an effective cooling system is used.

The aim of this work is to develop a method which allows accurate and reproducible measurements of electrophoretic mobilities during CE to be determined that are unburdened by Joule heating and to use these to calculate limiting ionic mobilities comparable to those in the literature by making corrections for ionic strength.

7.2 Experimental

The general instrumental details are given in Chapter 2. Detailed conditions are described below and given in each figure caption.

7.2.1 Chemicals

The BGE for analysis of inorganic anions, 5 mM $(NH_4)_2MoO_4$ was prepared by dissolving $(NH_4)_6Mo_7O_{24}$ (BDH, Sydney, Australia) and titrating the solution to pH 9.50 using concentrated ammonia solution (Sigma-Aldrich, Sydney, Australia). A 5 mM stock solution containing IO_3^-, BrO_3^-, NO_3^-, Cl^- and SO_4^{2-}, was prepared by dissolving their sodium or potassium salts (Williams and Hopkins, London, UK and BDH, Sydney, Australia). The sample solution was prepared by diluting the stock solution to 200 µM. An EOF modifier, 0.1 % hexadimethrine bromide in 30 mM $Na_2B_4O_7$ (Sigma-Aldrich, Sydney, Australia) was used as a pre-flush to reverse the EOF for analysis of anions.

The electrolyte for analysis of aromatic anions, 5.0 mM NaH_2PO_4 + 5.0 mM Na_2HPO_4 was prepared by titrating 10.0 mM H_3PO_4 with 13M NaOH to a pH of 7.21. Stock solutions of aromatic anions with a concentration of 10.0 mM were prepared for benzoic acid, salicylic acid (BDH, Sydney, Australia), 4-heptylbenzoic acid, 4-propylbenzoic acid, 2-aminobenzoic acid (Sigma-Aldrich, Sydney, Australia) and 4-aminophenylacetic acid (AJAX, Sydney, Australia) by dissolving the solids in Milli-Q water to which an equivalent amount of sodium hydroxide (BDH, Sydney, Australia) was added. Sample solutions were prepared by diluting the stock solutions to 100 µM.

LR grade acetone (BDH, Sydney, Australia), was used as neutral EOF marker for the separations of anions. A 5 % solution by volume of acetone was added to the sample so that the EOF could be determined.

7.2.2 Procedures

Separations of analytes were carried out at increments of 5 kV using normal EOF aromatic anions and reversed EOF for inorganic anions. Current and voltage were monitored at intervals of 0.01 min throughout each run using the Chemstation software and the mean conductance and power dissipated per unit length calculated for each run [3]. Indirect detection was carried out at 226 nm for inorganic anions using the diode array detector on the instrument. Direct detection of the EOF marker was carried out at 260 nm. Values of μ_{EOF}, μ_{ep} and *P/L* were calculated using Eqns 2- 3, 7- 4 and 2- 2, respectively. Values of μ_{ep} for each ion were plotted as a function of *P/L* and extrapolated to zero power to find electrophoretic mobilities corrected for Joule heating effects, $\mu_{ep}(0\ Wm^{-1})$. These values were later adjusted for the effect of ionic strength of the electrolyte using the Peakmaster 5.1 software. The parameters used for molybdic acid were: $pK_{A1} = 3.483$, $pK_{A2} = 6.0$[164], $\mu_{ep0}(MoO_4^{2-}) = -77.2 \times 10^{-9}\ m^2s^{-1}V^{-1}$ [165] and an estimate for the electrophoretic mobility of $HMoO_4^-$ was $\mu_{ep0}(HMoO_4^-) = -38.6 \times 10^{-9}\ m^2s^{-1}V^{-1}$.

7.3 Results and Discussion

Values of μ_{ep} are plotted as a function of *P/L* in **Figure 7- 2**. Extrapolated values for μ_{ep} at *P/L* = 4 Wm^{-1} and at *P/L* = 0 are tabulated in **Table 7- 1)**. **Figure 7- 2** shows that there was a linear variation of electrophoretic mobility with the power per unit length. There were significant variations in the observed values from day to day. This may have been related to variations in the room temperature, which was not controlled and varied by as much as 15 ºC during the course of the day. The ionic strength of the BGE used for inorganic anions led to significant Joule heating; *G* (4.00 Wm^{-1}) = 1.909 nS was about 23 % higher than *G*(0 Wm^{-1}) =1.556 nS so that the mean temperature of the electrolyte increased by about 11 ºC (see Section 4.2). Corresponding to this temperature increase, the average electrophoretic mobility increased by 22.8 % (RSD = 1.4 %). Over the same temperature range, the reciprocal of viscosity increased by 26.3 % [166]. It would appear that most of the variation in μ_{ep} of the inorganic anions could be attributed to changes to the viscosity that occur as a result of Joule heating. It is unclear what other factors may be influencing μ_{ep}.

At a pH of 9.50, the ionic strength of the 5mM $(NH_4)_2MoO_4$ solution used for the analysis of inorganic anions was approximately 23 mM. The simulation using

Peakmaster 5.1 calculated Λ_m = 0.9386 Λ_0; in other words the effect of the ionic strength correction was to reduce the limiting ionic mobility by 6.14 %. **Table 7- 1** shows that values of μ_{ep} at *P/L* = 4 Wm^{-1} were significantly larger than the theoretical values of limiting ionic mobilities μ_{ep}^0 but the values of μ_{ep} extrapolated to 0 Wm^{-1} were significantly lower. However, after making a correction for ionic strength using the Onsager-Fuoss equation, there was a great improvement in the experimental predictions of μ_{ep}^0. The slight differences involved may have been due to interactions between the anions and the cations of the buffer additive used to reverse the EOF.

Above a pH of 7, the electrophoretic velocity of most aromatic anions is significantly less that the velocity of the electroosmotic flow. This enables μ_{ep} to be determined without the need for EOF reversal. The variation of μ_{ep} with *P/L* is shown in **Figure 7- 2** and values of μ_{ep} at 4.0 Wm^{-1} and at 0 Wm^{-1} are shown in **Table 7- 2** along with predictions using Peak Master and the experimental and accepted values of limiting ionic mobility.

Figure 7- 3 shows that electrophoretic mobilities of aromatic anions were significantly affected by Joule heating and showed a linear dependence on *P/L*. *G* (4.00 Wm^{-1}) = 1.871 nS was about 21.0 % higher than *G*(0 Wm^{-1}) =1.546 nS, so that the mean temperature of the electrolyte increased by about 10.3 ºC (see Section 4.2).

This increase in μ_{ep} is larger than that which can be explained by the associated variation in $1/\eta$; 24.4 % over the same temperature range [166]. However, it is possible that at the elevated temperatures there was less association of the aromatic anions with the counter-ions in the BGE leading to a slight increase in the effective charge. This explanation is purely speculative.

After making an adjustment to μ_{ep} (0 Wm^{-1}) for ionic strength, excellent agreement was observed between the predicted values from experiment and the accepted values of μ_{ep}^0.

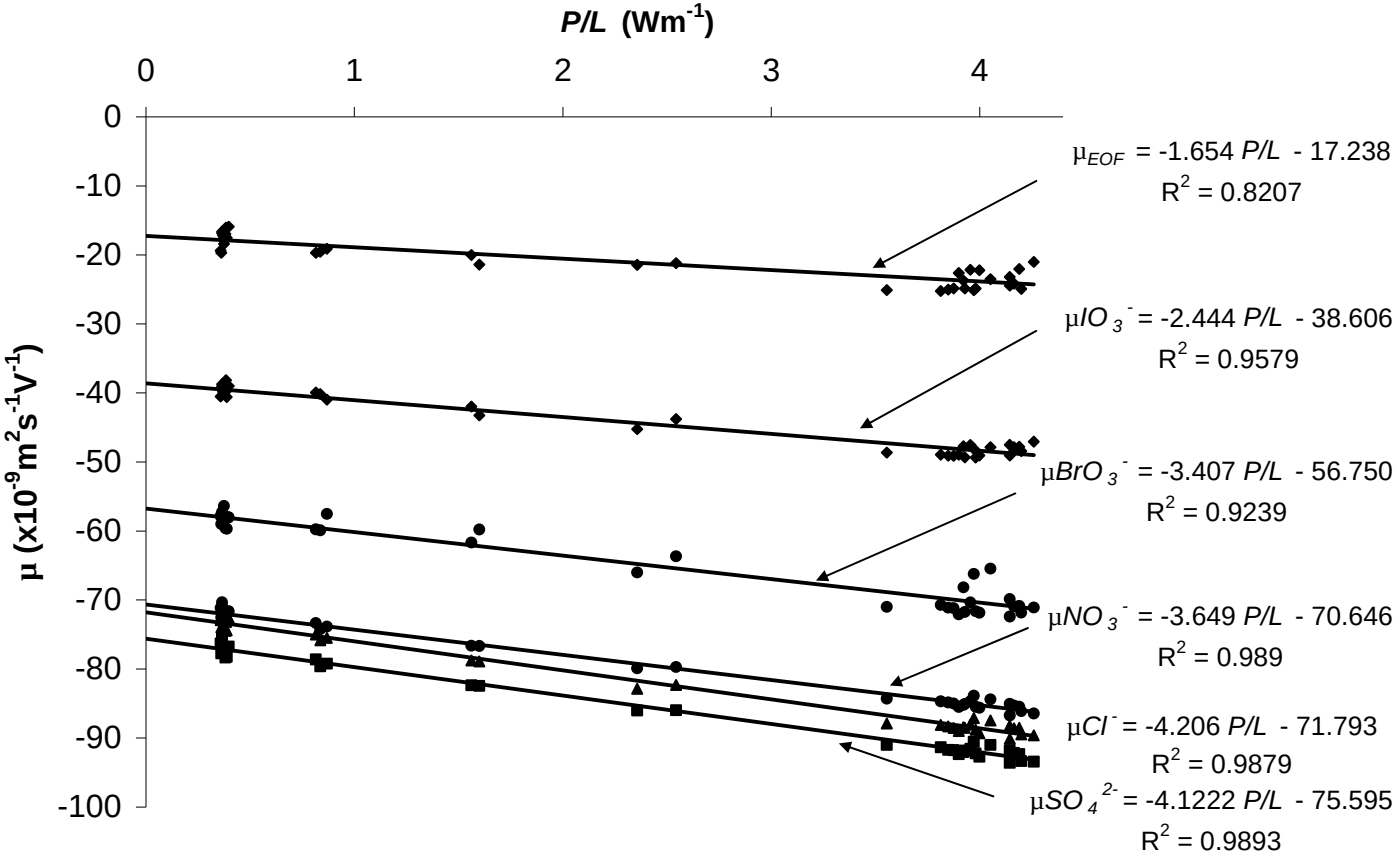

Figure 7- 2: Electrophoretic mobilities of inorganic anions as a function of the power per unit length.

Data taken from 7 days with error bars of ± 2 standard deviations

Conditions: BGE 5 mM $(NH_4)_2MoO_4$ adjusted to pH = 9.50 using conc. $NH_{3(aq)}$. Buffer electrolyte additive 0.1 % hexadimethrine bromide for EOF reversal. Capillary: fused-silica, d_i = 74.0 µm, d_o = 365 µm, L_{tot} = 41.8 cm, L_{det} = 32.8$_5$ cm (after sample injection) Injection: 2.0 kPa x 5.0s, injection length 0.45 cm Indirect UV detection of anions at 226 nm, detection of EOF marker at 260 nm. Set temperature 25.0 ºC.

Table 7- 1: Electrophoretic Mobilities of Inorganic Anions

Key: μ_{ep} (4 Wm^{-1}) and μ_{ep}(0 Wm^{-1})= experimental μ_{ep} extrapolated to *P/L* = 4.0 Wm^{-1} and to *P/L*= 0 Wm^{-1}, μ_{epPM} = Peak Master 5.1 predictions of μ_{ep} from limiting ionic mobility corrected for ionic strength, $\mu_{ep}^{0}{}_{(Experimental)}$ = μ_{ep} (0 Wm^{-1}) adjusted to zero ionic strength (predicted limiting ionic mobility) and $\mu_{ep}^{0}{}_{(Accepted)}$ = accepted μ_{ep}^{0} values based on limiting equivalent conductance using Eqn 7- 2.

Conditions: As in **Figure 7- 2**

Anion	μ_{ep}(4 Wm^{-1}) ($x10^{-9}m^2s^{-1}V^{-1}$)	μ_{ep}(0 Wm^{-1}) ($x10^{-9}m^2s^{-1}V^{-1}$)	μ_{epPM} ($x10^{-9}m^2s^{-1}V^{-1}$)	$\mu_{ep}^{0}{}_{(Experimental)}$ ($x10^{-9}m^2s^{-1}V^{-1}$)	$\mu_{ep}^{0}{}_{(Accepted)}$ ($x10^{-9}m^2s^{-1}V^{-1}$)
SO_4^{2-}	-91.94	-75.60	-74.41	-84.3	-82.9
Cl^-	-88.44	-71.79	-72.38	-78.5	-79.1
NO_3^-	-85.15	-70.65	-69.62	-75.2	-74.1
BrO_3^-	-70.36	-56.75	-53.94	-60.9	-57.8
IO_3^-	-48.11	-38.61	-38.64	-42.0	-42.0

It is interesting to note that the percentage increase in μ_{ep} associated with increasing *P/L* from 0 to 4 Wm^{-1} was essentially constant for each of the aromatic anions. The average increase was 28.2 % with RSD < 0.4 %.

Table 7- 2: Electrophoretic Mobilities of Aromatic Anions (x 10^{-9} $m^2s^{-1}V^{-1}$)

Key: μ_{ep} (4 Wm^{-1}) and μ_{ep}(0 Wm^{-1})= experimental μ_{ep} extrapolated to *P/L* = 4.0 Wm^{-1} and to *P/L*= 0 Wm^{-1}, μ_{epPM} = Peak Master 5.1 predictions of μ_{ep} from limiting ionic mobility corrected for ionic strength, $\mu_{ep}^{0}{}_{(Experimental)}$ = μ_{ep}(0 Wm^{-1}) adjusted to zero ionic strength (predicted limiting ionic mobility) and $\mu_{ep}^{0}{}_{(Accepted)}$ = accepted μ_{ep}^{0} values based on limiting equivalent conductance.

Conditions: BGE 10 mM H_3PO_4 adjusted to pH = 7.21 using conc. $NaOH_{(aq)}$. Capillary: fused-silica, d_i = 74.0 µm, d_o = 365 µm, L_{tot} = 41.8 cm, L_{det} = 32.8_5 cm(after sample injection) Injection: 2.0 kPa x 5.0s, Injection length 0.45 cm Direct UV detection of anions at 215 nm, detection of EOF marker at 260 nm. Normal EOF. T_{Set} = 25.0 ºC.

Anion	μ_{ep}(4 Wm^{-1}) ($x10^{-9}m^2s^{-1}V^{-1}$)	μ_{ep}(0 Wm^{-1}) ($x10^{-9}m^2s^{-1}V^{-1}$)	μ_{epPM} ($x10^{-9}m^2s^{-1}V^{-1}$)	$\mu_{ep}^{0}{}_{(Experimental)}$ ($x10^{-9}m^2s^{-1}V^{-1}$)	$\mu_{ep}^{0}{}_{(Accepted)}$ ($x10^{-9}m^2s^{-1}V^{-1}$)
$C_6H_4(OH)COO^-$	-39.98	-31.30	-31.38	-35.3	-35.4
$C_6H_5COO^-$	-37.99	-29.53	-29.61	-33.5	-33.6
$C_6H_4(NH_2)COO^-$	-37.38	-29.13	-27.52	-33.2	-31.6
$H_2NC_6H_4CH_2COO^-$	-33.13	-25.99	No data	-29.9	No data
$C_3H_7C_6H_5COO^-$	-31.09	-24.26	No data	-27.9	No data
$C_7H_{15}C_6H_5COO^-$	-26.22	-20.37	No data	-23.4	No data

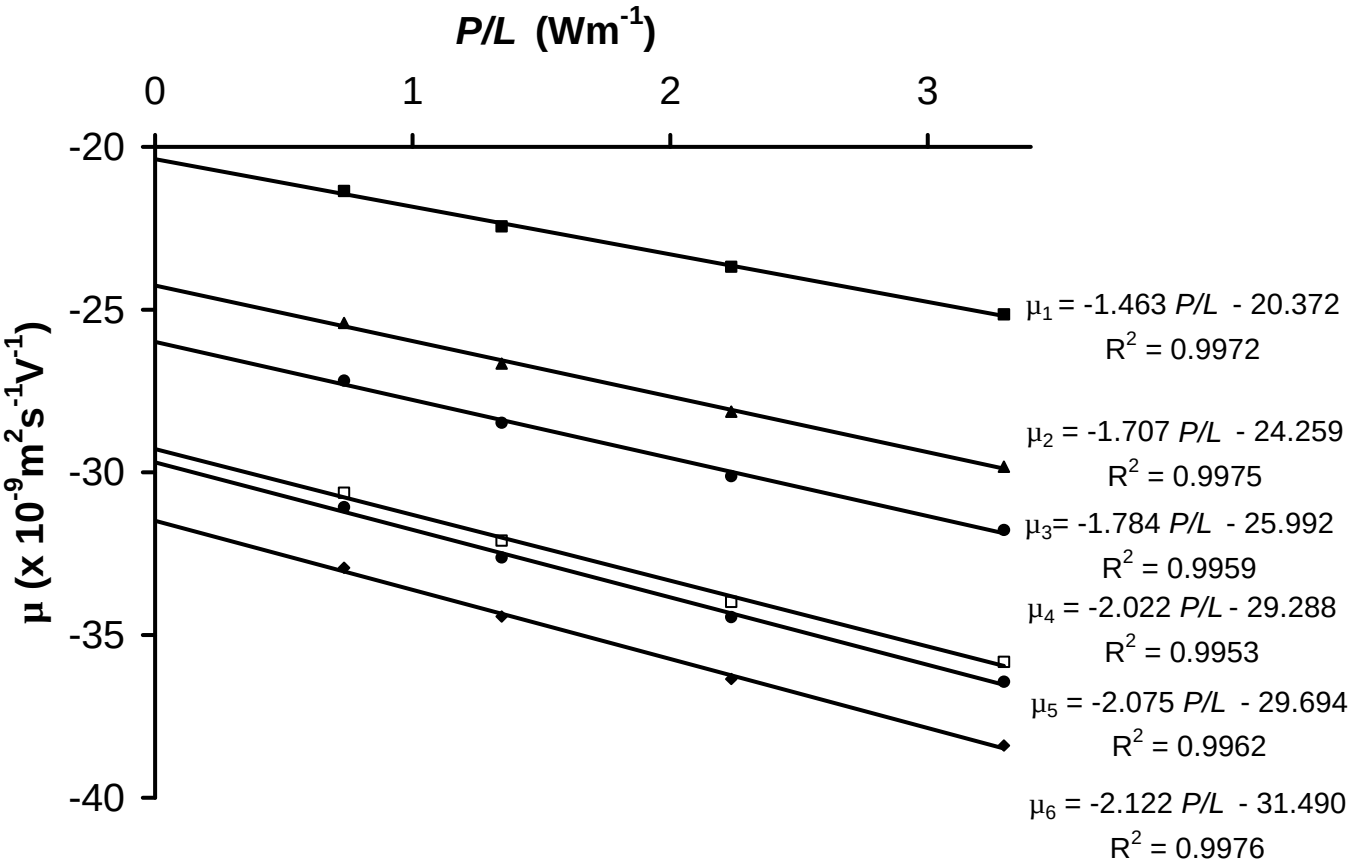

Figure 7- 3: Electrophoretic mobilities of aromatic anions as a function of *P/L*.
Data taken from a single day with error bars of ± 2 standard deviations
Conditions: As in **Table 7- 2**
Analytes: 1. 4-heptylbenzoate, 2. 4-propylbenzoate, 3. 4-aminophenylacetate, 4. 2-aminobenzoate, 5. benzoate, 6. salicylate

7.4 Conclusions

The accuracy of electrophoretic mobility measurements from CE can be improved by correcting for the influence of Joule heating which can introduce a variation of 20 % or more at moderate power levels. Values for the limiting ionic mobility can be obtained from μ_{ep} (0 Wm^{-1}) by correcting for the effects of the ionic strength of the electrolyte. These values were typically 13-15 % greater than μ_{ep} (0 Wm^{-1}) (the apparent electrophoretic mobility before performing the ionic strength correction) for the 10mM phosphate electrolyte used at pH = 7.21. The final accuracy of experimentally-determined μ_{ep}^{0} is limited by the lack of temperature control for parts of the capillary. It is anticipated that precision and accuracy could be further improved by applying active-cooling to the entire capillary.

8 General Conclusions

The following general conclusions can be made from the present work regarding thermal effects and temperature profiles in capillary electrophoresis (CE).

During CE, Joule heating results in a linear increase in the conductance (G) and the electroosmotic mobility (μ_{EOF}) as the power dissipated per unit length (P/L) is increased. Either G or μ_{EOF} may be used to determine the temperature of the electrolyte, but it has been demonstrated that these parameters indicate the electrolyte temperature at different radial positions in the capillary. G may be used to determine the mean electrolyte temperature (T_{Mean}) and μ_{EOF} may be used to determine T_{Wall}, the electrolyte temperature near the inner wall of the capillary (ie. where the electroosmotic flow is generated). The technique of extrapolating values of G or μ_{EOF} to $P/L = 0$ eliminates the influence of Joule heating and avoids the significant errors that are introduced by relying on measurements made at separation voltages of less than 5 kV.

A theoretical understanding of the relationship between the temperatures of the electrolyte at the central axis (T_{Axis}), near the inner wall (T_{Wall}) and the mean temperature of the electrolyte in the cross-section (T_{Mean}) indicates that T_{Mean} differs from T_{Axis} and T_{Wall} by $^1/_2 \Delta T_{Radial}$.

The accuracy of the temperatures determined during CE relies on an accurate knowledge of the temperature coefficient of the probe being used. G increases at approximately 2 % per ºC for most aqueous electrolytes, enabling the approximate increase in temperature to be determined simply. If the temperature coefficient of conductance is unknown, accurate temperature determinations require an initial calibration process which can be performed in a straightforward manner using a conductivity cell. The calibration of electroosmotic mobility as a temperature probe is a time-consuming process that requires great attention to detail and a significant amount of data processing.

Excellent results can be achieved using either G or μ_{EOF}. If sufficient experimental care is taken, the agreement between values of T_{Mean}, T_{Wall} or T_{Axis} determined from G or μ_{EOF} is within 0.1 ºC once the radial temperature difference is taken into account. Conductance is recommended as a routine probe for temperature determination due to its robust nature and the relative ease of its calibration.

Being able to make accurate temperature measurements using data collected directly from the CE instrument is significant in terms of cost saving and improved

precision but is most important when investigating kinetics say in affinity studies or in complexation reactions where small changes in temperature can alter the selectivity of a complexing ligand.

New equations have been developed to enable the temperature at any radial position within the capillary to be determined and a complete radial temperature profile to be plotted for any capillary including the temperature profile of the stagnant coolant layer surrounding the capillary. Modeling has shown that even when an efficient cooling system is used, the temperature drop across the air layer dwarfs all of the other temperature drops across the walls of the capillary and within the electrolyte itself. This explains why higher cooling efficiencies can be achieved by liquid cooling systems.

It has been demonstrated that a knowledge of the temperature difference across the stagnant air layer enables the heat transfer coefficient *h* for the capillary to be determined. This can also be achieved by curve-fitting the variation of conductance with voltage at relatively low separation voltages. The values of *h* reflect the cooling efficiency for the whole length of the capillary, not just the part that is actively cooled. Future research is needed to model the temperature profile in the zones of the capillary that experience different cooling modes so that the value of *h* for the whole capillary can be used to determine the cooling efficiency of the active-cooling system.

Some progress has been made in understanding the variation in zeta-potential (ζ) with temperature, an area that has not been addressed previously using CE. For the fused-silica capillaries used with a phosphate electrolyte at pH 7.21, ζ increased linearly with the absolute temperature (T) at a rate of 0.39 % K^{-1}. This value is about 4 times smaller than predictions made by earlier workers. The charge density on the inner surface of the capillary was found to be independent of temperature. This suggested that as the temperature increased, the increase in charge due to enhanced ionization of silanol groups was balanced by increased adsorption of counter-ions in the inner Helmholtz layer. To validate this hypothesis, the same experimental approach needs to be used to test the variation of ζ with T for a variety of electrolytes. An obvious limitation of this work is that it has only been carried out using one electrolyte system, at a single pH.

Extrapolating G to $P/L = 0$ facilitates the determination of internal diameters for capillaries of unknown dimensions. The same approach is applicable to determine the cross-sectional area of channels in microfluidic devices.

For polymer capillaries, the increase in electrolyte temperatures is approximately double that found in a fused-silica capillary of similar dimensions. ΔT_{Mean} increases with the reciprocal of the thermal conductivity of the capillary material. The implications of these findings are most significant for manufacturers of polymer-based electrodriven microfluidic devices. To minimise Joule heating in such devices, the polymer sheets employed should be made as thin as possible and attached to a material such as glass that has a much greater thermal conductivity.

A major criticism of CE has been its lack of reproducibility when compared with other separation techniques such as liquid chromatography. Joule heating and variations in the cooling efficiency in different CE instruments limits the reproducibility of electrophoretic mobility measurements. A solution to this problem has been to make measurements of μ_{Eff} over a range of *P/L* values and to extrapolate μ_{Eff} to *P/L* = 0 Wm^{-1} to obtain μ_{eff} free from the influence of Joule heating. These same values of μ_{eff} (0 Wm^{-1}) can be used to generate values of limiting ionic mobility after making a correction for ionic strength. Future research is needed to validate this method in other instruments.

9 References:

[1] Evenhuis, C. J., Guijt, R. M., Macka, M., Haddad, P. R., *Electrophoresis* 2004, *25*, 3602-3624.

[2] Guijt, R. M., Evenhuis, C. J., Macka, M., Haddad, P. R., *Electrophoresis* 2004, *25*, 4032-4057.

[3] Evenhuis, C. J., Guijt, R. M., Macka, M., Marriott, P. J., Haddad, P. R., *Electrophoresis* 2005, *26*, 4333-4344.

[4] Evenhuis, C. J., Guijt, R. M., Macka, M., Marriott, P. J., Haddad, P. R., *Electrophoresis* 2006, *27*, 672-676.

[5] Evenhuis, C. J., Guijt, R. M., Macka, M., Marriott, P. J., Haddad, P. R., *Anal. Chem.* 2006, *78*, 2684-2693.

[6] Kuban, P., Evenhuis, C. J., Macka, M., Haddad, P. R., Hauser*, P. C., *Electroanalysis* 2006, *18*, 1289-1296.

[7] Evenhuis, C. J., Guijt, R. M., Macka, M., Marriott, P. J., Haddad, P. R., in: Landers, J. P. (Ed.), *Handbook of Capillary Electrophoresis*, CRC Press, Boca Raton 2006, p. Submitted.

[8] Evenhuis, C. J., Guijt, R. M., Macka, M., Marriott, P. J., Haddad, P. R., 28th International Symposium on Capillary Chromatography & Electrophoresis, 2005, Las Vegas, poster no.59.

[9] Evenhuis, C. J., Guijt, R. M., Macka, M., Marriott, P. J., Haddad, P. R., International Symposium on Chromatography, Copenhagen, August 21-25, 2006 poster no. Pe01.

[10] Evenhuis, C. J., Guijt, R. M., Macka, M., Marriott, P. J., Haddad, P. R., International Symposium on Chromatography, Copenhagen, August 21-25, 2006 poster no. Pe03.

[11] Evenhuis, C. J., Guijt, R. M., Macka, M., Marriott, P. J., Haddad, P. R., International Symposium on Chromatography, Copenhagen, August 21-25, 2006 poster no. Pe04.

[12] Evenhuis, C. J., Guijt, R. M., Macka, M., Marriott, P. J., Haddad, P. R., International Symposium on Chromatography, Copenhagen, August 21-25, 2006 poster no. Pe05.

[13] Evenhuis, C. J., Guijt, R. M., Macka, M., Marriott, P. J., Haddad, P. R., 29th International Symposium on High Performance Liquid Phase Separations & Related Techniques - HPLC-2005, Stockholm, June 26-30, 2005 poster no.7:25.

[14] Evenhuis, C. J., Johns, C., Yang, W.-C., Schuman, P., Guijt, R. M., Haddad, P. R., Marriott, P. J., Macka, M., 25th International Symposium on Capillary Chromatography, Riva del Garda,, 31 May - 4 June 2004, oral keynote presentation No. KNL.10.

[15] Evenhuis, C. J., Guijt, R. M., Haddad, P. R., Marriott, P. J., Macka, M., International Symposium on Separation Science, Parubice, 12-15 September 2005, oral presentation No. L33, p. 43.

[16] Jandik, P., Bonn, G. K., *Capillary Electrophoresis of Small Molecules and Ions*, VCH, New York 1993, pp. 5-67.

[17] Andrews, A. T., *Electrophoresis: theory, techniques, and biochemical and clinical applications*, Clarendon Press, Oxford 1986, pp. 1-452.

[18] Baker, D. R., *Capillary electrophoresis*, Wiley, New York 1995, pp. 1-235.

[19] Bartle, K. D., Myers, P. J., *Capillary Electrochromatography*, RSC, Cambridge 2001, pp. 1-149.

[20] Camilleri, P., in: Camilleri, P. (Ed.), *Capillary Electrophoresis- Theory and Practice*, CRC Press, Boca Raton 1997, pp. 1-552.

[21] Deyl, Z., Svec, F., *capillary electrochromatography*, Elsevier, Amsterdam 2001, pp. 1-429.

[22] El Rassi, Z., *Carbohydrate analysis by modern chromatography and electrophoresis*, Elsevier, Amsterdam 2002, pp. 1-1223.

[23] Foret, F., Krivankova, L., Bocek, P., *Capillary zone electrophoresis*, VCH, Weinheim 1993, pp. 1-346.

[24] Frazier, R. A., Ames, J. M., Nursten, H. E., *Capillary electrophoresis for food analysis : method development*, Royal Society of Chemistry, Cambridge 2000, pp. 1-127.

[25] Grossman, P. D., Colburn, J. C., *Capillary electrophoresis: theory & practice*, Academic Press, San Diego 1992, pp. 1-352.

[26] Heiger, D. N., *High Performance Capillary Electrophoresis (3rd ed.)*, Hewlett Packard, Palo Alto 1997, pp. 1-136.

[27] Kuhn, R., Hoffstetter-Kuhn, S., *Capillary Electrophoresis: Principles and Practice*, Springer-Verlag, Berlin 1993, pp. 114-151.

[28] Krull, I. S., Stevenson, R. L., Mistry, K., Swartz, M. E., *Capillary Electrochromatography and Pressurised Flow Capillary Electrochromatography- An Introduction*, HNB publishing, New York 2000, pp. 1-240.

[29] Nelson, R. J., Burgi, D. S., in: Landers, J. P. (Ed.), *Handbook of Capillary Electrophoresis*, CRC Press, Boca Raton 1994, pp. 549-562.

[30] Landers, J. P., *Handbook of Capillary Electrophoresis (2nd Edition)*, CRC Press, Boca Raton 1997, pp. 1-894.

[31] Li, S. F. Y., Wei, H., *Capillary Electrophoresis-Principles, practice and applications*, Elseviers, Amsterdam 1992, pp. 1-582.

[32] Lunn, G., *Capillary electrophoresis methods for pharmaceutical analysis*, Wiley, New York 2000, pp. 1-1544.

[33] Lunte, S. M., Radzik, D. M., *Pharmaceutical and biomedical applications of capillary electrophoresis*, Pergamon, Oxford 1996, pp. 1-511.

[34] Rathore, A. S., Guttman, A., *Electrokinetic phenomena: principles and applications in analytical chemistry and microchip technology*, Marcel Dekker, New York 2004, pp. 1-476.

[35] Righetti, P. G., *Capillary electrophoresis in analytical biotechnology*, CRC Press, Boca Raton 1996, pp. 1-551.

[36] Shaw, D. J., *Electrophoresis*, Academic Press, London 1969, pp. 1-144.

[37] Shintani, H., Polonský, J., *Handbook of capillary electrophoresis applications*, Blackie Academic & Professional, London 1997, pp. 1-737.

[38] Thibault, P., Honda, S., *Capillary Electrophoresis of Carbohydrates*, Humana Press, Totowa 2003, pp. 1-318.

[39] Weinberger, R., *Practical capillary electrophoresis*, Academic Press, Boston 1993, pp. 1-312.

[40] Kirby, B. J., Hasselbrink, E. F. J., *Electrophoresis* 2004, *25*, 187-202.

[41] Qiao, R., *Langmuir* 2006, *ASAP 30/06/06*.

[42] van der Goor, A. A. A. M., Wanders, B. J., Everaerts, F. M., *J. Chrom.* 1989, *470*, 95-104.

[43] Jandik, P., Bonn, G. K., *Capillary Electrophoresis of Small Molecules and Ions*, VCH, New York 1993, pp. 23-24.

[44] Li, S. F. Y., *Capillary Electrophoresis-Principles, practice and applications*, Elseviers, Amsterdam 1992, p. 15.

[45] Pallandre, A., de Lambert, B., Attia, R., Jonas, A. M., Viovy, J.-L., *Electrophoresis* 2006, *27*, 584-610.

[46] Kirby, B. J., Hasselbrink, E. F., *Electrophoresis* 2004, *25*, 203-213.

[47] Hjerten, S., *Electrophoresis* 1990, *11*, 665-690.

[48] Hjerten, S., *Chromatog. Rev.* 1967, *9*, 122-219.

[49] Porras, S. P., Marziali, E., Gas, B., Kenndler, E., *Electrophoresis* 2003, *24*, 1553 - 1564.

[50] Xuan, X., Li, D., *J. Micromech. Microeng.* 2004, *14*, 1171-1180.

[51] Xuan, X., Xu, B., Sinton, D., Li, D., *Lab Chip* 2004, *4*, 230-236.

[52] Knox, J. H., *Chromatographia* 1988, *26*, 329-337.

[53] Knox, J. H., McCormack, K. A., *Chromatographia* 1994, *38*, 207-214.

[54] Grushka, E., McCormick, J. R. M., Kirkland, J. J., *Anal. Chem.* 1989, *61*, 241-246.

[55] Petersen, N. J., Nikolajsen, R. P. H., Mogensen, K. B., Kutter, J. P., *Electrophoresis* 2004, *25*, 253-269.

[56] Ikuta, N., Yamada, Y., Hirokawa, T., *Electrophoresis* 2000, *21*, 360-366.

[57] Xu, X., Kok, W., Poppe, H., *J Chromatogr. A* 1997, *786*, 333-345.

[58] Knox, J. H., McCormack, K. A., *Chromatographia* 1994, *38*, 279-282.

[59] McCormick, R. M., *Anal. Chem.* 1988, *60*, 2322-2328.

[60] Gobie, W. A., Ivory, C. F., *J. Chromatogr.* 1990, *516*, 191-210.

[61] Vinther, A., Soeberg, H., *J. Chromatogr. A* 1991, *559*, 27-42.

[62] Nelson, R. J., Paulus, A., Cohen, A. S., Guttman, A., Karger, B. L., *J. Chromatogr.* 1989, *480*, 111-127.

[63] Cifuentes, A., Kok, W., Poppe, H., *J. Microcolumn Sep* 1995, *7*, 365-374.

[64] Rush, R. S., Cohen, A. S., Karger, B. L., *Anal. Chem.* 1991, *63*, 1346-1350.

[65] Giordano, B. C., Horsman, K. M., Burgi, D. S., Ferrance, J. P., Landers, J. P., *Electrophoresis* 2006, *27*, 1355-1362.

[66] Kates, B., Ren, C. L., *Electrophoresis* 2006, *27*, 1967-1976.

[67] Tiselius, A., *Biochem. J.* 1932, *31*, 1464–1477.

[68] Camilleri, P., in: Camilleri, P. (Ed.), *Capillary Electrophoresis- Theory and Practice*, CRC Press, Boca Raton 1997, pp. 2-5.

[69] Engelhardt, H., Beck, W., Kohr, J., Schmitt, T., *Angewandte Chemie* 1996, *32*, 629-649.

[70] Tiselius, A., *Far. Soc. Disc.* 1953, *13*, 29-33.

[71] Mikkers, F. E. P., Everaerts, F. M., Verheggen, T. P. E. M., *J. Chromatogr.* 1979, *169*, 11-20.

[72] Jorgenson, J. W., Lukacs, K. D., *Anal. Chem.* 1981, *53*, 1298-1302.

[73] Mikkers, F. E. P., Everaerts, F. M., Verheggen, P. E. M., *J. Chromatogr.* 1979, *169*, 1-10.

[74] Harris, D. C., *Quantitative Chemical Analysis*, W.H. Freeman and Company, New York 2002, pp. 661-666.

[75] Mori, M., Hu , W., Haddad, P. R., Fritz, J. S., Tanaka, K., Tsue, H., Tanaka, S., *Anal. Bioanal. Chem.* 2002, *372*, 181-186.

[76] Coxon, M., Binder, M. J., *J. Chromatogr.* 1974, *101*, 1-16.

[77] Powell, R. W., Ho, C. Y., Liley, P. E., in: Weast, R. C. (Ed.), *CRC Handbook of Chemistry and Physics*, CRC Press, Cleveland 1978, p. E10.

[78] Polymicro_Technologies, Pheonix 2005, p. Product CD.

[79] National_Bureau_of_Standards, *CRC Handbook of tables for Applied Engineering Science*, CRC Press, Cleveland 1973, p. 11.

[80] Jones, A. E., Grushka, E., *J. Chromatogr.* 1989, *466*, 219-225.

[81] Liu, K.-L. K., Davis, K. L., Morris, M. D., *Anal. Chem.* 1994, *66*, 3744-3750.

[82] Tang, G. Y., Yang, C., Chai, C. J., Gong, H. Q., *Int. J. Heat Mass Transfer* 2004, *47*, 215-227.

[83] Hutchings, R., *Physics*, Macmillan Education Ltd., London 1990, pp. 517-518.

[84] Nishikawa, T., Kambara, H., *Electrophoresis* 1996, *17*, 1115-1120.

[85] Holman, J. P., *Heat Transfer*, McGraw-Hill, New York 1963, pp. 146-147.

[86] Knox, J. H., McCormack, K. A., *Chromatographia* 1994, *38*, 215-221.

[87] Palonen, S., *Chemistry*, Helsinki University Publishing House, Helsinki 2005, p. 96.

[88] Xuan, X. C., Li, D. Q., *Electrophoresis* 2005, *26*, 166-175.

[89] Bello, M. S., Righetti, P. G., *J. Chromatogr.* 1992, *606*, 103-111.

[90] Isono, T., *J. Chem.Eng. Data* 1984, *29*, 45-52.

[91] Fujii, T., Fujii, M., Honda, T., *Proceedings of the 7th International Heat Transfer Conference* 1982, pp. 311-316.

[92] Giddings, J. C., *Separation Science* 1969, *4*, 181-189.

[93] Guijt, R. M., *Chemistry*, Delft Technical University, Delft 2003, pp. 28-35.

[94] Harris, D. C., *Quantitative Chemical Analysis*, W.H. Freeman and Company, New York 2002, p. 563.

[95] Watanabe, I., Ui, N., Nakamura, M., *Journal of Physical Colloidal Chemistry* 1950, *54*, 1366-1370.

[96] Zhang, H., Li, Q., Hu, Z., Wang, R., Chen , X., *J Chromatogr. A* 2000, *709*, 353-356.

[97] Weisstein, E. W., 1996.

[98] Tallarek, U., Rapp, E., Scheenen, T., Bayer, E., Van As, H., *Anal. Chem.* 2000, *72*, 2292-2301.

[99] Rathore, A. S., *J. Chromatogr. A* 2004, *1037*, 431-443.

[100] Gas, B., *J. Chromatogr. A* 1993, *644*, 161-174.

[101] Xuan, X., Xu, B., Sinton , D., Li, D., *Lab on a Chip* 2004, *4*, 230-236.

[102] Burgi, D. S., Salomon, K., Chien, R.-L., *J.Liq. Chromatogr.* 1991, *14*, 847-867.

[103] Lacey, M. E., Webb, A. G., Sweedler, J. V., *Anal. Chem.* 2000, *72*, 4991-4998.

[104] Berezovski, M., Krylov, S. N., *Anal. Chem.* 2004, *76*, 7114-7117.

[105] Davis, K. L., Liu, K.-L. K., Lanan, M., Morris, M. D., *Anal. Chem* 1993, *65*, 293-298.

[106] Ryslavy, Z., Vacik, J., Zuska, J., *J. Chromatogr.* 1975, *114,*, 315-320.

[107] Terabe, S., Otsuka, K., Ando, T., *Anal. Chem.* 1985, *57*, 57, 834-841.

[108] Cross, R. F., Cao, J., *J. Chromatogr. A* 1998, *809*, 159–171.

[109] Chaudhari, A. M., Woudenberg, T. M., Albin, M., Goodson, K. E., *JMEMS* 1998, *7*, 345-355.

[110] Swinney, K., Bornhop, D. J., *Electrophoresis* 2001, *22*, 2032–2036.

[111] Mao, H., Yang, T., Cremer, P. S., *J. Am. Chem. Soc* 2002, *124*, 4432–4435.

[112] Rathore, A. S., Reynolds, K. J., Colon, L. A., *Electrophoresis* 2002, *23*, 2918.

[113] Ross, D., Gaitan, M., Locascio, L. E., *Anal. Chem* 2001, *73*, 4117-4123.

[114] Watzig, H., *Chromatographia* 1992, *33*, 445 - 448.

[115] Swinney, K., Bornhop, D. J., *Analyst* 2000, *125*, 1713-1717.

[116] Sakakibara, J., Adrian , R. J., *Experiments in Fluids* 1999, *26*, 7-15.

[117] Patil, V. A., Narayanan, V., *Microfluid Nanofluid* 2006, *2*, 291–300.

[118] Jorgenson, J. W., Lukacs, K. D., *Science* 1983, *222*, 266-272.

[119] NBS, in: Weast, R. C. (Ed.), *Handbook of Chemistry and Physics*, CRC Press, Cleveland 1977, p. F51.

[120] Kok, W., *Chromatographia* 2000, *51 (Suppl.)*, S24-27.

[121] Tang, G. Y., Yang, C., Chai, C. K., Gong, H. Q., *Anal. Chim. Acta* 2004, *507*, 27–37.

[122] Revil, A., Glover, P. W. J., Pezard, P. A., *J. Geophys. Res.* 1999, *104*, 20021–20032.

[123] Swinney, K., Bornhop, D. J., *Electrophoresis* 2002, *23*, 613-620.

[124] Thormann, W., Zhang, C.-X., Caslavska, J., Gebauer, P., Mosher, R. A., *Anal. Chem.* 1998, *70*, 549-562.

[125] Kok, W., *Chromatographia* 2000, *51 Supplement*, S28-S35.

[126] Hiemstra, T., Van Riemsdeijk, W. H., *J. Coll. Interf. Sci.* 1990, *136*, 132-150.

[127] Hamer, W. J., *Handbook of Chemistry and Physics*, CRC Press, Cleveland 1977, pp. E-61.

[128] Ishido, T., Mizutani, H., *J. Geophys. Res.* 1981, *86*, 1763-1775.

[129] Somasundaran, P., Kulkani, R. D., *J. Colloid Interface Sci.* 1973, *45*, 591-600.

[130] Dandeneau, R. D., Zerenner, E. H., *HRC & CC* 1979, *1*, 351-356.

[131] Dandeneau, R. D., Zerenner, E. H., *LC GC* 1990, *8*, 909-912.

[132] Eiceman, G. A., in: Meyers, R. A. (Ed.), *Encyclopedia of Analytical Chemistry*, John Wiley & Sons, Chichester 2000, pp. 10629-10630.

[133] Macka, M., Yang, W.-C., Zakaria, P., Shitangkoon, A., Hilder, E. F., Andersson, P., Nesterenko, P., Haddad, P. R., *J. Chromatogr. A* 2004, *1039*, 193-199.

[134] Caslavska, J., Thormann, W., *J. Microcol. Sep.* 2001, *13*, 69-83.

[135] Chen, S., Lee, M. L., *J. Microcol. Sep.* 1997, *9*, 57-62.

[136] Kvasnicka, F., *Electrophoresis* 2003, *24*, 860-864.

[137] Liu, P. Z., Malik, A., Kuchar, M. C., Vorkink, W. P., Lee, M. L., *J. Microcol. Sep.* 1993, *5*, 245-253.

[138] Deng, B., Chan, W.-T., *Electrophoresis* 2001, *22*, 2186-2191.

[139] Lukacs, K. D., Jorgenson, J. W., *HRC & CC* 1985, *8*, 407-411.

[140] Tanyanyiwa, J., Leuthardt, S., Hauser, P. C., *J. Chromatogr. A* 2002, *978*, 205-211.

[141] LAU ALDRICH, N. K., APPLERA CORP, LAU ALDRICH N K, USA, Patent No. WO2004104054 2004, pp. 1-66.

[142] Erickson, D., Sinton, D., Li, D., *Lab Chip* 2003, *3*, 141–149.

[143] Topas, Topas, www.topas.com/topas_brochure_english.pdf 2006.

[144] Pierson, H. O., *Handbook of Carbon, Graphite, Diamond and Fullerenes - Properties, Processing and Applications*, William Andrew Publishing, Noyes 1993, pp. 1-399.

[145] Kerbow, D. L., Sperati, C. A., in: Brandrup, J., Immergut, E. H., Grulke, E. A. (Eds.), *Polymer Handbook 4th Edition*, J. Wiley and Sons, Hoboken 1999, p. V/44.

[146] Dow-Corning, in: 10-898E-01, F. N. (Ed.), *http://www.dowcorning.com/DataFiles/090007b5802e201c.pdf* 2005.

[147] Kerbow, D. L., Sperati, C. A., in: Brandrup, J., Immergut, E. H., Grulke, E. A. (Eds.), *Polymer Handbook 4th Edition*, J. Wiley and Sons, Hoboken 1999, p. V/51.

[148] Mehta, R. H., in: Brandrup, J., Immergut, E. H., Grulke, E. A. (Eds.), *Polymer Handbook 4th Edition*, J. Wiley and Sons, Hoboken 1999, p. v/93.

[149] Wunderlich, W., in: Brandrup, J., Immergut, E. H., Grulke, E. A. (Eds.), *Polymer Handbook 4th Edition*, J. Wiley and Sons, Hobken 1999, p. v/88.

[150] Schrader, D., in: Brandrup, J., Immergut, E. H., Grulke, E. A. (Eds.), *Polymer Handbook 4th Edition*, J. Wiley and Sons, Hobken 1999, p. v/93.

[151] Kerbow, D. L., Sperati, C. A., in: Brandrup, J., Immergut, E. H., Grulke, E. A. (Eds.), *Polymer Handbook 4th Edition*, J. Wiley and Sons, Hoboken 1999, p. V/36.

[152] Kerbow, D. L., Sperati, C. A., in: Brandrup, J., Immergut, E. H., Grulke, E. A. (Eds.), *Polymer Handbook 4th Edition*, J. Wiley and Sons, Hoboken 1999, p. V/ 56.

[153] Zhang, Y., Bao, N., Yu, X.-D., Xu, J.-J., Chen, H.-Y., *J. Chromatogr. A* 2004, *1057*, 247–251.

[154] Macka, M., Appendix A Graphs and Tables for Capillary Electrophoresis ,Australian Centre for Research On Separation Science, University of Tasmania, Sandy Bay 2003, pp. 3,4.

[155] Hirokawa, T., Nishino, M., Aoki, N., Kiso, Y., Sawamoto, Y., Yagi, T., Akiyama, J.-I., *J. Chromatogr.* 1983, *271*, D1-D106.

[156] Jandik, P., Bonn, G. K., *Capillary Electrophoresis of Small Molecules and Ions*, VCH, New York 1993, pp. 15-18.

[157] Jandik, P., Bonn, G. K., *Capillary Electrophoresis of Small Molecules and Ions*, VCH, New York 1993, pp. 99-100.

[158] Pospichal, J., Gebauer, P., Bocek, P., *Chem. Rev.* 1989, *89*, 419-430.

[159] Onsager, L., Fuoss, R. M., *J. Phys. Chem.* 1932, *36*, 2689–2778.

[160] Atkins, P. W., *Physical Chemistry*, Oxford University Press, Oxford 1998, pp. 745-746.

[161] Atkins, P. W., *Physical Chemistry*, Oxford University Press, Oxford 2002, pp. 832-842.

[162] Vceláková, K., Zusková, I., Kenndler, E., Gaš, B., *Electrophoresis* 2004, *25*, 309-317.

[163] Jaros, M., Vceláková, K., Zusková, I., Gas, B., *Electrophoresis* 2002, *23*, 2667–2677.

[164] Kvaratskhelia, R., Kvaratskhelia, H., *Bulletin of the Georgian Academy of Sciences* 1997, *155*, 375-378.

[165] Vanysek, P., *CRC Tables of Chemistry and Physics (80th Ed.)*, CRC Press, Boca Raton 1999, p. 5_94.

[166] National-Bureau-of-Standards, *Handbook of Chemistry and Physics*, CRC Press, Cleveland 1977, pp. F-51.

[167] Chandra, A., Bagchi, B., *J. Chem. Phys.* 1999, *110*, 10024-10034.

[168] Horvath, A. L., *Handbook of Aqueous Electrolyte Solutions: Physical properties, estimation and correlation methods*, Ellis Horwood Ltd., Chichester 1985, pp. 254-255.

[169] National_Bureau_of_Standards, in: Bolz, R. E., Tuve, G. L. (Eds.), *CRC Handbook of tables for Applied Engineering Science*, CRC Press, Cleveland 1973, p. 11.

[170] Poferl, D. J., Svehla, R., in: Weast, R. C. (Ed.), *Handbook of Chemistry and Physics*, CRC Press, Cleveland 1978, p. F13.

10 Appendices

Appendix 1 - Derivation of Modified Debye-Hückel-Onsager Equation

Conductance, (G) is the inverse of resistance [161]. An equation for conductance is given in Eqn A1- 1 (previously 4- 3).

$$G = \frac{I}{V} = \frac{\kappa A}{L} \qquad \text{A1- 1 (previously 4- 3)}$$

where *I* is the current, *V* is the voltage, *κ* is the electrical conductivity, *A* is the cross-sectional area and *L* is the length of the conductor.

For electrolytes, *κ* can be calculated using the molar conductivity, (Λ_m) and concentration (c) as described in Eqn A1- 2.

$$\Lambda_m = \frac{\kappa}{c} \qquad \text{A1- 2}$$

An expression for the conductance of the electrolyte can be found by rearrangement and substitution to produce Eqn A1- 3.

$$G = \frac{c\Lambda_m A}{L} \qquad \text{A1- 3}$$

Kohlrausch's Law (Eqn A1- 4) can be used to determine the variation of the molar conductivity with electrolyte concentration [161].

$$\Lambda_m = \Lambda_0 - Kc^{1/2} \qquad \text{A1- 4}$$

where Λ_0 is the specific conductivity at infinite dilution, and *K* is a constant. As shown in Eqn A1- 4, *K* depends on the specific conductivity at infinite dilution of the electrolyte[161]and the Debye-Hückel-Onsager coefficients A and B [167].

$$K = A + B\Lambda_0 \qquad \text{A1- 5}$$

For electrolytes composed of monovalent ions (1:1 electrolytes) dissolved in water at 25 ^{o}C, A and B have values of 6.021 x10^{-3} $Sm^2mol^{-1}M^{-1/2}$ and 0.2289 $M^{-1/2}$ respectively. Under different conditions, the values for A and B can be found using Eqn A1- 6.

$$A = \left(\frac{z^2eF^2}{3\pi\eta}\right)\left(\frac{2}{\varepsilon RT}\right)^{1/2} \text{ and } \quad B = \left(\frac{q^* z^3 eF}{24\pi\varepsilon RT}\right)\left(\frac{2}{\varepsilon RT}\right)^{1/2} \qquad \text{A1- 6}$$

where z is the valency of the ions, e is the charge on an electron, F is Faraday's constant, η is the viscosity, ε is the electrical permittivity of the electrolyte, q is a parameter relating to the mobility of the ions and the stoichiometry of the electrolyte described in Eqn A1- 7, and the other symbols have their usual meaning[161]. For 1:1 electrolytes, Chandra and Bagchi [167] used Eqn A1- 7 to show that q^* = 0.586 (=2-√2) if the mobilities of the cations and anions ions are equal.

$$q^* = 2\left[1 - \left(\frac{1}{2}\sum_{\beta}\frac{\Lambda_\alpha}{\Lambda_\alpha + \Lambda_\beta}\right)^{\frac{1}{2}}\right] \qquad \text{A1- 7}$$

In Eqn A1- 7, Λ_α and Λ_β refer to the molar conductivities at infinite dilution of the cation and anion. Using the approximation that q = 0.586, and numerical values for the constants, in Eqn A1- 6, the expression for A and B may be simplified to Eqn A1- 8 [168].

$$A = \frac{82.03z^2}{\eta(\varepsilon_r T)^{1/2}} \quad \text{and} \quad B = \frac{8.205x10^5\left|z^3\right|}{(\varepsilon_r T)^{3/2}} \qquad \text{A1- 8}$$

where ε_r is the dielectric constant of the medium. The dielectric constant is the factor by which the electrical permittivity of a medium exceeds that of a vacuum; it is defined by Eqn A1- 9.

$$\varepsilon_r = \frac{\varepsilon}{\varepsilon_0} \qquad \text{A1- 9}$$

Walden's Rule (Eqn A1- 10) states that the specific conductivity at infinite dilution is inversely proportional to the viscosity.

$$\Lambda_0 = \frac{k}{\eta} \qquad \text{A1- 10}$$

where *k* is a constant for each particular electrolyte.

An expression for conductance can be found by combining Eqns A1- 3 to A1- 7 and Eqn A1- 10 to give Eqn A1- 11.

$$G = \frac{1}{\eta}\left(\frac{cA}{L}\right) \bullet \left\{ k - \left(\frac{z^2 eF^2}{3\pi}\right)\left(\frac{2c}{\varepsilon RT}\right)^{1/2} - q * k\left(\frac{z^3 eF}{24\pi\varepsilon RT}\right)\left(\frac{2c}{\varepsilon RT}\right)^{1/2} \right\} \qquad \text{A1- 11}$$

Appendix 2 – Calculation of *h* for Passively-cooled Capillaries

The Nusselts number can be evaluated using a set of empirical equations and approximations. N_u is a function of the Grashof number G_r and the Prandtl number P_r.

$$N_u = f(G_r P_r) \qquad \text{A2- 1}$$

The size of G_r depends on the outer diameter of the capillary, the temperature difference between the wall and the coolant and the kinetic viscosity of the coolant ($\nu_{Coolant}$) measured at the film temperature (the average of the ambient temperature and the temperature of the outer wall) [86].

$$G_r = \frac{g\beta {d_0}^3 \Delta T_{Coolant}}{\nu^2_{Coolant}} \qquad \text{A2- 2}$$

where g is the acceleration due to gravity = 9.80 ms^{-2}, β is the reciprocal of the film temperature (T_{Film}) and $\nu_{Coolant}$ is equal to the dynamic viscosity (η) divided by the density (ρ) at the film temperature) [85]

$$\beta = \frac{1}{\left(T_{set} + \frac{1}{2}\Delta T_{Coolant}\right)} \qquad \text{A2- 3}$$

Using the data from Knox and McCormack [86], it is possible to calculate G_r. For air at 34.1 ºC, the viscosity $\eta_{Air} \approx 1.893 \times 10^{-5}$ $kgm^{-1}s^{-1}$ [169] and the density can be calculated using the ideal gas equation with an average molar mass of 28.964 $gmol^{-1}$ [170].

$$\beta = \frac{1}{\left(T_{Ambient} + \frac{1}{2}\Delta T_{Coolant}\right)} = \frac{1}{\left(293.2K + \frac{1}{2}x\ 28.3K\right)} = 3.254x10^{-3}K^{-1}$$

$$\rho_{Air} = \frac{pM}{RT} = \frac{101.325\,x\,kPa\,x28.964x10^{-3}kgmol^{-1}}{8.3145\,x\,kPaLmol^{-1}K^{-1}x\,307.3K} = 1.1486\,kgm^{-3}$$

$$\nu = \frac{\eta_{Air}}{\rho_{Air}} = \frac{1.881x10^{-5}kgm^{-1}s^{-1}}{1.1486\,kgm^{-3}} = 1.637x10^{-5}m^2s^{-1}$$

$$\therefore G_r = \frac{9.80ms^{-2}\,x3.254\,x10^{-3}K^{-1}x(3.75x10^{-4}m)^3\,x\,28.3K}{(1.637x10^{-5}m^2s^{-1})^2} = 0.178$$

The Prandtl number is associated with the thickness (δ_t) of the thermal boundary layer (layer of coolant through which heat energy is transferred by conduction only). Pr is defined as the ratio of the kinematic viscosity (ν) of the coolant to its thermal diffusivity (α) [85]

$$P_r = \frac{\nu}{\alpha} = \frac{\eta_{Coolant} / \rho}{\lambda_{Coolant} / \rho c_p} = \frac{c_p \eta_{Coolant}}{\lambda_{Coolant}} \qquad \text{A2- 4}$$

where ρ is the density of the coolant and c_p is its specific heat capacity. For air at 34.1 ºC, $c_p \approx 1.0065 \times 10^3$ J kg^{-1}K^{-1}, $\eta_{Air} = 1.881 \times 10^{-5}$ kgm^{-1}s^{-1} and $\lambda_{Air} \approx 0.02680$ Wm^{-1}K^{-1} [169]. Substitution gives $P_r \approx 0.7064$ which is dimensionless [170].

The nature of the function in Eqn A2- 1 cannot be derived theoretically but experiments have shown that it depends on the product of G_r and P_r which is known as the Rayleigh number (R_a). For this example R_a = 0.182 x 0.7064 ≈ 0.129 For $10^{-2} < R_a < 10^2$, typical values found in CE [53], the function for the Nusselts number is given by A2- 5.

$$N_u = 1.02 \, R_a^{0.148} \qquad \text{A2- 5}$$

Substituting R_a = 0.129 in A2- 5 gives N_u = 0.753 and enables h to be calculated using Eqn 1- 20.

$$h = \frac{N_u \lambda_{Coolant}}{d_o} = \frac{0.753 \, x \, 0.02680 \, Wm^{-1}K^{-1}}{3.75 x 10^{-4} m} = 53.8 \; Wm^{-2}K^{-1}$$

This value agrees very well with the value of Nishikawa and Kambara [84] who used miniature thermocouples to measure the external temperature of capillaries but is about 60 % of the value for h previously calculated for Knox and McCormack's experimental data [53]. The discrepancy corroborates their hypothesis that tiny air currents were present.

By equating Eqns 1- 21 and A2- 5 Knox and McCormack were able to show that the rise in temperature of the electrolyte is not expected to increase linearly with P/L (= EI) for passive cooling. This was consistent with their previous observations at higher power levels [86].

$$N_u = 1.02 R_a^{0.148} = \frac{EI}{\pi \lambda_{Coolant} \Delta T_{Coolant}}$$

$$\therefore 1.02 \left(\frac{g \beta P_r d_0^{\,3} \Delta T_{Coolant}}{\nu^2_{Coolant}} \right)^{0.148} = \frac{EI}{\pi \lambda_{Coolant} \Delta T_{Coolant}}$$

$$\therefore \Delta T_{Coolant}^{\,1.148} \propto EI \quad or \quad \Delta T_{Coolant} \propto (EI)^{0.871} \qquad \text{A2- 6}$$

Appendix 3 – Derivations of Eqns 4- 27 and 4- 28

Eqn 1- 29 may be rearranged to produce Eqn A3- 1.

$$T_{Mean} = T_{Set} + \frac{\Delta T_{ref}}{2Bi'_{OA} - (k^*)^2} \qquad 1\text{- }29$$

Before Joule heating occurs, it is assumed that the electrolyte is at the set temperature. The increase in the mean temperature of the electrolyte (ΔT_{Mean}) is the difference between the final mean temperature and the set temperature (T_{Mean} - T_{Set}).

$$\Delta T_{Mean} = T_{Mean} - T_{Set}$$

$$\therefore \Delta T_{Mean} = \frac{\Delta T_{ref}}{2Bi'_{OA} - (k^*)^2} \qquad A3\text{- }1$$

$$G = G_0 + \gamma G_0 \Delta T_{Mean} \qquad 4\text{- }25$$

$$\Delta T_{ref} = \frac{\kappa_0 E^2 {r_i}^2}{\lambda} = \frac{G_0 L_{tot}}{\pi {r_i}^2} \bullet \frac{V^2 {r_i}^2}{\lambda {L_{tot}}^2} = \frac{G_0 V^2}{\pi \lambda L_{tot}} \qquad 4\text{- }32$$

$$k^* = \sqrt{\gamma \Delta T_{ref}} = \sqrt{\frac{\gamma G_0 V^2}{\pi \lambda L_{tot}}} \qquad 4\text{- }33$$

Substituting for ΔT_{ref} and k^* in Eqn A3- 1 leads to Eqn 4- 28

$$\Delta T_{Mean} = \frac{\frac{G_0 V^2}{\pi \lambda L_{tot}}}{\frac{2h_{OA} r_i}{\lambda} - \left(\sqrt{\frac{\gamma G_0 V^2}{\pi \lambda L_{tot}}}\right)^2}$$

$$= \frac{\frac{G_0 V^2}{\pi \lambda L_{tot}}}{\frac{2\pi L h_{OA} r_i}{\pi \lambda L_{tot}} - \frac{\gamma G_0 V^2}{\pi \lambda L_{tot}}}$$

$$= \frac{G_0 V^2}{2\pi L_{tot} h_{OA} r_i - \gamma G_0 V^2} \qquad 4\text{- }28$$

This allows an expression for G to be derived by substituting Eqn 4- 28 into Eqn 4- 34 leading to 4- 29

Substituting ΔT_{Mean} into Eqn 4- 25 gives

$$
\begin{aligned}
G &= G_0 + \frac{\gamma {G_0}^2 V^2}{2\pi r_i h_{OA} L_{tot} - \gamma G_0 V^2} \\
&= G_0 \left(1 + \frac{\gamma G_0 V^2}{2\pi r_i h_{OA} L_{tot} - \gamma G_0 V^2} \right) \\
&= G_0 \left(\frac{2\pi r_i h_{OA} L_{tot} - \gamma G_0 V^2 + \gamma G_0 V^2}{2\pi r_i h_{OA} L_{tot} - \gamma G_0 V^2} \right) \\
&= G_0 \left(\frac{2\pi r_i h_{OA} L_{tot}}{2\pi r_i h_{OA} L_{tot} - \gamma G_0 V^2} \right) \\
&= G_0 \left(\frac{1}{1 - \frac{\gamma G_0 V^2}{2\pi r_i h_{OA} L_{tot}}} \right) = \frac{G_0}{1 - k_1 V^2}
\end{aligned}
\qquad \text{4- 35}
$$

where $k_1 = \gamma G_0 / 2\pi r_i h_{OA} L_{tot}$.